

Investigating the contributions of the right temporoparietal junction in sensory reweighting and cybersickness

by

Alyssa Lynn

A thesis

presented to the University of Waterloo

in fulfillment of the

thesis requirement for the degree of

Master of Science

in

Kinesiology and Health Sciences

Waterloo, Ontario, Canada, 2025

© Alyssa Lynn 2025

Author's Declaration

I hereby declare that I am the sole author of this thesis. This is a true copy of the thesis, including any required final revisions, as accepted by my examiners.

I understand that my thesis may be made electronically available to the public.

Abstract

Accurate perception of body position relative to gravity relies on the integration of visual, vestibular, and proprioceptive inputs. In virtual reality (VR), conflict between these sensory inputs can cause cybersickness – a visually-induced form of motion sickness. Sensory reweighting – a neural mechanism which shifts perceptual reliance on specific sensory cues based on prior experience and cue availability – has been proposed as a mechanism to mitigate cybersickness. However, the higher-order neural mechanisms underlying sensory reweighting in VR remain unclear. This exploratory study examined the role of the right temporoparietal junction (rTPJ) — a region involved in sensory integration, salience, and conflict detection — in sensory reweighting and cybersickness mitigation. Before and after a high-intensity VR experience, participants completed the Oriented CHAracter Recognition Test (OCHART) to assess sensory cue weighting and ranked their cybersickness throughout the VR experience using the Fast Motion Sickness scale (FMS). During VR, transcranial direct current stimulation (tDCS) was applied to the rTPJ to modulate neural activity. We hypothesized that anodal stimulation would enhance rTPJ activity, promote more efficient sensory reweighting, and reduce cybersickness, whereas cathodal stimulation would have the opposite effects. Results showed no significant differences in sensory cue weighting or FMS scores across stimulation conditions. Additionally, there was no association observed between changes in sensory weights and cybersickness. These findings suggest that rTPJ stimulation before VR is insufficient to modulate sensory reweighting or alleviate cybersickness. Future research should investigate the effect of rTPJ tDCS before and after VR and consider vestibular-specific reweighting measures, such as the subjective visual vertical or postural measures, such as sway path length. More specific measures of sickness, such as the Simulator Sickness Questionnaire (SSQ) should also be considered to better quantify the changes in cybersickness subtypes.

Acknowledgements

First, I would like to extend my gratitude to my supervisor, Dr. Michael Barnett-Cowan. I deeply appreciate all your support and patience throughout the many stages of this ever-evolving project. Thank you for believing in my ideas and for encouraging curiosity throughout. I would also like to thank the members of the Multisensory Brain and Cognition Lab for their continued support and guidance. I am incredibly thankful to have met a great group of mentors and friends through this degree.

Thank you to my committee members, Dr. Sean Meehan and Dr. Richard Staines, for providing valuable perspective and feedback to help me realize my research goals. Thank you to Dr. Benjamin Thompson and the Human Visual Neuroscience Lab for generously lending their neuroConn Stimulator when ours was out for repair. Finally, thank you to everyone who participated in my study and to those who volunteered their time to help with data collection.

Table of Contents

Author’s Declaration.....	ii
Abstract.....	iii
Acknowledgements.....	iv
List of Figures.....	viii
List of Tables.....	ix
List of Abbreviations.....	x
1.1 Introduction.....	1
1.2 Multisensory Integration in the Brain.....	2
1.3 Perception for Action.....	5
1.4 Motion Sickness.....	7
1.4.1 Motor Control and Motion Sickness.....	7
1.4.2 Visual Perception in VR.....	8
1.5 Cybersickness in VR.....	10
1.6 Postural Instability Theory.....	11
1.7 Sensory Conflict Theory.....	12
1.8 Sensory Reweighting.....	14
1.8.1 Measuring Sensory Reweighting.....	15
1.9 The Temporoparietal Junction.....	19
1.9.1 Multisensory Convergence and Integration.....	20
1.9.2 Ventral Attention Network.....	21
1.9.3 Body Perception.....	22
1.9.4 Verticality Perception.....	22
1.9.5 Sensory Conflict.....	23

1.9.6 TPJ Dysfunction.....	24
1.10 Transcranial Direct Current Stimulation (tDCS)	25
1.10.1 tDCS Mechanisms.....	25
1.10.2 tDCS Applications	27
1.11 Rationale	28
1.11.1 Sample Size Estimation	28
1.12 Hypotheses.....	30
2.1 Methods.....	31
2.1.1 Participants.....	31
2.1.2 Screening Criteria	31
2.1.3 Procedure	31
2.2 Apparatus and Stimuli.....	32
2.2.1 Laptop and Structure.....	32
2.2.2 Oculus CV1 Virtual Reality Headset.....	34
2.2.3 neuroConn DC-STIMULATOR PLUS.....	35
2.2.4 tDCS Preparation	36
2.3 Data Analysis.....	37
2.3.1 OCHART	37
2.3.2 OCHART Example Analysis.....	38
2.3.3 Vector Sum Model.....	39
2.4 Fast Motion Sickness Scale (FMS).....	42
3.1 Results.....	43
3.1.1 Pre-VR Cue Weight	43
3.1.2 Hypothesis 1 – Change in Cue Weights.....	43

3.1.3 Perceptual Upright	48
3.1.4 Hypothesis 2 – tDCS Condition Cybersickness Relative to Sham	56
3.1.5 Sensory Reweighting and Cybersickness Modelling	66
4.1 Discussion	68
4.1.1 Hypothesis 1 - No Change in Cue Weights across tDCS Conditions	70
4.1.2 Hypothesis 2 - No Difference in Change in Cybersickness Between tDCS Conditions.....	77
4.1.3 Cybersickness and Sensory Reweighting.....	78
4.2 Limitations and Future Directions	80
4.2.1 PU and OCHART Interpretations	80
4.2.2 VR Exposure Limitations.....	80
4.2.3 Fast Motion Sickness (FMS) Scale vs Simulator Sickness Questionnaire (SSQ)	81
4.2.4 tDCS Limitations	82
4.2.5 Online tDCS vs Offline tDCS	83
4.2.6 Cybersickness and tDCS Aftereffect Assumptions.....	85
4.2.7 Future Measure Suggestions	86
4.2.8 Effect Size and Sample Size Estimation	88
4.3 Conclusion	88
References.....	90

List of Figures

Figure 1	17
Figure 2	19
Figure 3	20
Figure 4	27
Figure 5	32
Figure 6	33
Figure 7	33
Figure 8	34
Figure 9	35
Figure 10	36
Figure 11	36
Figure 12	39
Figure 13	45
Figure 14	46
Figure 15	48
Figure 16	50
Figure 17	53
Figure 18	54
Figure 19	57
Figure 20	59
Figure 21	64
Figure 22	67
Figure 23	68

List of Tables

Table 1	40
Table 2	47
Table 3	47
Table 4	50
Table 5	52
Table 6	54
Table 7	56
Table 8	58
Table 9	58
Table 10	60
Table 11	62
Table 12	65
Table 13	67

List of Abbreviations

ABS: absolute

AG: angular gyrus

CNS: central nervous system

cTBS: continuous theta burst stimulation

EEG: electroencephalography

fMRI: functional magnetic resonance imaging

FMS: Fast Motion Sickness scale

IPL: inferior parietal lobe

LTP: long-term potentiation

MST: medial superior temporal

MT: middle temporal

OBE: out of body experience

OCHART: oriented character recognition task

pSTG: posterior superior temporal gyrus

PSE: point of subjective equality

PU: perceptual upright

RSD: right side down

rTPJ: right temporoparietal junction

SMG: supramarginal gyrus

SMGp: posterior supramarginal gyrus

SSQ: Simulator Sickness Questionnaire

SVV: subjective visual vertical

tDCS: transcranial direct current stimulation

VAC: vergence accommodation conflict

VOR: vestibulo-ocular reflex

VR: virtual reality

V1: primary visual cortex

V2: secondary visual cortex

1.1 Introduction

Every day we perceive multisensory events through various distinct sensory systems. Our central nervous system (CNS) recognizes sensory events which are spatially and temporally congruent and binds them for multisensory perception (Holmes & Spence, 2005; Stein & Stanford, 2008). However, the process of binding sensory information can be imperfect and can lead to integration errors. For example, co-occurring yet incongruent sensory information presents a perceptual challenge. When sensory information is related but conflicting, the integration of this information can drive feelings of unease known as motion sickness (Reason, 1978). Conflicting sensory information is common when exposed to passive motion on planes, boats or in microgravity environments. In spaceflight for example, motion sickness is caused by the absence of gravitational cues detected by the vestibular system and a consequently an inability to align the body axis with the spatial vertical (Cohen et al., 2019; Dyde et al., 2009).

In simulated environments like virtual reality (VR), our sensory perception is challenged further. Though immersive, VR technology suffers from display lags, visual glitches, and unnatural depth portrayal (Allison et al., 2001; Costello, 1997; Davis et al., 2015; Harris et al., 2019; Saredakis et al., 2020; Wurtz & Kandel, 2021; Zhan et al., 2020). More specifically, the sensory systems engaged during VR (i.e. visual, vestibular, and proprioceptive systems) are challenged when it comes to processing co-occurring but incongruent sensory information. For example, a space flight simulator in VR presents the visual system with visual motion while the vestibular and proprioceptive systems are not detecting the same motion. The incongruent sensory information can lead to discomfort in VR; a sensation known as cybersickness. Cybersickness is a form of motion sickness however, it differs from traditional motion sickness as it is driven by visual motion. Highly dynamic visual input in the absence of congruent vestibular input can result in a sense of vection, or illusory sense of self- motion (Chang et al., 2020). Vection can happen outside of VR environments however, VR experiences typically provoke prolonged vection and therefore are more sickness-inducing than vection in natural environments. Similarly to motion sickness, cybersickness is characterised by oculomotor, disorientation, and nausea- type symptoms (Curry, 2019; LaViola, 2000; Weech et al., 2019).

Previous research suggests that those who subconsciously shift their reliance on visual, vestibular, versus bodily cues during VR are less likely to get sick. By contrast, those who are less flexible in their cue prioritization are more likely to experience cybersickness (Chung & Barnett-Cowan, 2023). This insight provides a helpful framework for exploring the neural mechanisms which drive multisensory integration and the consequences of the integration process. The remainder of this introduction will cover the underlying theories, summarize the sensory systems, and explain the study rationale.

1.2 Multisensory Integration in the Brain

Our ability to recognize and bind co-occurring sensory events is known as multisensory integration (Stein & Stanford, 2008). For almost 50 years, there has been a well-established and growing literature surrounding multisensory integration and processing in the CNS (Alais et al., 2010; Peterka, 2018; Spence, 2012; Stein & Stanford, 2008; A. M. Treisman & Gelade, 1980). When multisensory information is presented congruently in space and time, multisensory integration facilitates the efficient and accurate identification of the co-occurring information (Alais & Burr, 2019; Amso & Scerif, 2015; Eördegh et al., 2022; Holmes & Spence, 2005; Murray et al., 2016; Spence, 2012). It is thought that multisensory integration was developed for the benefit of survival to inform our behaviour and interactions with the environment (Stein & Stanford, 2008). It is beyond the scope of this thesis to cover all types of multisensory integration, however the integration of the visual, vestibular and proprioceptive systems for detecting orientation, position and motion will be discussed.

Sensory information from our environment first arrives at specialized sensory receptors. Each sensory system has specialized receptors sensitive to important stimulus qualities for perception within that modality. Within the visual system, rods and cones in the retina support the visual sensation of light and colour (Purves et al., 2001a). Visual information travels from the retina through the optic tract, the lateral geniculate nucleus of the thalamus and arrives at the primary visual cortex (V1) in the occipital lobe of the brain (Martin, 2012; Moraes & Gustavo, 2013). The somatotopic organization of visual information is preserved along the visual pathway so that spatial organization of stimuli within a visual field is represented during processing. Next,

V1 projects to either higher- order visual cortices, the contralateral V1 through the corpus callosum or visuomotor regions in the midbrain. Information about colour and object properties is carried along the ventral stream of visual processing while information about motion, direction and speed is carried along the dorsal stream of visual processing (Harris et al., 2019; Martin, 2012). Along the dorsal stream of visual processing, V1 projections travel from the secondary visual cortex (V2) to middle temporal lobe (MT) and terminate in the posterior parietal lobe (Cook et al., 2025; Harris et al., 2019). At V2, integrated visual information from V1 can be processed based on colour, pattern, orientation and spatial frequency (Huff et al., 2025). Along the ventral stream, projections from V1 travel to V2, visual area V4 and terminate in the inferior temporal lobe (Cook et al., 2025; Harris et al., 2019; Martin, 2012). At V4, shape, orientation, depth and curvature information are processed. Across hemispheres, projections from V1 to the contralateral primary visual cortex helps to unify visual perception from both hemifields while projections from V1 to the superior colliculus and oculomotor nuclei of brainstem control saccadic eye movements when moving eyes to an object of interest (Martin, 2012).

Vestibular receptors within the ampullae of the semicircular canals detect changes in head rotation and receptors within the maculae of the saccule and utricle detect linear acceleration (American Psychological Association, 2018; Collard, 1994; Martin, 2012). Vestibular information from the superior, medial and inferior vestibular nuclei is relayed from the ventral posterior nucleus of the thalamus to the posterior parietal lobe to inform our bodily awareness and orientation. Vestibular information also travels to the somatosensory cortex and integrates with inputs from proprioceptive afferents in the neck to detect head position (Martin, 2012; Ventre-Dominey et al., 2003). Descending projections from the vestibular complex to the spinal cord inform changes in muscle tone when linear or angular acceleration is detected while projections to brainstem extraocular nuclei support the vestibulo-ocular reflex (VOR; Martin, 2012; Swenson, 2017). Communication between the thalamus and the vestibulocerebellum may also inform adjustments to vestibular responses when faced with environmental change (Swenson, 2017). The parieto-insular vestibular cortex helps respond to translations or rotations of the head and body and efferent projections to the vestibular nuclei allow for top-down control over the vestibular brainstem reflexes. The parieto-insular vestibular cortex also projects to the

temporo-parietal junction (TPJ) for self-motion perception and egocentric representation (Frank & Greenlee, 2018).

Mechanoreceptors detect different skin contact sensations such as vibration, pressure, and pain and with proprioceptors (Golgi tendon organs, joint receptors, and muscle spindles) to inform our sense of bodily position. Together, mechanoreceptors and proprioceptors inform our sense of body relative to our environment and help detect changes to our body state during movement, and action (Taylor, 2009; Tuthill & Azim, 2018). Input from somatosensory receptors travels to the ventral posterolateral thalamic nucleus to the primary somatosensory cortex where shape, size and texture features are identified (Raju & Tadi, 2022). Proprioception works closely with our visual and vestibular systems to inform our understanding of limb location, relative to our body, gravity, and environment (Blanke et al., 2005; Blanke & Arzy, 2005; Martin, 2012). Proprioception is especially helpful in maintaining balance and coordination in the absence of visual information (i.e. eyes closed). The secondary somatosensory cortex receives sensory information from the primary somatosensory cortex and then processes, stores, and retains it (Raju & Tadi, 2022). The secondary somatosensory cortex also projects to the hippocampus for the integration of sensory information with previous experiences and decision making (Kropf et al., 2018; Raju & Tadi, 2022). Finally, secondary somatosensory cortex projections synapse at the insular cortex and then project to the lateral, central, and basal nuclei of the amygdala to encode for the emotional significance of sensory stimuli (Kropf et al., 2018).

Sensory information from the specialised sensory cortices and the thalamus may also travel to association cortices for multisensory integration and behaviour generation (Purves et al., 2001b). For example, visual and vestibular information converges at the medial superior temporal (MST) and MT lobes which process location, orientation, and motion for the dorsal stream of visual processing (Cook et al., 2025; Olman, 2022). Output from the association cortices and multisensory brainstem regions may then travel to the basal ganglia, the thalamus, the cerebellum, and other association cortices (Purves et al., 2001b). The basal ganglia support sensorimotor coordination, visual perception and somatosensory discrimination and exercise cross-modal facilitatory and inhibitory interactions for evaluating changes in the environment and

determining how we react to or interact with these changes (Brown et al., 1997; Nagy et al., 2006). The thalamus acts as a sensory relay point for afferent inputs from the sensory systems directly or via the brainstem nuclei. The thalamus may also receive higher-order projections from association cortices to be sent to other association cortices. The thalamus, specifically the thalamic reticular nucleus facilitates sensory gating through bidirectional connections with the cortex and inhibitory projections to the other thalamic nuclei (León-Domínguez et al., 2013).

1.3 Perception for Action

Perception of multisensory information involves the interpretation of integrated sensory information as well as probabilistic estimates. The term “unconscious inference”, coined by Hermann von Helmholtz in 1924, refers to the perceptual inferences made based on prior knowledge of previous sensory events (Alais & Burr, 2019). Under a Bayesian framework of perception, our estimation of a sensory event is dependent on our pre-existing expectations or knowledge (prior) and the incoming noisy sensory signals (likelihood; Alais & Burr, 2019). If information across sensory modalities is congruent, it is integrated however if it is incongruent, the most reliable stream is identified based on prior knowledge and prioritized over the other streams (Körding & Wolpert, 2004). How we perceive sensory events is crucial for informing subsequent actions therefore the sensory and motor systems are closely interrelated.

1.3.1.1 Motor System

The primary motor cortex, located at the precentral gyrus, is the origin of many descending motor pathways. In tandem with the premotor cortex and supplementary motor area, the primary motor cortex coordinates sequences of movements, and plans voluntary actions based on behavioral and environmental context (Knierim, 2020; Yip et al., 2025). Like the primary visual cortex, the primary motor cortex is somatotopically organized and has larger cortical representations for the hand, arm, leg, and torso (Knierim, 2020; Martin, 2012). The primary motor cortex is involved in initiating the motor commands and the amount of movement force required to carry out an action and encodes the speed, direction, and distance of movement. The supplementary motor and premotor areas are located rostrally to the primary motor cortex and are associated with planning and deciding on the most appropriate motor response and

sequencing muscle contractions (Knierim, 2020; Pearson, 2000). The premotor cortex specifically, is involved in preparation of planned movement and behavioral context of movements while the supplementary motor area coordinates bilateral movements, complex sequence movements and stabilization (Knierim, 2020; Yip et al., 2025).

The posterior parietal cortex and the prefrontal cortex are motor association areas which also project to the premotor and primary motor areas. The posterior parietal cortex is involved in informing voluntary motor commands based on sensory input and bridging attention and motor control (Pearson, 2000). The posterior parietal cortex is also involved in representing exocentric space for movement which allows for a reliable representation of space regardless of individual orientation or position (Knierim, 2020). The prefrontal cortex is also involved in motor control and contributes to motor decision-making by evaluating the consequences of actions based on context and imagining the execution of a movement (Henley, 2021; Knierim, 2020). Connections from the secondary somatosensory cortex to the primary somatosensory cortex to the motor cortex are associated with the perception of motion and object manipulation (Kropf et al., 2018). Further, multisensory areas like the right temporoparietal junction (rTPJ) are involved in integrating visual and motor information for adaptation and recalibration of eye-hand coordination (Clower et al., 2001; Fogassi & Luppino, 2005).

1.3.1.2 Cerebellum

Our interactions with the environment are constantly being adapted based on discrepancies between incoming sensory information and expected outcomes from the motor commands (Popa & Ebner, 2019). The cerebellum is involved in regulating motor pathways, maintaining equilibrium, controlling muscle tone, posture, and coordinating voluntary movements. The cerebellum receives input from the vestibular system, the spinal cord and the posterior parietal lobe, and the limbic association cortex. Vestibular, spinal, and cortical inputs converge so that motor commands and sensory input can be compared to determine if intended movement outcomes were achieved (Martin, 2012; Popa & Ebner, 2019). The spinocerebellum receives direct input from the spinal cord and assists in controlling posture and movement of trunk and limbs as well as coordinating eye movements with vestibular input. The cerebrocerebellum is

involved in planning of movement and the regulation of skilled movements and complex sequences of movement and the vestibulocerebellum is involved in coordinating head and eye movements and maintaining balance (Martin, 2012; Purves et al., 2001b). Cerebellar output is sent to the ventrolateral thalamus where it is then relayed to the motor cortex for correcting errors and informing motor output and to the frontal and parietal lobes for adapting motor performance (Clower et al., 2001).

1.4 Motion Sickness

Motion sickness can occur whenever there is real or perceived motion as detected by the visual, somatosensory, and vestibular systems. Specifically, unexpected motion or perturbations trigger a neural mismatch signal which can cause an emetic response. It is theorized that the nausea and discomfort symptoms of motion sickness were evolved to encourage the purge of potential neurotoxins. Both motion sickness and the ingestion of neurotoxins are associated with disturbances in sensory perception and coordination and therefore share similar autonomic symptoms (Treisman, 1977). Further, motion sickness is closely tied to motion detection through the vestibular system (Cohen et al., 2019; Takeda et al., 2001). Motion sickness does not occur in humans with defective vestibular systems or animals who have had their vestibular system removed underscoring the contributions of the vestibular system in motion sickness manifestation (Takeda et al., 2001; Uno et al., 2000).

1.4.1 Motor Control and Motion Sickness

When a motor command is sent from the motor cortex, an efference copy is also sent to the somatosensory cortex and cerebellum to predict the anticipated sensory outcomes of that motor command. This efference copy helps prepare the sensory systems for the sensory stimulation that occurs as result of a motor command. The sensory systems determine the sensed body state (integration of visual, vestibular, and proprioceptive input) which is then compared to the expected body state (based on efference memory and efference copy memory) generated by the internal model of the body (Takeda et al., 2001). External perturbations such as motion on a plane or car can result in an actual body state that does not match that of the internal model of the body. In other words, conflict between the sensed body state and expected state is considered

conflict which can result in motion sickness (Bos et al., 2010). The internal model accounts for sensory conflict signals and generates an error signal to trigger sensory-motor adaptation for motor control (Bos et al., 2010; Oman, 1982; Takeda et al., 2001). The cerebellum specifically is involved in predicting and adjusting to any errors in self-motion and contributes to motion sickness mitigation by supporting adaptations in motor performance (Denise & Darlot, 1993).

1.4.2 Visual Perception in VR

When perceiving objects in the real world, where we focus our eyes (accommodation cues) and how we rotate our eyes (vergence cues) are congruent based on the distance of the object (Zhan et al., 2020). Integration of binocular vision then occurs at V1 where slightly different images from each eye can be compared for stereopsis (Wurtz & Kandel, 2021). The difference between binocular vision images in combination with our vergence and accommodation cues allow us to perceive depth. In VR, virtual visual scenes and optic flow are simulated using near-eye binocular displays however, VR is challenged by the vergence accommodation conflict (VAC). In VR, objects (regardless of their distance), are projected via a near-eye display plane and while object distance can be simulated on the VR display plane, the accommodation distance is always proportional to the distance from the display plane to the eyes. Therefore, the vergence cues which suggest the object is distant, and the accommodation cues, which suggest the object is positioned at the display plane, are in conflict. Discomfort from VAC can manifest as dizziness and nausea. Issues from VAC are being addressed as VR display configurations continue to advance. More modern displays may use multiple image planes to display an image on the display plane in a way that aligns vergence and accommodation cues. Multifocal displays for example, layer multiple image planes behind the display plane to match the appropriate vergence and accommodation distances based on simulated object distance (Yin et al., 2021). These displays, however, are not widely available for consumer use and are limited by their weight and their need for advanced computational resources (Harris et al., 2019; Yin et al., 2021).

High intensity VR experiences can also induce the sense ofvection – the illusory sense of self motion when stationary. Vection occurs when visual motion is perceived in the absence of vestibular motion and the visual input is prioritized over the vestibular input (Hughes et al.,

2024). When in VR, users are especially susceptible tovection due to highly immersive visual experiences rich in optic flow. Interestingly, estimations of optic flow in VR have been shown to vary between individuals. In a treadmill VR experiment, most participants rated optic flow as being slower than their physical running speed when the speeds were equally matched. This suggests matching optic flow in VR to physical speed in real life does not account for individual visual feedback expectations and may explain why matching visual motion with physical motion does not always eliminate cybersickness in VR (Caramenti et al., 2018). Similarly, VR users tend to underestimate distances by about 10% when walking. However, when a first-person avatar is present and embodied, distance estimation errors decrease (Gonzalez-Franco et al., 2019). These results emphasize how visual motion in VR and individual perceptual differences interact and give rise to altered motion perception in VR.

The VOR also plays a key role in vision perception in VR. The VOR allows us to keep an image focused on our retina despite head rotations. When head rotation is detected by the semicircular canals of the vestibular system, a compensatory eye movement is initiated through excitatory and inhibitory connections with the medial and lateral rectus extraocular muscles. Latency for VOR is about 20ms, however in VR the VOR is challenged by the latency delays of up to 50ms for head movement tracking putting users at risk of visual slip (Warburton et al., 2023). Tracking delays present challenges when attempting to stabilize vision during head motion resulting in visual-vestibular conflict in VR. One study, which investigated postural control following a dynamic VR rollercoaster experience concluded that the opto-kinetic reflex, which helps stabilize gaze when perceiving visual motion, is upweighted to reduce retinal slippage and compensate for the unreliable VOR. Post-VR, improved postural control in conditions which rely on visual and vestibular input suggested an adaptive upweighting of the opto-kinetic reflex and down weighting of the VOR (Warchoł et al., 2024). This decrease in VOR gain has been measured post-VR for up to 30-minutes providing further evidence for adaptive changes in vestibular weighting when exposed to incongruent visual and vestibular motion during head turns in VR (Di Girolamo et al., 2001).

1.5 Cybersickness in VR

As VR technology has evolved, innovations in visual display resolution, movement latency and VAC have drastically improved user experience. Despite these innovations, cybersickness manifests in many users suggesting incongruent and unpredictable sensory information may underly cybersickness. A notable distinction between cybersickness and motion sickness is that motion sickness is caused by visuo-vestibular conflict in the presence of physical motion, while cybersickness is primarily visually induced and can occur in the absence of physical motion (LaViola, 2000). For this reason, individuals experiencing visual motion in VR can suffer from cybersickness symptoms even when stationary. Interestingly, non-invasive stimulation of the rTPJ, an area involved in processing visuo-vestibular information has been found to reduce cybersickness in VR users (Takeuchi et al., 2018).

When considering the VR devices themselves, ergonomics and display capacity limitations reduce the realism of portrayal and therefore subject users to distorted sensory experiences (Saredakis et al., 2020; Stanney et al., 2020). For example, most headsets offer an adjustment feature to accommodate various interpupillary distances, however not all physiological variability is accounted for. The interpupillary adjustment range in the Oculus Rift S for example, does not encapsulate roughly 16% of female users therefore making them more susceptible to cybersickness due to increased VAC (Stanney et al., 2020). These visual challenges are common in many commercially available headsets and can increase the susceptibility of vulnerable users (i.e. women) to cybersickness symptoms such as eyestrain and headaches.

Interestingly, sickness severity varies significantly among VR users. A meta-analysis examining VR sickness found an average participant dropout rate of 15.6% across 46 VR studies (Saredakis et al., 2020). A separate study which used a VR rollercoaster had approximately 67% of participants stop the VR experience before the 14-minute exposure was complete. Despite all being exposed to the same environment, some participants experienced more intense cybersickness than others (Nesbitt et al., 2017). Cybersickness researchers have proposed many theories to make sense of this variability. However, most theories suggest differences in sensory processing underly cybersickness susceptibility (Takeda et al., 2001). One study which

investigated the relationship between sensory processing and sickness used VR to present visual cues and stereoscopic movies and assessed motion sensitivity. The study findings suggest a greater sensitivity to motion parallax cues is predictive of more severe cybersickness (Fulvio et al., 2021). Under this theory, those who are more sensitive to sensory cues are more likely to detect misaligned sensory events in VR and are more likely to experience cybersickness symptoms as a result (Weech et al., 2019).

Differences in cybersickness recovery have also been observed in VR study participants. A study investigating sickness recovery used a VR video in which participants flew through a landscape scene and made various twists and turns across all axes. Following the 10-minute video, researchers used electroencephalography (EEG) to monitor participants' sickness recovery. Researchers were interested in examining EEG changes in delta power as previous research has found an association between VR sickness and delta power in the frontal, central, parietal, occipital and temporal lobes (Kim et al., 2005). Following VR, sensitive individuals required 11.3 ± 6.6 min to recover from sickness while non-sensitive individuals only took 9.1 ± 5.2 min to recover. Delta power increased during participant recovery though no significant differences in delta power were found between sensitive and non-sensitive individuals (Woo et al., 2023). Cybersickness susceptibility has not yet been identified through cybersickness recovery brain activity however, other cybersickness research has found links to postural control and sensory processing as possible cybersickness susceptibility indicators.

1.6 Postural Instability Theory

The postural instability theory of motion sickness proposes that motion sickness occurs in situations where animals have not yet developed effective strategies for the maintenance of postural stability (Ricchio & Stoffregen, 1991). Under this theory, the intensity of motion sickness is determined by the amount of postural instability experienced in each environment (Warwick-Evans et al., 1998). Evidence for this theory comes from an experiment that exposed participants to large-field optic flow resembling that of unperturbed postural sway (between 0.1 and 0.4 Hz). Postural sway was found to precede motion sickness and significant differences in

postural sway were identified when comparing those who experienced motion sickness and those who did not (Riccio & Stoffregen, 1991).

Researchers interpreted these findings as evidence for postural instability theory because motion sickness manifested in the absence of highly conflicting sensory input. Evidence disproving postural instability theory was found shortly following the theory proposal. Researchers exposed participants to a motion video while they were either free standing, lying down or lying down restrained. Various positions and levels of restraint were used to test the notion that limiting physical mobility and therefore postural instability, would reduce motion sickness. A point-of view video walking around campus was either presented at normal speed or played at 2x speed to increase intensity of sensory conflict. Researchers found that limiting physical mobility in the lying down unrestrained and lying down restrained conditions did not reduce motion sickness (Warwick-Evans et al., 1998). A more recent study found additional evidence for an association between reduced postural stability in those who experienced cybersickness but not consistently across all participants (Litleskare, 2021). Further, cybersickness may manifest before postural instability is observed (Akiduki et al., 2003). These findings suggest that postural stability does not always protect against cybersickness. Therefore, postural instability is not a requirement for motion sickness manifestation however it is still associated with motion sickness as those who experience more postural instability are more susceptible to cybersickness in VR (Akiduki et al., 2003; Arcioni et al., 2019; Litleskare, 2021; Warwick-Evans et al., 1998).

1.7 Sensory Conflict Theory

Due to evidence against postural instability theory, sensory conflict theory remains the dominant theory in motion sickness research. Formerly referred to as the sensory rearrangement theory, sensory conflict theory posits that conflicting sensory cues and therefore cues that misalign with previous sensory experiences, cause motion sickness (Reason & Brand, 1975). Specifically, sensory conflict theory concerns the incongruence between sensory systems responsible for detecting motion and orientation —the visual, vestibular, and proprioceptive systems (Chung & Barnett-Cowan, 2023; Reason, 1978). Sensory incongruence can present as one of the following:

simultaneous signaling that is unrelated or contradictory, or one system signalling in the absence of an expected signal from the other system. One example of sensory conflict in the natural environment is reading a book in a car (Reason, 1978). The visual system is processing stationary information from the book whereas the vestibular system is detecting linear motion from the car moving. This is an example of simultaneous signalling that is unrelated or contradictory and typically results in motion sickness. Similarly, astronauts can experience a form of motion sickness after prolonged exposure to zero-gravity conditions (Davis et al., 2015). The transition into orbit can cause perceptual confusion for the vestibular, proprioceptive, and visual systems of astronauts leading to atypical experiences of motion and orientation (Souvestre et al., 2008).

A subsidiary hypothesis of sensory conflict theory proposes that symptoms are proportional to the magnitude of conflict. However, there is conflicting evidence for this subsidiary hypothesis. Evidence for moderately conflicting visual motion via a walking video presented at a normal pace produced more motion sickness than high- conflict visual motion via a walking video at 2x speed (Warwick-Evans et al., 1998). A recent study however found that higher speed passive driving VR experiences resulted in greatervection as well as greater cybersickness compared to lower speed passive driving scenarios (Hughes et al., 2024). It is possible that the magnitude of conflict is proportional to symptoms when high- motion is presented via immersive VR while non-immersive high-motion videos do not have the same predictable effect.

In natural environments, sensory conflict and the resulting motion sickness typically only occurs in moving vehicles or in micro-gravity environments. In artificial environments however, sensory conflict is much more common and can occur in all types of environments due to a lack of congruent sensory cues. In VR, co-occurring sensory events may lack the temporal synchrony or coherence that would otherwise occur in the natural world. Display lags and visual motion in the absence of vestibular motion can present challenges to typical sensory processing. When manipulating objects in VR or interacting with different spaces, user experience is also limited by the lack of haptic feedback. Visually, users may see they are holding an object that possesses different physical properties than the provided VR controllers. This incongruence between the

proprioceptive and visual systems can result in cybersickness. Additionally, the restrictions of play space and the range of the VR headset does not allow participants to interact with the virtual space organically. As a result, visual interaction and motion within the virtual space may not align with vestibular and proprioceptive cues (Gallagher & Ferrè, 2018). Further, physical motion can cause passive movement of the internal organs. In VR however, simulated visual motion can result in erroneous re-ference predictions and trigger cybersickness (Denise & Darlot, 1993; Oman, 1982).

Past studies have coupled VR visual motion with incongruent motion to facilitate sensory conflict and have found that a mismatch in visual and vestibular motion increases cybersickness ratings among participants (Chung & Barnett-Cowan, 2023; Ng et al., 2018; Nishiike et al., 2013). Further, incongruent participant-initiated motion and VR visual motion has been found to increase the risk of cybersickness. If VR visual motion latency or axis of rotation does not match a user's head turn, this can increase cybersickness severity (Palmisano et al., 2023). The principles behind sensory conflict theory also hold up in congruent sensory conditions. When congruent visual and vestibular motion are paired, cybersickness ratings are found to decrease among participants (Ng et al., 2018). Though widely accepted, sensory conflict theory fails to account for why sickness severity varies across individuals who are exposed to the same degree of conflicting sensory information in VR.

1.8 Sensory Reweighting

Individual differences in sickness severity may be modulated by a mechanism called sensory reweighting. Sensory reweighting refers to our ability to adjust the contributions of different sensory modalities based on sensory availability and suitability to the task. For example, a previous study which paired VR with noisy vestibular stimulation found that unreliable vestibular signals were down weighted and visual signals were upweighted. This reweighting reduces sensory incongruence and can therefore protect against cybersickness manifestation (Chung & Barnett-Cowan, 2023; Gallagher & Ferrè, 2018; Weech et al., 2020).

When sensory signals become unreliable, our perceptual systems recalibrate and optimise the remaining sensory inputs for informing our interactions with the environment (Assländer &

Peterka, 2014). Individuals who are adept at sensory reweighting may be able to better accommodate VR's sensory incongruities, consequently reducing cybersickness (Chung & Barnett-Cowan, 2023; Stanney et al., 2020). Existing research supports sensory reweighting's role in diminishing VR-induced cybersickness, but the processes underlying this neural mechanism remain unexplored.

1.8.1 Measuring Sensory Reweighting

1.8.1.1 Postural Control

Postural control requires coordination of inputs from our visual, vestibular, and somatosensory systems. To investigate contributions of these interacting sensory systems, centre of pressure and sway measurements can be taken before, during and after VR in various conditions to determine the contributions of each system at a given time. One study investigated the effects of VR on postural control in congruent and incongruent conditions. In the congruent condition, participants walked and experienced congruent optic flow via the VR headset. In the incongruent scenario, the participants stood still and experienced the same optic flow as the congruent condition. Following the incongruent condition, participants reported more motion sickness and dizziness and displayed more postural sway with eyes open and closed. Notably, the ratio of sway with eyes closed to eyes open decreased following incongruent VR suggesting a decreased reliance on vision for postural control following VR (Nishiike et al., 2013). The sensory systems supporting postural control work to reduce postural sway therefore changes in our centre of mass across different sensory conditions can provide insight into the contributions of each sensory system at a given time.

1.8.1.2 Subjective Visual Vertical

Determining the direction of up is important for accurate and efficient recognition of letters, objects, and people. The direction of up is highly subjective and depends on visual, vestibular, and somatosensory cues. Measuring the subjective upright may help us better understand the contributions of each sensory system in informing our orientation perception. The 'subjective visual vertical' (SVV) task was developed to measure the perception of up by having participants set a line to the gravitational vertical (Aubert, 1861; Dyde et al., 2006). Using the gravitational

cues, visual cues and body axis information from the orientation of the head and trunk, weighted vectors can be calculated to determine the magnitude of contribution by each set of sensory cues (i.e. gravity, vision, body; Dyde et al., 2006; Mittelstaedt, 1983).

One study had participants complete the SVV in upright and right side down (RSD) body orientations and had them orient the line over various visual backgrounds rich in upright visual cues or over an unpolarized grey background. Using a weighted vector model to quantify the contributions of body and gravitational cues in the SVV responses, it was revealed that the gravitational cues were prioritized when making judgements on the true vertical. The model revealed that the vectors of vision, body and gravity could be represented respectively as a ratio of 0.1:0.2:1.0. These findings suggest a considerable influence of gravitational cues on the SVV relative to bodily and visual cues (Dyde et al., 2006).

The estimate of the SVV, however is strongly influenced by body tilt. Previous research has shown that the SVV tends to shift toward the longitudinal body axis; this effect is referred to as the idiotropic factor (Mittelstaedt, 1983). There are two recognized effects which emphasize the impact of the idiotropic factor on the SVV: the Aubert effect (A-effect) and the Entgegengesetzt Effect (E-Effect; Aubert, 1861; De Vrijer et al., 2009). The E-effect refers to the shift in SVV in the opposite direction of the head tilt when the tilt angle is less than 60° due to ocular counter torsion or otolith errors. Conversely the A-effect occurs when the head is tilted beyond 60°. At a tilt of 60° or greater, the SVV is biased toward the direction of the head tilt suggesting an underestimation of perceived body tilt. These effects are typical in healthy populations and emphasizes our ability to account for smaller body tilts which we encounter more frequently (Winnick et al., 2022). Contributions from our CNS and interactions between our sensory systems ensure that there are not large E-effects at small head or body tilts.

1.8.1.3 Oriented Character Recognition Task (OCHART)

The OCHART is used to evaluate an individual's subjective perception of upright. Interpretation of the visual world is highly dependent the perception of upright as it aids in the efficient recognition of faces and objects (Dyde et al., 2006; H. Jenkin et al., 2007). The OCHART was developed to assess the perceptual upright (PU) which is the orientation at which objects are

most easily perceived. When completing the OCHART, participants are presented with a ‘p’ symbol ($3.1^\circ \times 1.9^\circ$ of visual arc) at the same position as the fixation point. The letter probe ‘p’ is presented over grey background or a visual background at one of 24 orientations from 0° - 345° in 15° increments. The visual background depicts a scene of a woman sitting at a table with a ladder in the background (Figure 1). This scene is rich in polarized cues which are in alignment with gravity and indicate direction (i.e. shelf and plant vines, woman looking left) The visual background is presented at one of 24 orientations in 0° increments from 345° . Including the grey background, there are a total of 7 background options for the letter probe to be presented over. Each of the total 24 letter probe orientations is paired with each of the 7 background options and each combination is presented to the participant 8 times for a total of 1344 ($24 \times 7 \times 8$) trials. The participant’s body orientation is also manipulated to determine the influence of body cues on perceptual upright (PU) when completing the OCHART.

The PU values are calculated based on response averages across the 7 presentations of a certain letter orientation over a certain visual background orientation (see Data Analysis). When the letter is presented in an orientation where the participant is equally likely to judge it as a ‘p’ or a ‘d’ (response average 50%) this is considered a point of subjective equality (PSE). The PSE for the transition from ‘p’ to ‘d’ and ‘d’ to ‘p’ are averaged and 180° is subtracted from the average to determine the PU for that visual background.



Figure 1. Oriented Character Recognition Task (OCHART) Probe and visual background at 0° . The OCHART probe may be presented over either the grey background or one of the visual backgrounds at one of the six $+60^\circ$ orientations about 360° .

1.8.1.4 The Vector Sum Model

The PU values can then be used in the vector sum model. The vector sum model uses the PU values for each combination of body orientation and visual background to determine the relative contributions of body cues, vision cues and gravity cues on the PUs. A change in the PU from upright to RSD against one visual background is attributed to changes in body cues. A change in PU across visual backgrounds when the body orientation remains constant is attributed to changes in visual cues. The vector sum model assigns vectors to vision cues and body cues based on the change in PU evoked by each manipulation (Figure 2). Gravity cues also contribute to a participant's PU however gravity is not manipulated in the OCHART task; therefore, the gravity vector is assigned a constant value of 1. In the vector sum model, more reliable (lower variance) cues are weighted higher than cues with lower reliability (Dyde et al., 2006). This weighting model is derived from the Bayesian model of sensory processing (Alais & Burr, 2019). Sensory vector lengths are representative of the magnitude of contribution of a cue in determining the PU across each visual condition (visual background) and body orientation. The vector sum model uses an optimization algorithm (Marquardt-Levenberg technique) to optimize the length of the vision and body vectors so that the direction of the observed PU can be predicted from the predicted PU vector (otherwise known as the vector sum).

Previous research using the OCHART had 11 participants complete the task in three body positions: upright, right side down (RSD) and supine. The study results revealed a greater influence of body cues on the PU relative to vision and gravity cues. Additionally, results showed that PU judgements in the RSD orientation causes a disproportional pull towards the direction of gravity (away from the body axis). On average, the three vectors determined the ratio of 1.2:2.6:1 for vision, body, and gravity, respectively. While the specific ratio can differ from person to person, this research suggests that overall, individuals rely the most on body and visual cues when completing the OCHART (Dyde et al., 2006; Fraser et al., 2018).

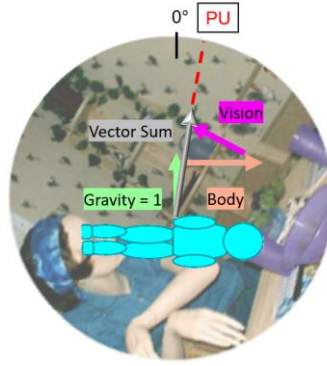


Figure 2. Example sensory vector contributions as estimated by the vector sum model for a right side down (RSD) trial on a 300° visual background. The vector sum (grey arrow) is in alignment with the perceptual upright (PU) vector (red dashed line). Sensory vector lengths are optimized to predict the PU.

The PU and cue weight estimations can also be influenced by motion cues and environmental conditions. When the OCHART is superimposed over a motion scene (i.e. people walking) rather than a static scene there is a stronger effect of visual cues on the PU (Jenkin et al., 2011). Further, astronauts who had returned from a ~168 day space flight relied less on gravity cues when completing the OCHART possibly due to prolonged exposure to unreliable gravity cues while in space (Dyde et al., 2009). Cue reliance may also differ within clinical populations. Some stroke and Parkinson’s patients display a lower reliance on body cues than healthy individuals, suggesting a shift in reliance on to visual cues for balance control in these populations (Fraser et al., 2018).

1.9 The Temporoparietal Junction

The TPJ, also known as the temporo-parietal region (Figure 3), refers to the region dorsal to the lateral sulcus where the inferior parietal lobe (IPL), the posterior superior temporal sulcus and the lateral occipital cortex meet (Decety & Lamm, 2007; Donaldson et al., 2015; Eddy, 2016; Mars et al., 2012). The TPJ includes portions of the angular gyrus (AG), the IPL, the superamarginal gyrus (SMG), and the posterior superior temporal gyrus (pSTG; Donaldson et al., 2015). Bilaterally, the rTPJ and left TPJ are involved in attention, multisensory integration and self-other processing however, the right and the left TPJ have distinct lateralized functions as well (Donaldson et al., 2015). The rTPJ is associated with spatial localization, body perception, orientation perception and conflict detection (Blanke & Arzy, 2005; Kheradmand & Winnick,

2017; Papeo et al., 2010). Alternatively, the left TPJ is involved in speech, left-lateralized language pathways, and in right-handed individuals, overlaps the superior portion of Wernicke's area (Javed et al., 2023; Kucyi et al., 2012).

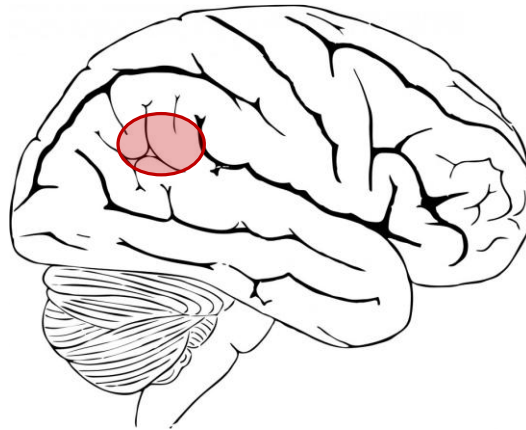


Figure 3. Right temporoparietal junction (rTPJ) shown in red. *Adapted from Human Brain Images, by D. Hudson, 2007, PublicDomainPictures.net (<https://www.publicdomainpictures.net/>). Public domain image retrieved May 18, 2025.*

A study using diffusion-weighted imaging tractography and functional magnetic resonance imaging (fMRI) to examine resting-state structural and functional connectivity revealed three distinct rTPJ subregions based on functional connectivity: the dorsal IPL, the anterior TPJ, and the posterior TPJ. The IPL was connected to the anterior prefrontal cortex, the intraparietal sulcus, and the caudate nucleus to support attention and cognition. The anterior TPJ was found to be involved in the ventral attention network through its connections with the ventral prefrontal cortex, anterior insula, and middle frontal gyrus. The posterior TPJ was involved in social cognition and had strong connections with the anterior medial prefrontal cortex, the temporal poles, the posterior cingulate cortex and the precuneus of the medial parietal cortex (Mars et al., 2011).

1.9.1 Multisensory Convergence and Integration

Evidence for the role of the TPJ in multisensory integration and processing has been found in invasive and non-invasive studies. In an invasive study, researchers examined the electrophysiological responses evoked by various stimuli in a cohort of epilepsy patients with

subdural electrodes in the right and left TPJ. Neuronal responses were recorded when presented with somatosensory stimuli, auditory stimuli, and visual motion stimuli providing evidence for bilateral multisensory convergence on the TPJ (Matsushashi et al., 2004).

Further, the rTPJ projects to the vestibular complex, particularly the medial vestibular nuclei to support balance and posture and is involved in the processing of both visual and vestibular information (Decety & Lamm, 2007; Takeuchi et al., 2018; Ventre-Dominey, 2014; Ventre-Dominey et al., 2003). Research using animal models has identified connections between the TPJ, the medial and superior vestibular nuclei for vestibular-ocular mechanisms and to the inferior vestibular nucleus for the cerebello-spinal system (Ventre & Faugier-Grimaud, 1988). In humans, the rTPJ also exercises top-down control to regulate the VOR and stabilize the eyes once the head has stopped moving (Ventre-Dominey, 2014).

1.9.2 Ventral Attention Network

The rTPJ is also involved in attentional processes and has been identified as a critical region for directing attention to relevant stimuli (Corbetta & Shulman, 2002; Donaldson et al., 2015). The ventral attention network refers to a network of connectivity between the anterior rTPJ, the anterior insula, the intraparietal sulcus, the ventral frontal cortex and the frontal eye fields for bottom-up attentional control (Donaldson et al., 2015; Kucyi et al., 2012; Vossel et al., 2014). Evidence from fMRI studies shows that these regions are activated when registering salient visual, auditory, and somatosensory stimuli (Kucyi et al., 2012). More specifically, the rTPJ plays a role in the reorientation or attention to unattended stimuli which are behaviorally relevant or task-related (Kucyi et al., 2012; Masina et al., 2022). When novel and behaviorally relevant stimuli are detected, connections between the rTPJ and the intraparietal sulcus can interrupt top-down attention so that the novel stimuli is attended to (Corbetta and Shulman, 2002). The rTPJ also has asymmetrical connections to the insula which support the rTPJ's role in awareness and detection of salient stimuli (Kucyi et al., 2012). Interestingly, one set of fMRI results found bilateral activation of the TPJ and the salience network occurred in tandem with activity in the noradrenergic system suggesting a link between the ventral attention network and sympathetic responses (Kucyi et al., 2012). While both the rTPJ and left TPJ are involved in processing

salient sensory information, the left TPJ has been linked to the integration of sensory information with contextual knowledge whereas the rTPJ is associated with salience detection (Corbetta & Shulman, 2002; Kucyi et al., 2012; Papeo et al., 2010).

1.9.3 Body Perception

The SMG and the AG of the rTPJ are specifically involved in multisensory integration for body schema (Donaldson et al., 2015). Inputs from the posterior insula, the parieto-insular vestibular cortex, areas of MT and MST, and the somatosensory cortex all converge on the SMG and the AG to inform bodily awareness and perception. Projections are then sent to the intraparietal sulcus, the premotor cortex and cerebellum to inform behaviour (Donaldson et al., 2015; Ramnani, 2012).

There is also evidence to suggest that the TPJ is involved in multisensory integration for self-body processing. Out of body experiences (OBEs) have been reported in patients with lesioned rTPJ and can also be induced by delivering direct cortical electrical stimulation via subdural electrodes to the rTPJ. Many patients with OBEs report vestibular symptoms (i.e., floating, inversion) emphasizing the interactions between the rTPJ and vestibular perception for embodiment (Blanke & Arzy, 2005; Godefroy, 2013). The rTPJ's involvement in OBE generation was further investigated by having healthy individuals imagine themselves as a presented avatar and determine if the marked avatar hand was the right or the left. Performance on the embodiment task was significantly impaired by single-pulse TMS over the rTPJ suggesting that the rTPJ contributes to OBE generation and own-body mental imagery. Interestingly, participant performance on a letter rotation task was not impaired by TMS to the rTPJ. These findings provide evidence for the contributions of the rTPJ to self- processing and not simply spatial processing or mental rotation (Blanke & Arzy, 2005).

1.9.4 Verticality Perception

Multisensory integration at the rTPJ is also important for body perception. Specifically, there is evidence for the role of the posterior SMG (SMGp), within the TPJ, in multisensory processing for upright perception. One study investigated the effect of continuous theta burst stimulation (cTBS) over the right SMGp on the perception of upright using the SVV task.

Participants completed the SVV upright and with their heads tilted 20° to the right or 20° to the left. Applying cTBS over the SMGp tilted the SVV in the opposite direction of participant head tilt. Interestingly, applying cTBS to the AG and the STG did not cause significant differences in tilt and no-tilt SVV responses. These results were interpreted as evidence for the SMGp in body-related perception and integration across proprioceptive, visual, and vestibular input. More specifically, these results suggest that cTBS to the SMGp impairs the integration of cues from head tilt, ocular torsion and retinal cues resulting in misjudgments of upright (Kheradmand et al., 2015).

Another study investigated the role of the rTPJ in the perception of verticality using a Rod- and-Frame test in which participants had to align a rod with the gravitational vertical. Researchers used cTBS over the rTPJ and found that participant performance on the Rod- and-Frame test was impaired but not performance on a Gabor Patch orientation task. These results were evidence for the rTPJ's role in the integration of visual, vestibular, and proprioceptive information to specifically inform our perception of verticality (Fiori et al., 2015).

1.9.5 Sensory Conflict

The rTPJ is also associated with the detection and resolution of sensory conflict. One group of researchers used a mirrored hand-illusion paradigm to see how congruent and incongruent visuo-tactile conditions are perceived when the rTPJ activity is disrupted. The middle or ring fingers of the hidden hand and the mirrored hand were touched synchronously either congruently or incongruently. When single-pulse TMS was applied to the rTPJ, incongruent trial performance improved in speed and accuracy providing evidence for the rTPJ's involvement in intersensory conflict detection (Papeo et al., 2010). In other words, the rTPJ detects the visual-tactile conflict and when interference was introduced through TMS, that conflict is detected less leading to more veridical perception.

Another study investigated the rTPJ's involvement in visual and proprioceptive conflict detection. In this study, participants hands were passively moved using a mouse-like device as they were presented either congruent or incongruent visual cursor motion. Results from the fMRI revealed greater activity in the rTPJ during incongruent trials providing evidence for the rTPJ in

orienting attention to conflicting or unexpected sensory events. Further, this study provides evidence for rTPJ involvement in conflict detection of passive motion which involved no motor-planning (Balslev et al., 2005).

Other studies have suggested that the rTPJ plays a role in conflict resolution rather than conflict detection. One study which used anodal tDCS over the rTPJ before a VR rollercoaster found that postural instability and cybersickness decreased post-VR relative to the sham condition. This finding was interpreted as evidence for the rTPJ's role in conflict resolution between visual and vestibular inputs during VR (Takeuchi et al., 2018). Though the role of the rTPJ in sensory conflict detection or resolution is unclear, its involvement in sensory conflict perception is well supported.

1.9.6 TPJ Dysfunction

Lesions to the rTPJ and its specific sub-regions are associated with atypical perceptual experiences. One potential outcome of rTPJ dysfunction is OBEs where an individual's visual and bodily experience has departed from their veridical body positioning (Blanke & Arzy, 2005). Hemiasomatognosia, a loss of awareness of body parts or illusory sensations that limbs are absent or alien can also occur as result of stroke or seizure at the rTPJ (Godefroy, 2013). Further, damage to ventral attention network or the connections between the right parietal lobe and the rTPJ can impair one's ability to respond or orient to salient objects and events contralesionally and result in visuospatial neglect (Corbetta & Shulman, 2002; Donaldson et al., 2015; Friedrich et al., 1998; Halligan et al., 2003; Kucyi et al., 2012; Masina et al., 2022; Matsushashi et al., 2004; Ventre-Dominey, 2014). This pathology emphasizes the role of the rTPJ in contralateral visual attention. Similarly, TMS -induced lesions to the rTPJ disrupt stimulus-driven attention providing additional evidence for the involvement of the rTPJ in orienting attention to salient sensory events (Corbetta & Shulman, 2002; Kucyi et al., 2012). The rTPJ is also involved in oculomotor reflexes and it has been found that patients with unilateral temporoparietal lesions can experience vestibulo-ocular deficits causing decreased VOR gain (Ventre-Dominey et al., 2003).

1.10 Transcranial Direct Current Stimulation (tDCS)

1.10.1 tDCS Mechanisms

The present study uses transcranial direct current stimulation (tDCS) to stimulate the rTPJ. As a non-invasive neurostimulation technique, tDCS can either increase or decrease the likelihood of neural firing (Bikson et al., 2016). Anodal and cathodal tDCS use a weak electrical current to induce sub-threshold changes in membrane polarization (Chew et al., 2015). Setup for tDCS requires two electrodes to be placed on the head, a reference electrode, and a target electrode. Weak electrical currents will travel through these electrodes and penetrate the skull to either increase or decrease cortical excitability depending on stimulation polarity (Lefaucheur & Wendling, 2019; Thair et al., 2017; Yamada & Sumiyoshi, 2021). Factors like skull density and grey or white matter volume can all impact tDCS current density (Bikson et al., 2016; Polanía et al., 2018). The electrical currents produced by tDCS can pass more easily through thinner skulls and grey matter making anatomical variability a key consideration in tDCS efficiency (Bikson et al., 2016; Ciecchanski et al., 2018). Once the electrical current passes through the skin and the skull, it diffuses and therefore the current that reaches the brain is less intense than the current that is delivered through the stimulator (Bikson et al., 2016).

Depending on the desired stimulation, the placement of electrodes and current path will differ. For anodal tDCS, the anodal electrode is placed over the region of interest increasing the chance that the neurons below that electrode become depolarized. For cathodal tDCS, the cathodal electrode is placed over the region of interest for stimulation therefore decreasing the chances that the neurons below the electrode become depolarized (Pelletier & Cicchetti, 2015). The current produced by tDCS is not enough to evoke action potentials however, the presence of the tDCS current causes membrane polarization changes (Lefaucheur & Wendling, 2019; Yamada & Sumiyoshi, 2021). Effects of tDCS however, can vary based on individual brain state, anatomical differences and current density (Bikson et al., 2016).

Research on the neural mechanisms of tDCS is limited but continues to emerge as its applications grow (Giordano et al., 2017; Lefaucheur & Wendling, 2019). The neuromodulatory effects of tDCS are associated with long-term potentiation (LTP) however the exact mechanisms

are not well understood. There is evidence to suggest that anodal direct current stimulation alters postsynaptic membrane potential as result of sustained synaptic activity therefore enhancing LTP. These enhancements follow principals of Hebbian plasticity, therefore only pathways undergoing synaptic plasticity displayed enhanced LTP via stimulation (Polanía et al., 2018). Conversely, cathodal stimulation induced long term depression (LTD) -like changes at the post-synaptic membrane. The application of tDCS can therefore supplement endogenous Hebbian plasticity for adaptive learning and sensorimotor adaptation (Kronberg et al., 2020). However, long-term changes to brain function are typically only observed when tDCS and task performance is repeated over multiple days (Polanía et al., 2018).

Consistent with existing tDCS literature involving the rTPJ, electrodes in the current study were placed over points Cz and CP6 located using the EEG 10-20 system (Donaldson et al., 2015; Takeuchi et al., 2018). Figure 4 depicts the active electrode placement for rTPJ tDCS. For anodal stimulation of the rTPJ, the anode will be placed over area CP6 on the head and the cathode will be placed on area Cz. For cathodal stimulation of the rTPJ the anode will be placed over area Cz and the cathode will be placed over CP6. Electrode placement for sham tDCS could follow the anodal configuration. Following specified and long-established guidelines, tDCS poses a negligible risk to the participants of research studies (Bikson et al., 2016). The set up for tDCS differs depending on the type of stimulation desired. The recommended electrical current for a 5-to-30-minute tDCS session is between 1- 2 mA with 2mA being the upper threshold for human studies (Thair et al., 2017). Studies using non- invasive stimulation on the TPJ typically apply currents between 1mA and 2mA (Donaldson et al., 2015; Takeuchi et al., 2018).

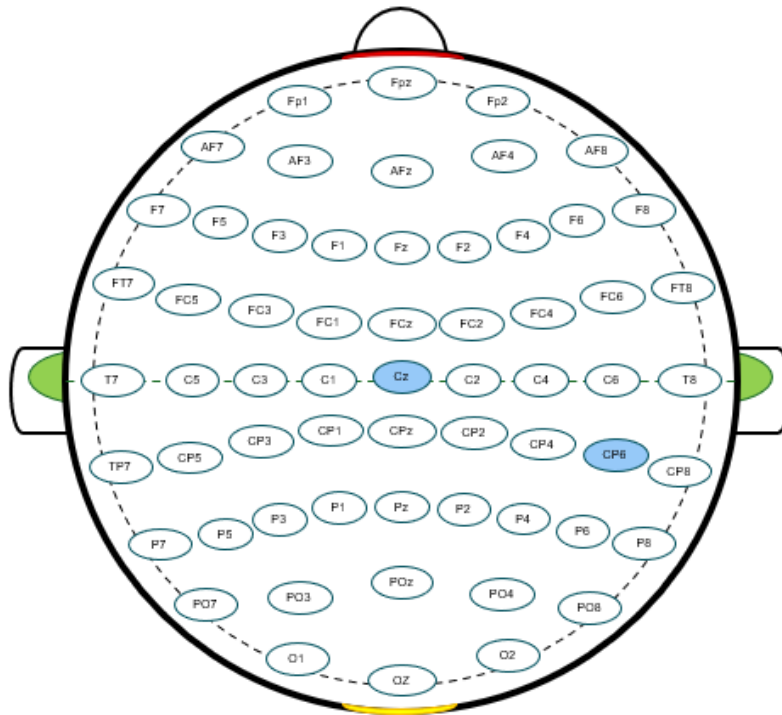


Figure 4. Electroencephalography (EEG) 10-20 electrode location for transcranial direct current stimulation (tDCS) of the right temporoparietal junction (rTPJ). The active electrode stimulating the rTPJ is placed over CP6; the reference electrode is placed over Cz. Adapted from Krol, 2020.

1.10.2 tDCS Applications

In the past, tDCS has been paired with VR for rehabilitation in improving pain management, postural control and gait patterns in clinical populations (Masseti et al., 2017). In healthy populations, tDCS has also been effective at improving postural stability. One study found that anodal tDCS to the rTPJ increased postural stability on an unstable surface when eyes were closed whereas cathodal tDCS to the rTPJ decreased postural stability. In this study, anodal stimulation was linked to improved efficacy in updating the body schema in the unfamiliar environment whereas cathodal stimulation was linked to decreased sensory integration at the rTPJ (Kamada & Takeuchi, 2023). With respect to cybersickness research, one study investigated cybersickness- mitigation strategies by applying tDCS to the rTPJ during VR. Both vestibular and visual information is processed at the temporoparietal junction making it an area of interest as visuo-vestibular conflict underlies cybersickness.

Anodal tDCS was found to reduce disorientation, postural instability and overall feelings of sickness during VR, providing evidence for the contributions of the rTPJ in cybersickness mitigation (Takeuchi et al., 2018).

1.11 Rationale

This study aims to investigate cybersickness mechanisms in the CNS through the lens of sensory conflict theory. While previous studies have shed light on the relationship between sensory reweighting and cybersickness severity, there is insufficient research on the higher-order brain regions involved in this relationship (Chung & Barnett-Cowan, 2023). Based on existing literature, we hypothesise that variability in sickness severity can be manipulated through stimulation of the rTPJ (Takeuchi et al., 2018). Under this hypothesis, anodal stimulation will increase the likelihood of rTPJ neurons to fire, increasing the efficiency of sensory reweighting and decreasing cybersickness severity caused by sensory conflict in VR. Under the same hypothesis, cathodal stimulation will decrease the likelihood of rTPJ neuronal firing, decreasing the efficiency of sensory reweighting and increasing cybersickness severity. The present study examines how tDCS of the rTPJ during VR affects sensory weightings as measured by the OCHART. Previous research has found evidence to suggest that those who display more change sensory weights following VR are less likely to experience cybersickness (Chung & Barnett-Cowan, 2023). Therefore, we are interested in determining whether the modulation of cybersickness via rTPJ tDCS is reflected in the OCHART results.

1.11.1 Sample Size Estimation

The sample size for this study was determined for a two-way repeated measures ANOVA investigating the effect of tDCS condition and sensory modality on change in cue weight using a simulated power calculation ($n = 2000$ simulations). Effect sizes were generated based on expected cue weight changes seen in astronauts and perception matched controls (Harris et al., 2017). Anodal change was estimated based on astronaut change in sensory cue weights (-4.6% vision, +11.9% body, -6.9% gravity), cathodal change was estimated based on changes in perception matched controls (-1.3% vision, -1.8% body, +3.8% gravity) and sham change was estimated based on the average change between astronauts and perception matched controls (-

3.0% vision, +5.0% body and -1.5% gravity). The expected standard deviations of the change in cue weights ranged between 0.083 and 0.15 and were calculated using the pre and post standard error from the reference study (Harris et al., 2017).

Correlation among repeated measures was estimated at 0.5. A sample of 20 participants yielded 100% power to detect a tDCS condition x sensory modality interaction in this ANOVA design. This sample size estimation assumes that changes from pre-VR to post-VR with anodal tDCS are similar to the changes observed after long-term exposure to microgravity. While drawing comparisons between space flight and VR exposure may be farfetched, sample size estimations are limited by the designs of previous OCHART studies. In the reference paper, both an experimental group and a control group are measured on the OCHART pre- and post-VR making it the closest OCHART study design available for the sample size estimation of the present study. The grey background PU data was used to estimate sample size as it is the OCHART data in closest alignment with the SVV as used by Chung and Barnett-Cowan (2023). An anticipated effect of $\eta^2 = 0.11$ was estimated based on the results of Chung and Barnett-Cowan (2023) where the high-intensity VR exposure resulted in significantly lower SVV scores compared to baseline. The estimated sample size for a two-way repeated measures ANOVA investigating the effect of sensory modality and tDCS condition on change in cue weights with $\eta^2 = 0.11$, $\alpha = 0.05$, $\beta = 0.80$ was 18 participants.

Another sample size was estimated for a two-way repeated measures ANOVA investigating the effect of time and tDCS condition on cybersickness using G*Power. An anticipated effect of $\eta^2 = 0.20$ was estimated from Takeuchi and colleagues (2018) where the anodal condition resulted in higher cybersickness compared to the sham and cathodal conditions. The estimated sample size for a two-way repeated measures ANOVA investigating the effect of time and condition on cybersickness with $\eta^2 = 0.20$, $\alpha = 0.05$, $\beta = 0.80$ was 6 participants. Therefore, to satisfy all power requirements for the study analyses, recruitment was set up for a minimum of 20 participants.

1.12 Hypotheses

We hypothesize that the rTPJ is involved in sensory reweighting and therefore anodal stimulation of the rTPJ during VR will cause a greater change in vector sum cue weights pre- to post-VR relative to sham stimulation. Conversely, we would expect cathodal stimulation of the rTPJ to cause a smaller change in cue weights relative to the sham condition.

A secondary hypothesis concerns sickness severity. Under this hypothesis we would expect less sickness to develop post-VR in the anodal condition compared to the sham condition. We would also expect more sickness to develop post-VR in the cathodal condition compared to the sham condition.

2.1 Methods

2.1.1 Participants

Participants were recruited from the University of Waterloo or were interested residents of Waterloo. Participants were recruited via email, word of mouth, or from posters. The total number of subjects recruited for this study was 24. However, 2 participants dropped out before completing all three testing sessions. Of the 22 participants whose data is represented in this study (10 male, 11 female, 1 non-specified; mean age = 24.7 ± 3.6) eleven were volunteers and eleven were remunerated \$10/h of their participation. This study was approved by the University of Waterloo Research Ethics Committee, and all participants provided written consent prior to participating in the study.

2.1.2 Screening Criteria

First, participants were given an information letter and screening form electronically to determine their eligibility. To be eligible for this study, participants had to be at least 18 years old and no older than 35. To participate in the study, participants had no history of any neurological deficits (e.g., migraine, seizures), uncorrected visual deficits, uncorrected auditory impairments, or balance (vestibular) disorders. Participants were not eligible to participate if they had metal implants in the head, face, or neck. In accordance with the Oculus Rift safety and health guidelines, participants with an inner ear infection, a pacemaker or other implanted medical devices or participants who were experiencing fatigue, under stress or anxiety, or suffering from cold/flu/headaches were excluded. Individuals who were pregnant are also excluded as VR may impact balance and increase risk of falls, as well as exacerbate symptoms of nausea and vomiting which are common during pregnancy. Sections in the screening form and information letter informed participants of the potential risks of wearing a mask while using a VR headset.

2.1.3 Procedure

The study collection took place over 3 separate days. The study duration for Day 1 was about 2.5 hours with the following Days 2 and 3 taking about 2 hours each. Day 1, Day 2 and Day 3 were

counterbalanced across participants to avoid order effects. Figure 5 below depicts the study design.

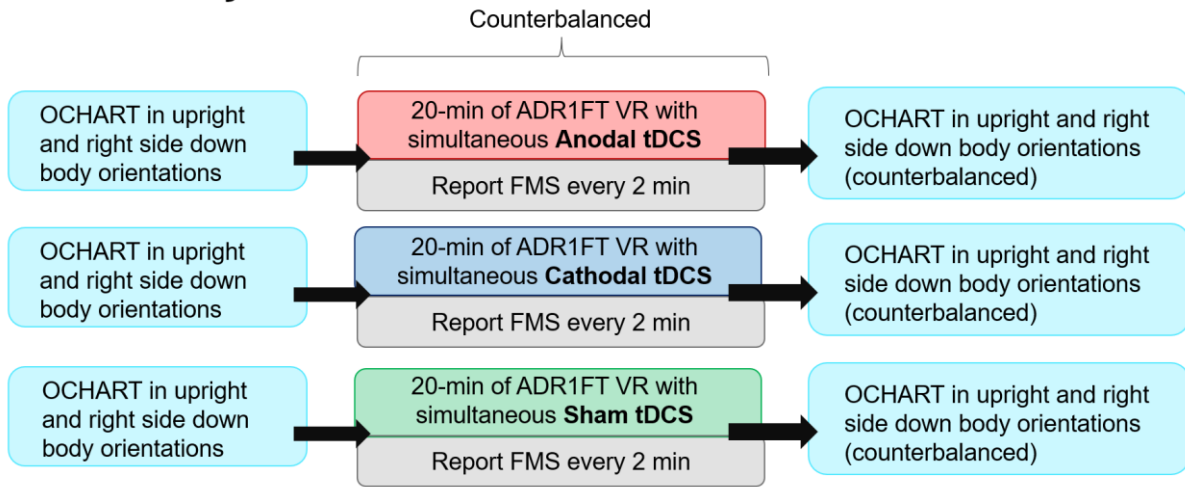


Figure 5. Study procedure flowchart. Testing takes place over three sessions, each separated by at least one week. Participants first completed the Oriented CHARACTER Recognition Task (OCHART) in both upright and right side down body orientations. Stimulation conditions were counterbalanced across the three days, and stimulation took place simultaneously with virtual reality (VR). The VR exposure took place over 20 minutes or until the participant became too sick to continue. Participants reported their Fast Motion Sickness (FMS) every 2 minutes throughout the VR exposure. Following VR, participants immediately completed the OCHART in both body orientations.

The participants first completed the Oriented Character Recognition Task (OCHART) task. Participants answered whether the character appeared as a ‘p’ or a ‘d’ on an Xbox controller using the buttons X and B for ‘p’ and ‘d’ respectively. The OCHART task was completed once sitting upright in a chair and once lying on their right side.

2.2 Apparatus and Stimuli

2.2.1 Laptop and Structure

The OCHART was performed on a 2011 Apple MacBook Pro laptop with a 20cm diameter viewing tube to restrict peripheral orientation cues as the task was completed. Participants viewed the OCHART through the viewing tube in both upright and RSD positions (Figure 6). A massage table 29 inches above the ground was used when participants were completing the OCHART in the RSD position. A firm foam pillow was used to support the head and ensure alignment between the head, neck, and body. The task laptop was mounted to a metal structure

that allowed the participant to view the task at the appropriate angle (90° from upright) as they laid RSD on the massage table. Responses on the OCHART were recorded using a Logitech Gamepad F310 which was connected to the MacBook Pro via USB cord.

Each trial of the OCHART presented the letter probe at one of the 24 orientations from 0°- 345° in 15° increments (Figure 7). The letter probe was presented over a grey background or a visual background. The visual background was presented at one of 6 orientations from 0°- 300° in 60° increments. Including the grey background, there were a total of 7 background options for the letter probe to be presented over. Each of the 24 letter probe orientations were paired with each of the 7 background options and each combination was presented to the participant 8 times for a total of 1344 trials (24 x 7 x 8). The letter probe and background pairings were presented for 500ms and then replaced with a screen of the same mean luminance and the task typically took about 15-20 minutes to complete (Dyde et al., 2006).



Figure 6. Upright and right side down (RSD) body orientations with the Oriented CHAracter Recognition Task (OCHART) laptop apparatus viewing tube.



Figure 7. Twenty-four letter probe orientations rotated at +15° increments about 360° (depicted over a grey background) and six visual backgrounds.

2.2.2 Oculus CV1 Virtual Reality Headset

An Oculus CV1 was used for the VR sessions. The CV1 uses an OLED display with a 90Hz refresh rate (VR image updates 90 times every second) and a 1,080 x 1,200-pixel resolution per eye. The CV1 field of view extended approximately $\pm 110^\circ$ diagonally and had a sudden movement latency of ~ 21.6 ms and a continuous movement latency of ~ 1.9 ms with stabilization occurring within 25-33ms from motion onset (McManus & Harris, 2023; Warburton et al., 2023). The Oculus CV1 was connected to a computer via an Oculus C4-A cable. Oculus sensors were placed 15 inches apart on a desk adjacent to the designated play space. The play space was 2.52m^2 and was covered with foam tiles.

ADR1FT VR, a game developed on Unreal Engine available on Steam, was used during VR exposures. The game settings were set to EVA Free, Solaris (free play) for VR exposure. ADR1FT was selected because it is a single-player microgravity game with many opportunities for visual motion along all axes and the potential to induce cybersickness. Figure 8 shows a screenshot of ADR1FT VR from the player's perspective. Participants were encouraged to explore the game and interact with various objects and space shuttle rooms. A wireless controller for Xbox one was used to navigate the VR environment.

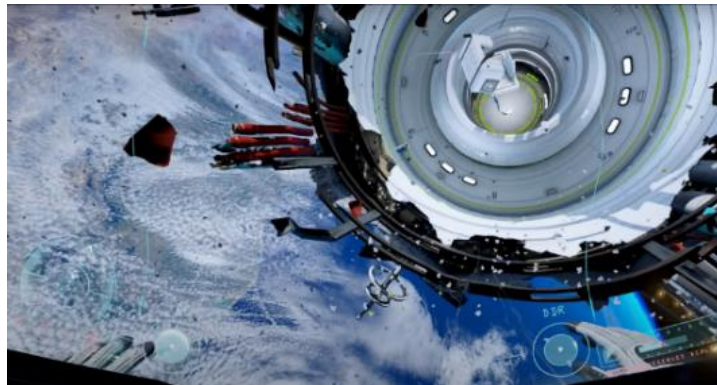


Figure 8. ADR1FT VR EVA Free Solaris player point of view. Participants played ADR1FT VR for 20 minutes or until they become too sick to continue.

2.2.3 neuroConn DC-STIMULATOR PLUS

The neuroConn DC-STIMULATOR PLUS with reusable 35cm² silicone electrodes was used to deliver tDCS. The tDCS delivered at a current of 1.5mA and the stimulation reached a maximum current density of 0.04mA/cm² which is within normal range for tDCS of the TPJ (Donaldson et al., 2015). Parker Spectra 360 Electrode Gel was used to facilitate conduction, and 3M clear medical tape was used to secure electrodes to the head. A small backpack was used to keep the neuroConn DC-STIMULATOR PLUS stimulator on the participant during the VR sessions.

Active stimulation current slowly faded in over 8 seconds and then occurred continuously over the course of the stimulation period (~20 minutes). The current then slowly faded out over 5 seconds. Figure 9 illustrates the current intensity changes over the course of anodal and cathodal stimulation. A sham tDCS condition was used to control for placebo effects of tDCS set up. Using the neuroConn DC-stimulator, sham stimulation deployed a small current pulse every 550ms for 3ms as opposed to a continuous current. The tDCS faded in for 8 seconds, followed by 30 seconds of direct current, a 5 second fade out and then 1200s of impedance control only. Figure 10 illustrates the current pattern for the sham tDCS. Sham tDCS used small current pulses to stimulate the feeling of normal tDCS on the skin. As average current overtime does not exceed 2 mA, there is no therapeutic effect of the sham tDCS (neuroConn, 2024).

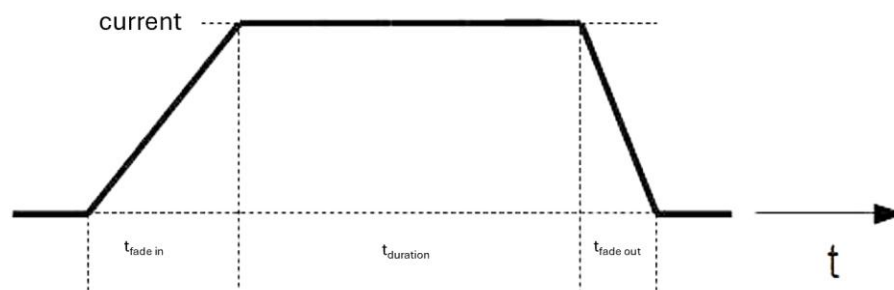


Figure 9. Current pattern for transcranial direct current stimulation (tDCS) during active (anodal/cathodal) stimulation. Adapted from the neuroConn Programmable Direct Current Stimulator DC-STIMULATOR User Manual (2024).

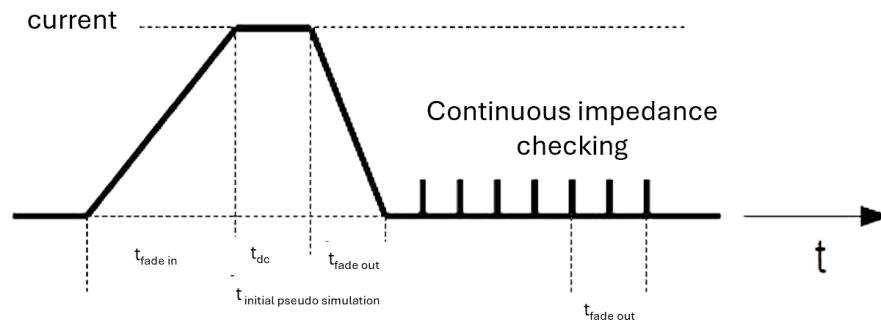


Figure 10. Current pattern for transcranial direct current stimulation (tDCS) during sham stimulation. Adapted from the neuroConn Programmable Direct Current Stimulator DC-STIMULATOR User Manual (2024).

2.2.4 tDCS Preparation

After completing the OCHART, participants were prepped for tDCS. Head measurements were taken using a measuring tape and following the 10-20 method of EEG placement (Morley & Hill, 2016). Figure 11 illustrates the 10-20 measurement process for locating points Cz and CP6. Point Cz is the midpoint between the nasion (red) and the inion (yellow) as well as the midpoint between the two pre-auricular points (green).

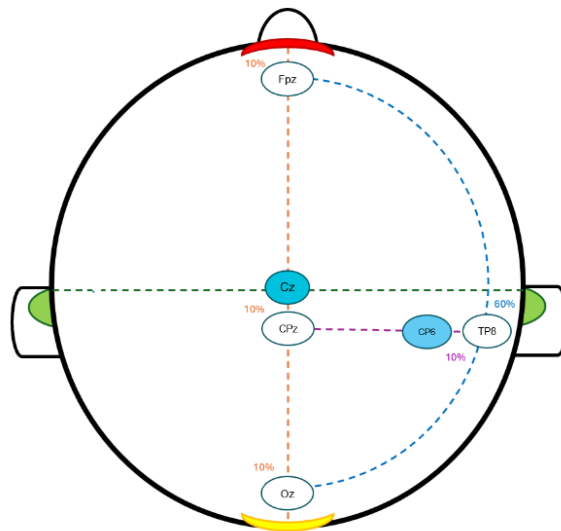


Figure 11. Electrode locating and placement using the EEG 10-20 method. The nasion and inion are represented in red and yellow respectively. Preauricular points are represented in green. Percentages (%) represent the distance from a landmark to an anatomical mark or between anatomical marks (i.e. Fpz marked at the 10% distance from the nasion to the inion, TP8 marked at the 60% distance from Fpz to Oz). The stimulating electrode was placed on area CP6 and the reference electrode was placed on area Cz.

Once the tDCS electrodes were set up, participants were assisted in carefully placing the VR headset over the electrodes. Prior to full stimulation, a test current of 1.5mA was administered to see if the participant was comfortable. Next, tDCS current ramped up to 1.5mA. In the anodal and cathodal conditions, the current remained at 1.5mA for the duration of the VR experience. For sham stimulation, the 1.5mA current was delivered briefly for 30 seconds and then quickly ramped down.

In the VR exposure (ADR1FT), participants explored a low gravity simulation spaceship as an astronaut in first person. Using an Xbox controller, they controlled their avatar's hands to grab objects in the virtual world and push themselves around. Since there was no gravity in the simulation, it was easy for the avatar to rotate easily and cause cybersickness. Throughout the VR exposure, participants were asked to rank their cybersickness every 2 minutes. Cybersickness rankings were made on the Fast Motion Sickness scale (FMS) which ranges from 0 to 20, where 0 represents no sickness and 20 represents severe sickness. Following the VR exposure, participants completed the OCHART again in both body orientations. The order of the body orientations was counterbalanced to reduce the risk of body orientation order effects. Once the post-VR OCHART was complete, participants had completed testing for that day.

2.3 Data Analysis

2.3.1 OCHART

The OCHART was used to evaluate the participants' PU. The PU was calculated for each visual background each time the OCHART was completed. Therefore, because there are 7 backgrounds used, there were 7 PUs for each OCHART. In total, each day of the study yielded 28 PU (7 upright pre-VR + 7 RSD pre-VR + 7 upright post-VR + 7 RSD post-VR). To calculate the PU for one visual background, the average response for all letter presentations was taken. Recall each letter orientation was presented over each visual background 8 times. An average response across those 8 presentations was taken to determine how likely the participant judged the letter as the letter 'p' when it was presented in that given orientation. When the participant responded 'p' or 'd' it was coded as '1' or '0' respectively. Therefore, if a participant perceived the letter as a 'p' 100% of the time at a certain orientation, the response average was 1 whereas if

the participant perceived the letter as a ‘d’ 100% of the time, the response average was a ‘0’. Uncertainty in responses yielded response averages between 0.875 and 0.125. We were interested in the response average at 0.5 as this indicated the transition point from perceiving ‘p’ to ‘d’ or ‘d’ to ‘p’.

Across the 24 letter orientations from 0-360°, two points were identified where the letter is equally likely to be perceived as a ‘p’ or as a ‘d’. These transition points were identified using a 2-parameter sigmoidal regression and are known as the points of subjective equality (PSE). Next, an average of the two PSE was taken and -180° was subtracted from the average to calculate the PU. These steps were completed for each of the 7 visual backgrounds and yielded the 7 PU for one OCHART trial. The PUs were then used in the vector sum model to determine the sensory cue weights for gravity, vision and body. The PUs within one OCHART trial were compared across visual background orientations to determine the effect of visual manipulation on PU. The PU between upright and RSD OCHART trials were compared to determine the effect of body orientation on PU. Each PU across all four OCHART trials was associated with one background orientation and one body orientation. When using the vector sum model, we also assumed that gravity did not change and therefore set its vector value to 1. By inputting the body orientation and visual background orientation that corresponded with the PU into the model, we can solve for the vectors of body and vision. Given the visual background orientation and body orientation, the sum of the vision, body and gravity vectors is in alignment with the PU (Jenkin et al., 2007).

2.3.2 OCHART Example Analysis

Response averages across each letter probe orientation were organized in a 7 x 24 table. Next the p-d (1-0) and d-p (0-1) transitions were extracted manually from the data table for the 2-parameter sigmoidal regression analysis (Figure 12). Using the 2-parameter sigmoidal regression, we estimated an inflection point where the participant was equally likely to identify the letter probe as a ‘p’ or a ‘d’ against a certain background. All sigmoidal regressions fit to the data with an $R^2 \geq 0.5$. Next, using the PSE (x_0) for the p-d transition and the d-p transition we calculated the PU for the visual background (Equation 1). Each OCHART trial yielded 7 PU values — one for each background. Only the PU for the 6 visual backgrounds were used in the

vector sum model. Next, the vector sum was calculated using the PU for pre-VR upright and RSD trials as well as the PU for post-VR upright and RSD trials.

Equation 1. Perceptual upright (PU) calculated using the two points of subjective equality (PSE) as estimated by the 2-parameter sigmoidal regression.

$$PU = \frac{(x_{01} + x_{02})}{2} - 180^\circ$$

$$PU = \frac{(93^\circ + 270^\circ)}{2} - 180^\circ = 1.5^\circ$$

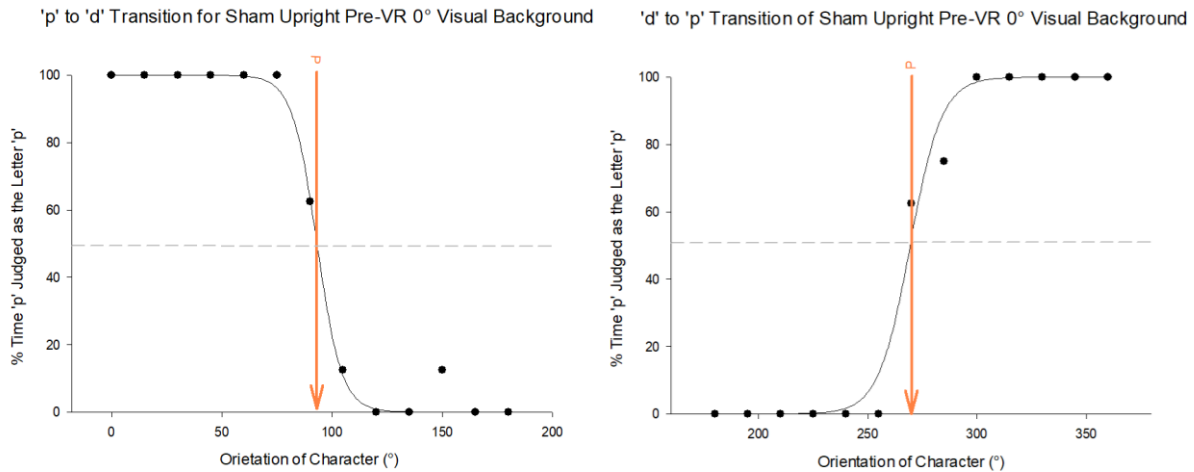


Figure 12. Perceptual upright (PU) calculation using the two points of subjective equality (PSE). The PSE (shown in orange) is located at the 50% judgement point where the letter is equally likely to be judged as a 'p' or a 'd' as predicted by the 2-parameter sigmoidal regression. Two PSE are estimated to cover the two transitions that occur about 360°.

2.3.3 Vector Sum Model

For each time point (pre-VR or post-VR) the OCHART was done in two body orientations. For one time point, the PUs for each visual background across both body orientations were entered into the vector sum model (Table 1). Using the body orientations, the visual background orientations and the PU, two sensory vectors were generated per OCHART: a vision vector and a body vector. The horizontal and vertical components of the vision vector were represented by v_x and v_y respectively. Visual harmonics $2v$ and $4v$ were included to capture ambiguity in perceptual responses under certain visual conditions (e.g. similar PU over 0° and 180° visual backgrounds). Under the vector sum model, the body's influence was assumed to be aligned with gravity in the upright condition, the tilt value adjusted that assumption to align the body vector

with RSD body orientation when necessary. The gravity vector was represented as a constant ($g = 1$) and influenced both the x and y estimates based on the body orientation (Equation 2). When the body orientation was upright (0°) and aligned with gravity, the product of the gravity and body contributions to the y and x estimate were 1 and 0 respectively. When the body orientation was RSD (90°), it was no longer aligned with gravity and the product of the gravity and body contributions to the y and x estimate were 0 and 1 respectively.

The model accounted for visual harmonics where certain visual background orientations were expected to have symmetrical influences on the PU. The first visual harmonic $\cos(v)$ and $\sin(v)$ accounted for the directional bias in the visual background (polarized cues which signaled an “up” direction based on gravity-aligned elements) so that the PU was angled toward the actual background angle.

Table 1. Example data for vector sum model input.

Body Orientation (<i>tilt</i>)	Visual Background Orientation (<i>v</i>)	PU (<i>f</i>)
0°	0°	1.30°
0°	60°	4.76°
0°	120°	0.92°
0°	180°	-0.66°
0°	240°	-9.20°
0°	300°	5.23
90°	0°	-28.40°
90°	60°	-27.26°
90°	120°	-44.96°
90°	180°	-39.74°
90°	240°	-49.38°
90°	300°	-43.80

Equation 2. Vector sum model used for estimating sensory cue reliance based on perceptual upright (PU) data. In the model v = visual background orientation, $tilt$ = body orientation, f = PU, g = gravity constant = 1, vis_1, vis_2, vis_3 = weight of visual cues, bod = body vector along y-axis.

$$vy = vis \cdot \cos(v) + vis_2 \cdot \cos(2v) + vis_3 \cdot \cos(4v)$$

$$vx = vis \cdot \sin(v) + vis_2 \cdot \sin(2v) + vis_3 \cdot \sin(4v)$$

$$y = bod + v_y + g \cdot \cos(tilt)$$

$$x = v_x + g \cdot \sin(tilt)$$

$$f = \tan^{-1}\left(\frac{x}{y}\right)$$

The second visual harmonic, $\cos(2v)$ and $\sin(2v)$, accounted for 180° symmetry, where polarized cues in the visual background provided similar gravitational information at 180° orientation differences. For example, a letter probe was perceived similarly over a 0° and 180° visual background as gravity cues were represented at the same angle in both scenes. The fourth harmonic $\cos(4v)$ and $\sin(4v)$ represented 90° symmetry where the PU was biased to the nearest 90° depending on visual background orientation, body orientation and cue weights.

Each vector length was proportional to the contribution of a certain cue at that time point. The sum of all the sensory vectors, known as the vector sum, was calculated for the pre-VR and post-VR data in each tDCS condition. Each sensory cue weight was determined as the quotient of the sensory vector divided by the vector sum (Equation 3). The sensory cue weights are relative proportions and sum to 1 (Equation 4). A total of six sets of sensory cues were generated for the analysis: sham pre-VR, sham post-VR, anodal pre-VR, anodal post-VR, cathodal pre-VR and cathodal post-VR. The vectors can then combined to generate the PU vector using the body orientation and visual background orientation for that trial (Equation 5; Dyde et al., 2006).

Equation 3. Example calculation for the weighted vision vector (w_v). The vision vector (\overrightarrow{vision}) and body vector (\overrightarrow{body}) are the outputs of the vector sum model. The gravity vector ($\overrightarrow{gravity}$) is assigned a value of 1 as gravity is a constant which is not manipulated during the OCHART. The vision vector is divided by the

vector sum and the quotient is the relative cue weight for the vision vector.

$$w_v = \frac{\overrightarrow{vision}}{(\overrightarrow{vision} + \overrightarrow{gravity} + \overrightarrow{body})}$$

Equation 4. The weighted sensory vectors are compositional values which sum to 1.

$$w_v + w_g + w_b = 1$$

Equation 5. The perceptual upright (PU) vector estimate is equal to the product of each sensory cue orientation and the respective cue weight, summed. The PU vector estimate can be calculated for each combination of visual background orientation and body orientation.

$$\overrightarrow{PU} = \text{visual background orientation} (w_v) + \text{gravity} (w_g) + \text{body orientation} (w_b)$$

2.4 Fast Motion Sickness Scale (FMS)

The FMS is a simple Likert scale measure of sickness that is used to measure visually induced motion sickness (Chang et al., 2020; Keshavarz & Hecht, 2011; Merchant & Kirollos, 2022). On the FMS, participants verbally rank their sickness on a scale from 0 (no sickness) to 20 (frank sickness; Keshavarz & Hecht, 2011). Frank sickness may present as overwhelming and intolerable nausea, unease, or disorientation. Pre- and post-VR FMS scores are compared for the sham, anodal and cathodal conditions to determine the change in cybersickness severity for each tDCS condition.

3.1 Results

3.1.1 Pre-VR Cue Weight

Of the total 22 participants collected, accurate sensory vectors could not be estimated using the vector sum model for three participants. The three participants whose data did not fit the vector sum model displayed either unpredictable or minimal change in responses across visual backgrounds or body orientations making it difficult to estimate the contributions of vision and body cues. Therefore, 19 participants are included in the analysis of cue weights. A Shapiro-Wilk test confirmed normality of residuals in pre-VR cue weights. Three separate one-way ANOVAs were run to confirm there were no significant differences in pre-VR vision, body, and gravity cue weights across tDCS conditions. In this analysis, tDCS condition was treated as a repeated measure.

A one-way repeated-measures ANOVA was conducted to determine the effect of tDCS condition on pre-VR vision cue weights. A Greenhouse Geisser correction was applied to tDCS condition as it violated the assumption of sphericity. The main effect of tDCS condition [$F_{2,36} = 0.27$, $\varepsilon = 0.72$, $p = 0.69$, $\eta p^2 = 0.015$] was not significant. Another one-way repeated measures ANOVA was conducted to determine the effect of tDCS condition on pre-VR body cue weights. The main effect of tDCS condition [$F_{2,36} = 1.11$, $p = 0.34$, $\eta p^2 = 0.058$] was not significant. Finally, a one-way repeated-measures ANOVA was conducted to determine the effect of tDCS condition on pre-VR gravity cue weights. The main effect of tDCS condition [$F_{2,36} = 0.98$, $p = 0.38$, $\eta p^2 = 0.052$] was not significant. Therefore, pre-VR cue weights for all cues remained consistent across all conditions.

3.1.2 Hypothesis 1 – Change in Cue Weights

Within the current OCHART and vector sum model literature, exclusions based on vector sum model fit are unclear. Therefore, for the sake of comparison with the existing literature, participants with poor R^2 were not excluded from the primary analysis. As mentioned earlier, three participants were excluded from the analysis. Therefore, the analysis of cue weights was

conducted with data from 19 participants. First, the absolute change in sensory cue weight (ABS Δ Cue Weight) for each participant was calculated across sensory modalities in each tDCS condition. The change scores were calculated using Equation 6.

Equation 6. Absolute cue weight change (ABS Cue Weight) formula where Cue Weight is either w_v , w_g or w_b .

$$ABS \Delta Cue Weight = |Post VR Cue Weight - Pre VR Cue Weight| \times 100\%$$

A Shapiro-Wilk test revealed the assumption of normality of residuals was violated. An ART ANOVA with the factors tDCS condition (sham, anodal and cathodal) and sensory modality (vision, body, gravity) was conducted to examine the effect of tDCS condition and sensory modality on ABS Δ Cue Weight. Sensory modality and tDCS condition were treated as repeated measures. The two-way repeated measures ART ANOVA revealed a significant main effect of sensory modality [$F_{2,144} = 12.56, p < 0.001, \eta_p^2 = 0.15$] and a non-significant main effect of tDCS condition [$F_{2,144} = 1.64, p = 0.19, \eta_p^2 = 0.022$]. Further, the interaction between tDCS condition and sensory modality was not significant [$F_{4,144} = 0.58, p = 0.68, \eta_p^2 = 0.016$]. The ART contrast tests revealed that ABS Δ Cue Weight was significantly larger for body cues compared to vision cues ($p = 0.0001$, body = $5.67\% \pm 0.85\%$, vision = $2.53\% \pm 0.38\%$) and for gravity cues compared to vision cues and ($p = 0.0001$, gravity = $6.14\% \pm 0.97\%$, vision = $2.53\% \pm 0.38\%$). Absolute change data is illustrated in Figure 13.

Next, non-absolute Δ Cue Weight was investigated to determine if there was a directional effect of tDCS condition and sensory modality. Cue weights are interdependent compositional scores which sum to 1. Therefore, to satisfy the assumption of independence, a centered log ratio transformation was applied to the cue weights before Δ Cue Weight was calculated for each sensory modality. A Shapiro-Wilk test on the Δ Cue Weight data revealed a violation of normality of residuals. Therefore, a two-way repeated measures ART ANOVA was conducted to investigate the effect of tDCS condition and sensory modality on Δ Cue Weight. Sensory modality and tDCS condition were treated as repeated measures.

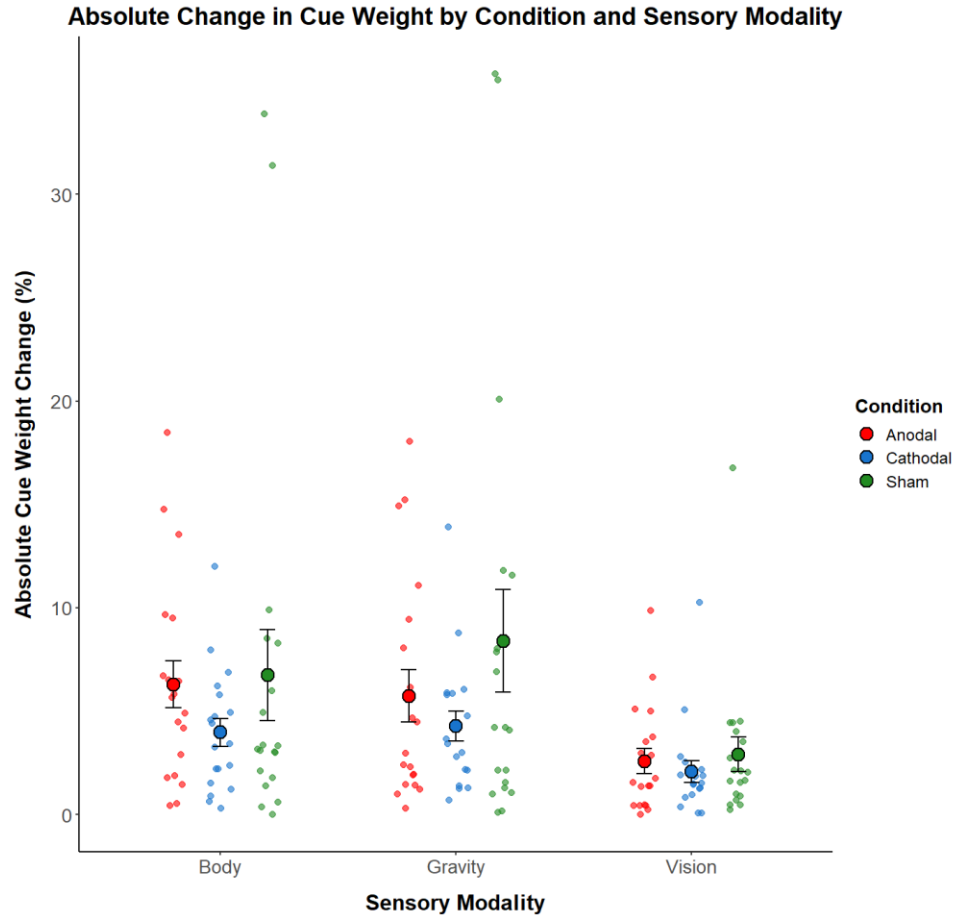


Figure 13. Absolute cue weight change (ABS Δ Cue Weight) by sensory modality and tDCS condition. Mean absolute cue weight change is represented by points outlined in black. Error bars represent standard error.

The ART ANOVA revealed a main effect of sensory modality trending toward significance [$F_{2,144} = 2.97, p = 0.054, \eta_p^2 = 0.04$] no significant effect of tDCS condition [$F_{2,144} = 2.57, p = 0.034, \eta_p^2 = 0.034$]. The interaction between tDCS condition and sensory modality was also not significant [$F_{4,144} = 0.71, p = 0.59, \eta_p^2 = 0.019$]. Figure 14 illustrates the average directional change in cue weights from pre-VR to post-VR.

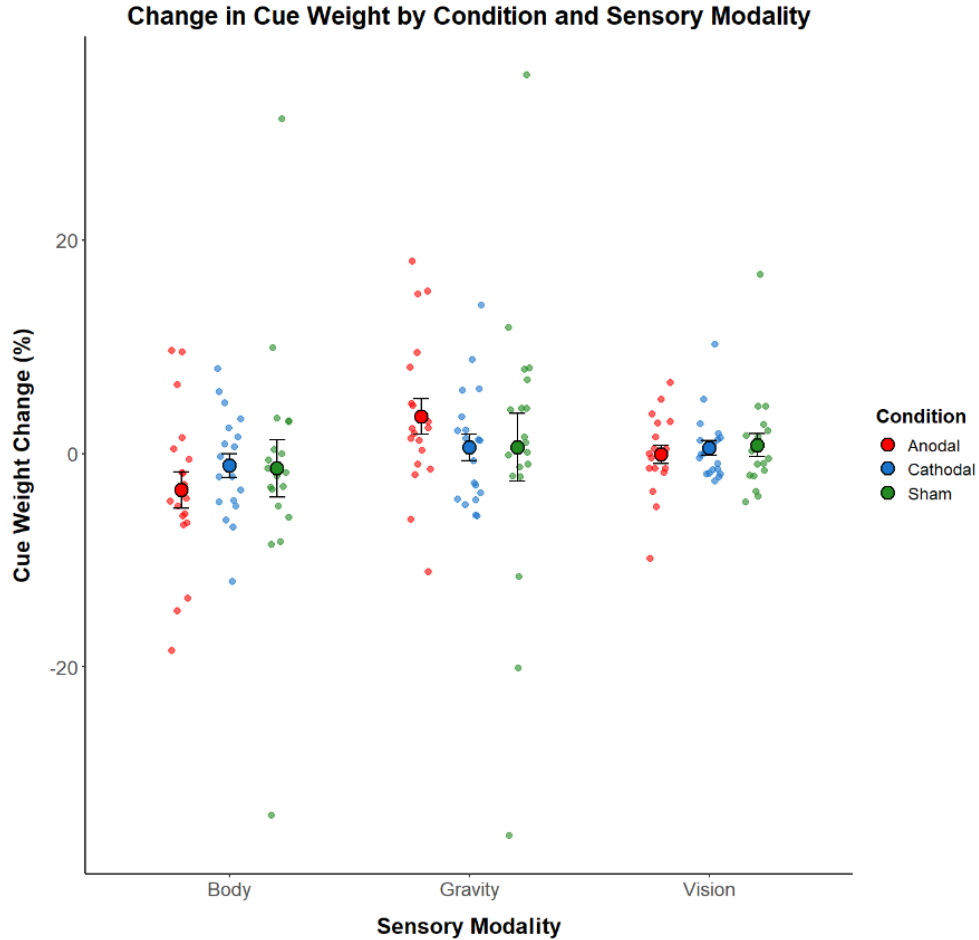


Figure 14. Average cue weight change as a function of tDCS condition and time. Negative % change indicates down weighting of that sensory cue post-VR.

3.1.2.1 Vector Sum Model Fit to averaged PU

Individual PU data has a high level of variability and therefore fitting the vector sum model to individual data resulted in models with poor fits (low R^2). Within the existing literature, participant average PU values have been used in the vector sum model to estimate sensory vectors and relative cue weights within a sample. Cue weights and relative cue weights for average data are represented below in Table 2. The ratio for pre-VR cue vectors for vision, body and gravity cues respectively were 0.333: 1.446: 1 for sham, 0.352:1.380; 1 for anodal and 0.400: 1.379: 1 for cathodal. The ratio for post-VR cue vectors for vision, body and gravity cues respectively were 0.331: 1.380: 1 for sham, 0.352: 1.315: 1 for anodal and 0.370: 1.352: 1 for

cathodal. The change in relative cue weights from pre-VR to post-VR is represented in Table 3 and illustrated in Figure 15.

Table 2. Average parameter estimates of the vector model for vision, body and gravity cues pre-VR by tDCS condition. Standard error for relative cue weight was estimated from the proportion of standard error for the pre-VR vector length.

Sensory Cue	tDCS Condition	Vector Length Pre	S.E. Pre	Relative Cue Weight Pre	S.E. Pre	Vector Length Post	S.E. Post	Relative Cue Weight Post	S.E. Post
Vision (v)	Sham	0.333	0.13	12%	0.05	0.331	0.17	12.2%	0.06
	Anodal	0.352	0.13	12.9%	0.05	0.352	0.13	13.2%	0.05
	Cathodal	0.4	0.11	14.4%	0.04	0.37	0.11	13.6%	0.04
Body (b)	Sham	1.446	0.19	52.0%	0.07	1.38	0.25	50.9%	0.09
	Anodal	1.38	0.19	50.5%	0.07	1.315	0.18	49.3%	0.07
	Cathodal	1.379	0.16	49.6%	0.06	1.352	0.15	49.7%	0.06
Gravity (g)	Sham	1	0	36%	0	1	0	36.9%	0
	Anodal	1	0	36.6%	0	1	0	37.5%	0
	Cathodal	1	0	36%	0	1	0	36.7%	0

Table 3. Relative change in cue weights by sensory cue and tDCS condition. Pre-VR and Post-VR R^2 for the vector sum model (VSM) fit.

		tDCS Condition					
Sensory Cue		Sham		Anodal		Cathodal	
Δ Relative Cue Weight	Vision	+0.2%		+0.3%		-0.8%	
	Body	-1.1%		-1.2%		+0.1%	
	Gravity	+0.9%		+0.9%		+0.7%	
VSM R^2		Pre-VR	Post-VR	Pre-VR	Post-VR	Pre-VR	Post-VR
		0.66	0.23	0.68	0.68	0.81	0.81

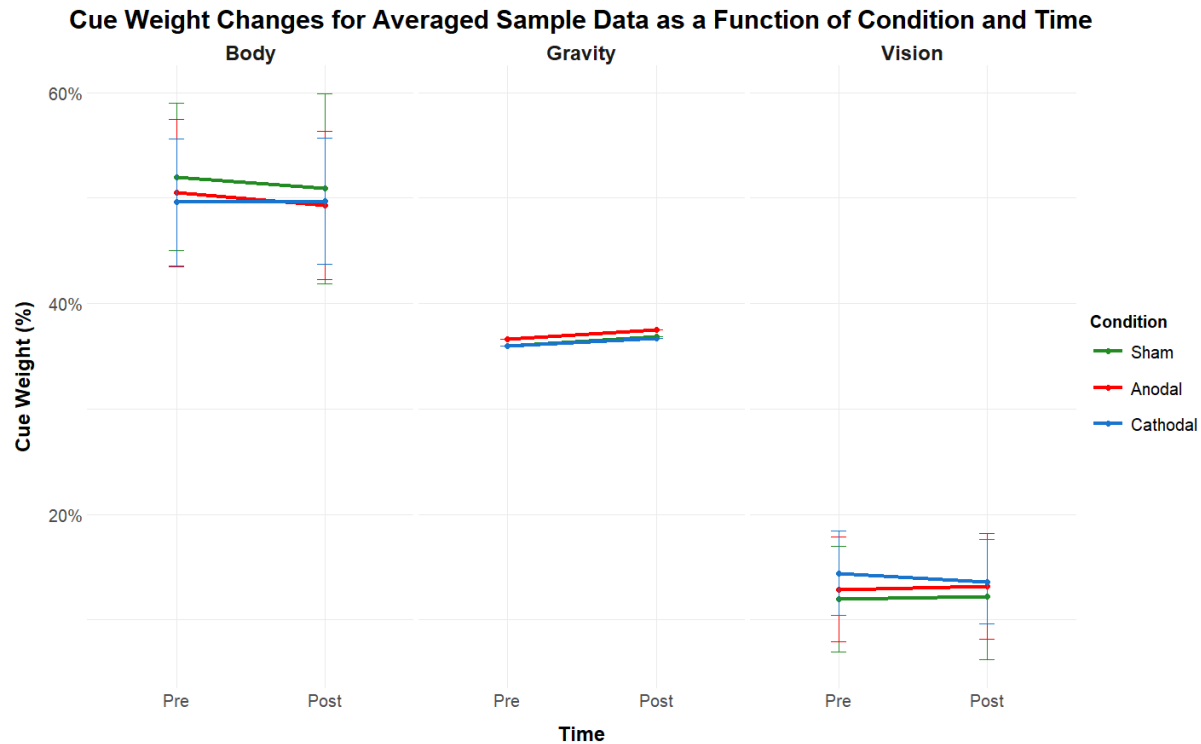


Figure 15. Cue weight changes in averaged sample data as a function of tDCS condition and time. Standard error was calculated by multiplying the relative cue weight by the quotient of the standard error divided by the vector length. Error bars represent standard error.

3.1.3 Perceptual Upright

3.1.3.1 Visual Background PU Analysis

Data from all 22 participants included in the PU analysis over visual backgrounds. The average PU for each tDCS condition, time, body orientation, and visual background was calculated and plotted (Figure 16). A Shapiro-Wilk test revealed non-normality in the residuals; therefore, an ART ANOVA was used to examine the differences between PU across the factors tDCS condition, time, visual background and body orientation. The factors were all treated as repeated measures. The ART ANOVA revealed significant main effects of body orientation [$F_{1,1491} = 1520.92, p < 0.0001, \eta_p^2 = 0.505$] and visual background [$F_{5,1491} = 124.17, p < 0.0001, \eta_p^2 = 0.29$] and non-significant main effects of condition [$F_{2,1491} = 2.45, p = 0.087, \eta_p^2 = 0.03$], and time [$F_{1,1491} = 2.50, p = 0.11, \eta_p^2 = 0.002$]. The two-way interaction between body orientation and visual background was also significant [$F_{5,1491} = 11.50, p < 0.001, \eta_p^2 = 0.037$]. The remaining two-way

interactions between tDCS condition and time [$F_{2, 1491} = 0.31, p = 0.73, \eta_p^2 = 0.0004$], tDCS condition and body orientation [$F_{2, 1491} = 2.56, p = 0.077, \eta_p^2 = 0.03$], time and body orientation [$F_{1, 1491} = 0.039, p = 0.466, \eta_p^2 = 0.00003$], tDCS condition and visual background [$F_{10, 1491} = 0.18, p = 0.18, \eta_p^2 = 0.001$], time and visual background [$F_{5, 1491} = 0.37, p = 0.87, \eta_p^2 = 0.001$] were not significant. The following three-way interactions did not reach significance: tDCS condition, time and body orientation [$F_{2, 1491} = 0.38, p = 0.68, \eta_p^2 = 0.001$], tDCS condition, time and visual background [$F_{10, 1491} = 0.15, p = 1.00, \eta_p^2 = 0.001$], tDCS condition, body orientation and visual background [$F_{10, 1491} = 0.44, p = 0.93, \eta_p^2 = 0.003$], time, body orientation and visual background [$F_{5, 1491} = 0.47, p = 0.80, \eta_p^2 = 0.002$]. The four-way interaction between tDCS condition, time, body orientation and visual background was also not significant [$F_{10, 1491} = 0.16, p = 1.00, \eta_p^2 = 0.001$].

Contrast tests for the ART ANOVA revealed that the average PU was significantly smaller and therefore shifted significantly more leftward from the body orientation when RSD compared to upright ($p < 0.001, \text{RSD} = -36^\circ \pm 0.86^\circ, \text{upright} = -11.2^\circ \pm 0.76^\circ$). ART contrast tests also revealed that PU was significantly larger when the visual background was presented at 0° compared to 180° ($p < 0.0001, 0^\circ = -17.9^\circ \pm 1.27^\circ, 180^\circ = -28.7^\circ \pm 1.72^\circ$), 240° ($p < 0.0001, 0^\circ = -17.9^\circ \pm 1.27^\circ, 240^\circ = -34.9^\circ \pm 1.48^\circ$), 300° ($p < 0.0001, 0^\circ = -17.9^\circ \pm 1.27^\circ, 300^\circ = -29.1^\circ \pm 1.34^\circ$), at 60° compared to 120° ($p < 0.0001, 60^\circ = -13.4^\circ \pm 1.54^\circ, 120^\circ = -17.6^\circ \pm 1.75^\circ$), 180° ($p < 0.0001, 60^\circ = -13.4^\circ \pm 1.54^\circ, 180^\circ = -28.7^\circ \pm 1.72^\circ$), 240° ($p < 0.0001, 60^\circ = -13.4^\circ \pm 1.54^\circ, 240^\circ = -34.9^\circ \pm 1.48^\circ$), and 300° ($p < 0.0001, 60^\circ = -13.4^\circ \pm 1.54^\circ, 300^\circ = -29.1^\circ \pm 1.34^\circ$), at 120° compared to 180° ($p < 0.0001, 120^\circ = -17.6^\circ \pm 1.75^\circ, 180^\circ = -28.7^\circ \pm 1.72^\circ$), 240° ($p < 0.0001, 120^\circ = -17.6^\circ \pm 1.75^\circ, 240^\circ = -34.9^\circ \pm 1.48^\circ$), 300° ($p < 0.0001, 240^\circ = -34.9^\circ \pm 1.48^\circ, 300^\circ = -29.1^\circ \pm 1.34^\circ$), at 180° compared to 240° ($p < 0.0001, 180^\circ = -28.7^\circ \pm 1.72^\circ, 240^\circ = -34.9^\circ \pm 1.48^\circ$), 300° ($p = 0.0138, 180^\circ = -28.7^\circ \pm 1.72^\circ, 300^\circ = -29.1^\circ \pm 1.34^\circ$) and finally 240° compared to 300° ($p = 0.0003, 240^\circ = -34.9^\circ \pm 1.48^\circ, 300^\circ = -29.1^\circ \pm 1.34^\circ$). ART contrast test results for

the interaction between body orientation and visual background are summarized in Table 4.

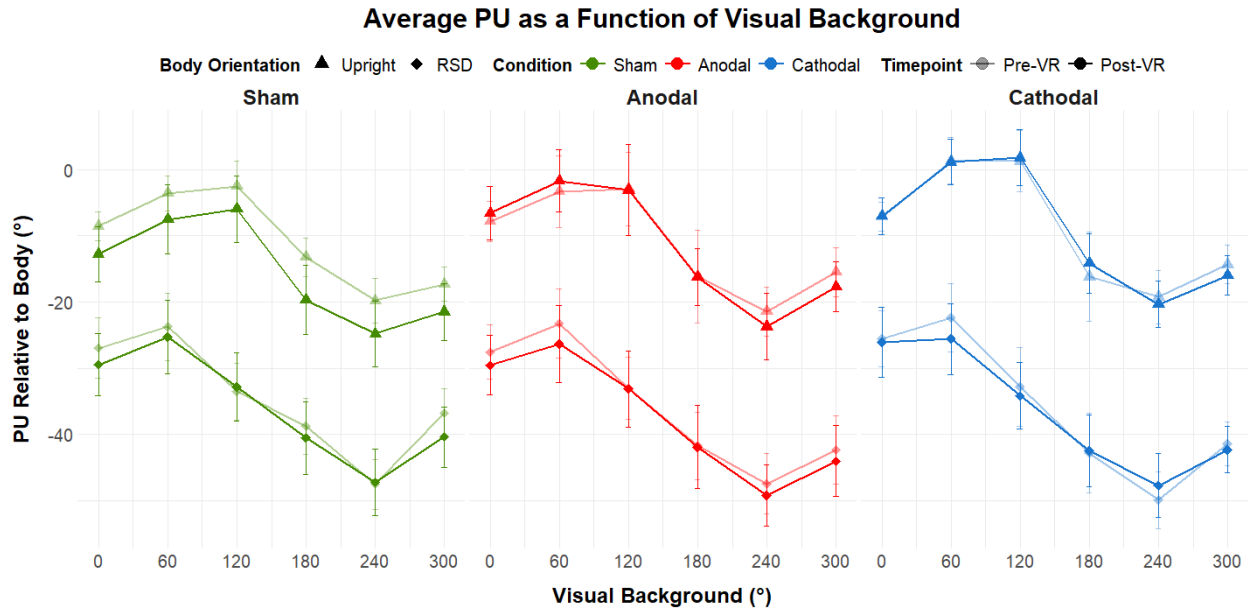


Figure 16. Average PU as a function of visual background across tDCS conditions. Lines connecting points are to illustrate a pattern in responses across visual backgrounds. Error bars represent standard error.

Table 4. Contrast test results for the interaction between body orientation and visual background on perceptual upright (PU).

Comparison	<i>p</i>
Upright 0° < Upright 60°	0.0098
Upright 0° < Upright 120°	0.0815
Upright 0° > Upright 180°	0.0055
Upright 0° > Upright 240°, 300°	<0.0001
Upright 60° > Upright 180°, 240°, 300°	<0.0001
Upright 120° > Upright 60°	1.00
Upright 120° > Upright 180°, 240°, 300°	<0.0001
Upright 180° > Upright 240°	<0.0001
Upright 180° < Upright 300°	0.15
Upright 240° < Upright 300°	0.26
RSD 0° < RSD 60°	0.98 (ns)
RSD 0° > RSD 120°	0.0015
RSD 0° > RSD 180°, 240°, 300°	<0.0001

RSD 0° < Upright 0°, 60°, 120°, 180°, 300°	<0.0001
RSD 0° < Upright 240°	0.015
RSD 120° < RSD 60°, 240°	<0.0001
RSD 120° < RSD 180°	0.044
RSD 120° < RSD 300°	0.0009
RSD 120° < Upright 0°, 60°, 120°, 180°, 240°, 300°	<0.0001
RSD 180° > RSD 60°	<0.0001
RSD 180° > RSD 240°	0.0035
RSD 180° > RSD 300°	1.00 (ns)
RSD 180° < Upright 0°, 60°, 120°, 180°, 240°, 300°	<0.0001
RSD 240° < RSD 60°	<0.0001
RSD 240° < RSD 300°	0.12 (ns)
RSD 240° < Upright 0°, 60°, 120°, 180°, 240°, 300°	<0.0001
RSD 300° < RSD 60°	<0.0001
RSD 300° < Upright 0°, 60°, 120°, 180°, 240°, 300°	<0.0001
RSD 60° < Upright 0°, 60°, 120°, 180°, 300°	<0.0001
RSD 60° < Upright 300°	0.0001
RSD 60° < Upright 240°	0.47 (ns)

3.1.3.2 Grey Background PU Analysis

Of the total 22 participants collected, data from one participant was excluded because the participant mistook the grey trials for a loading screen and was responding randomly (n=21). The averaged grey PU data is represented relative to the visual background PU data in Figure 17. A Shapiro-Wilk test indicated a violation of the normality of residuals in the grey background data therefore a three-way repeated measures ART ANOVA was conducted to examine the effect of tDCS condition, time and body orientation on PU. All factors were treated as repeated measures. The three-way repeated measures ART ANOVA revealed a significant main effect of body orientation [$F_{1, 220} = 433.91, p < 0.0001, \eta_p^2 = 0.66$] and non-significant main effects of tDCS condition [$F_{2, 220} = 2.57, p = 0.079, \eta_p^2 = 0.023$] and time [$F_{1, 220} = 0.25, p = 0.62, \eta_p^2 = 0.001$]. The following two-way interactions were non-significant: tDCS condition and time was not [$F_{2, 220} = 0.58, p = 0.56, \eta_p^2 = 0.005$], tDCS condition and body orientation [$F_{2, 220} = 0.48, p = 0.62,$

$\eta_p^2 = 0.004$] and time and body orientation [$F_{1, 220} = 0.15, p = 0.7, \eta_p^2 = 0.001$]. The three-way interaction between tDCS condition, time and body orientation was not significant [$F_{2, 220} = 0.32, p = 0.72, \eta_p^2 = 0.003$]. Contrasts tests revealed that the PU over a grey background is significantly smaller and therefore shifted more leftward from the body orientation when RSD ($p < 0.0001, RSD = -36.2^\circ \pm 1.92^\circ, upright = -12.0^\circ \pm 1.46^\circ$). The average PU over grey background was summarized for each tDCS condition, time, and body orientation (Table 5).

Table 5. Average perceptual upright (PU) over a grey (unpolarized) visual background by tDCS condition, time and body orientation. Standard error (s.e.) is listed for each averaged PU.

tDCS Condition	Time	Body Orientation	PU (relative to body)	SE
Sham	Pre-VR	Upright	-11.09°	2.59°
	Pre-VR	RSD	-34.81°	4.45°
Sham	Post-VR	Upright	-14.70°	4.54°
	Post-VR	RSD	-36.47°	4.40°
Anodal	Pre-VR	Upright	-13.61°	4.28°
	Pre-VR	RSD	-38.58°	4.58°
Anodal	Post-VR	Upright	-13.38°	3.81°
	Post-VR	RSD	-38.56°	4.50°
Cathodal	Pre-VR	Upright	-10.76°	2.42°
	Pre-VR	RSD	-36.16°	4.25°
Cathodal	Post-VR	Upright	-8.54°	3.56°
	Post-VR	RSD	-32.86°	6.21°

3.1.3.3 Sham Grey Background PU Analysis

The same sample of 21 participants was used in an analysis of the sham data over the grey background. A Shapiro-Wilk test indicated a violation of normality in the residuals; therefore, a two-way repeated measures ART ANOVA was conducted to examine the effect of time and body orientation on PU in the sham condition. All factors were treated as repeated measures. The two-way repeated measures ART ANOVA revealed a significant main effect of body orientation [$F_{1, 60} = 97.25, p < 0.0001, \eta_p^2 = 0.62$]. There was no significant main effect of time [$F_{1, 60} = 0.15, p = 0.70, \eta_p^2 = 0.002$] and no significant interaction between time and body orientation [$F_{1, 60} =$

0.02, $p = 0.89$, $\eta_p^2 < 0.0001$]. Contrasts tests revealed that the PU over a grey background is significantly smaller and therefore shifted more leftward from the body orientation when RSD ($p < 0.0001$, $RSD = -35.6^\circ \pm 3.09^\circ$, upright = $-12.9^\circ \pm 2.60^\circ$). The grey background PU data is represented on Figure 17 relative to the visual background PU data.

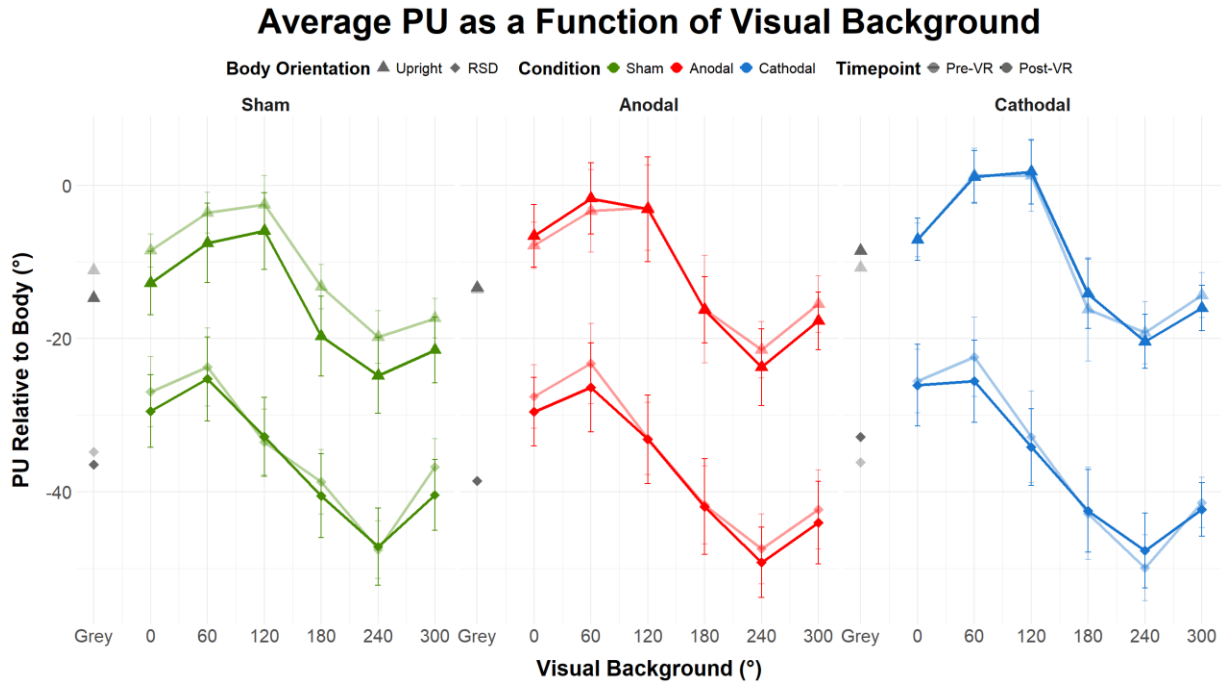


Figure 17. Average perceptual upright (PU) as a function of background including grey background PU data. Error bars represent standard error.

3.1.3.4 Visual Effect

The visual effect was calculated to quantify the effect of vision on OCHART responses without using the vector sum model. The visual effect quantifies the strength of the visual background's effect on PU by looking at the maximum PU (least shifted) and minimum PU (most shifted) at the individual level (Jenkin et al., 2011). Average visual background orientations for the maximum and minimum PU are listed in Table 6 and average visual effects are listed in Table 7. The equation for the visual effect is shown below (Equation 7).

Equation 7. Visual effect calculation. PU = perceptual upright.

$$visual\ effect = PU\ max - PU\ min$$

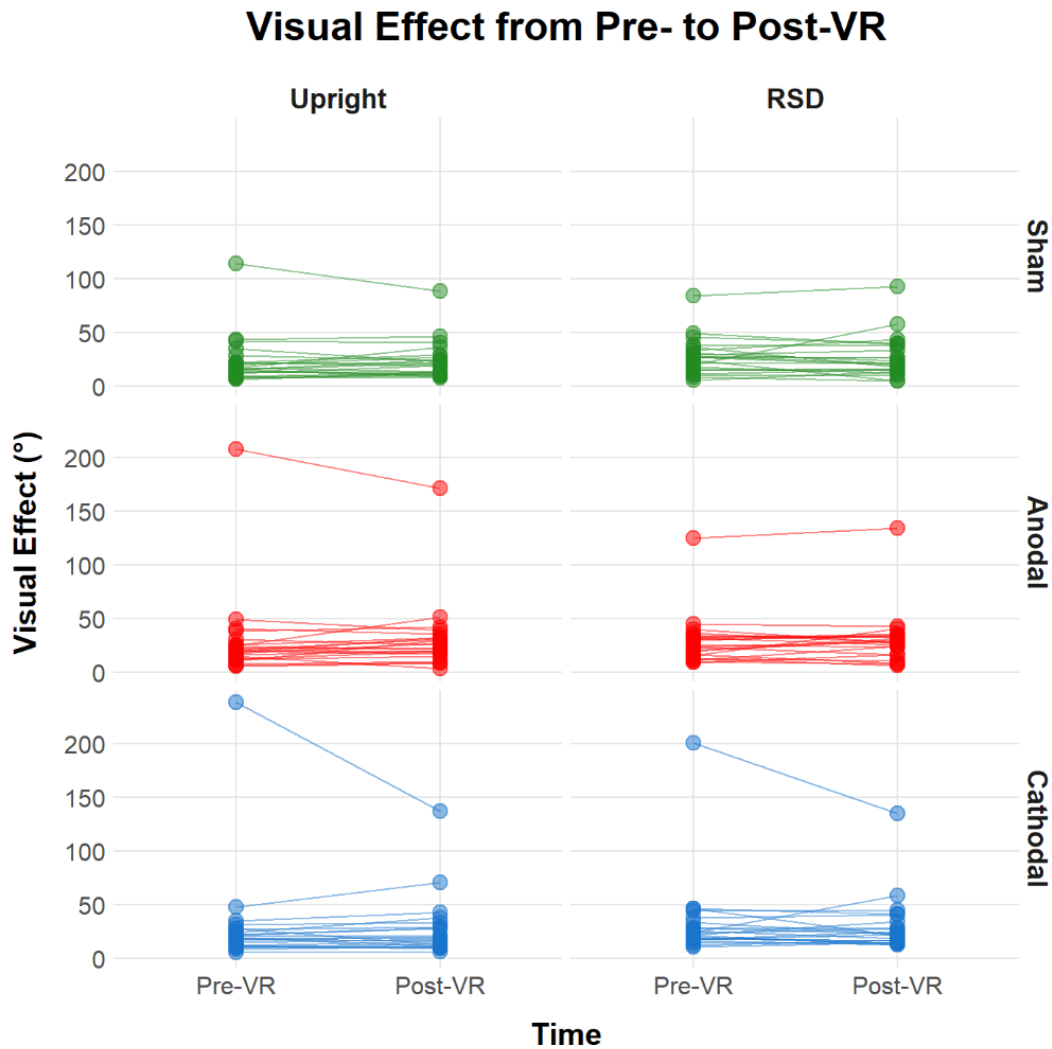


Figure 18. The visual effect across time, body orientation and stimulation condition. Data belonging to the same participant is connected by a line.

Table 6. Mean and standard deviation of visual backgrounds at which participants displayed their maximum and minimum PU.

Condition	Time	Body Orientation	PU Type	Visual Background Mean \pm SD (°)
Sham	Pre-VR	Upright	Max	84.5 \pm 54.5
			Min	245 \pm 41
Sham	Pre-VR	RSD	Max	73.6 \pm 84.7
			Min	218 \pm 62.9

Sham	Post-VR	Upright	Max	87.3 ± 44.3
			Min	248 ± 38.4
Sham	Post-VR	RSD	Max	65.5 ± 71.5
			Min	240 ± 45.4
Anodal	Pre-VR	Upright	Max	98.2 ± 60.1
			Min	221 ± 70.2
Anodal	Pre-VR	RSD	Max	76.4 ± 89.2
			Min	226 ± 45.1
Anodal	Post-VR	Upright	Max	90 ± 63.5
			Min	243 ± 47.1
Anodal	Post-VR	RSD	Max	60 ± 61.4
			Min	240 ± 52.4
Cathodal	Pre-VR	Upright	Max	95.5 ± 57.5
			Min	224 ± 81.1
Cathodal	Pre-VR	RSD	Max	54.5 ± 71.5
			Min	237 ± 39.2
Cathodal	Post-VR	Upright	Max	98.2 ± 54.1
			Min	235 ± 63.9
Cathodal	Post-VR	RSD	Max	40.9 ± 65.2
			Min	224 ± 46

All 22 participants were included in the visual effect analysis. A Shapiro-Wilk test indicated a violation of normality in the residuals therefore a three-way repeated measures ART ANOVA was conducted to examine the effect of time, body orientation and tDCS condition on the visual effect. All factors were treated as repeated measures. The three-way repeated measures ART ANOVA revealed a significant main effect of body orientation [$F_{1,231} = 16.08, p < 0.0001, \eta^2 = 0.065$]. There was no significant main effect of time [$F_{1,231} = 1.05, p = 0.31, \eta^2 = 0.005$] or tDCS condition [$F_{2,231} = 2.13, p = 0.12, \eta^2 = 0.018$]. The following interactions were not significant: tDCS condition and time [$F_{2,231} = 0.77, p = 0.46, \eta^2 = 0.007$], tDCS condition and body orientation [$F_{2,231} = 0.17, p = 0.84, \eta^2 = 0.001$], time and body orientation [$F_{1,231} = 1.58, p = 0.21, \eta^2 = 0.007$] and the three-way interaction between tDCS condition, time and body

orientation [$F_{2,231} = 0.13, p = 0.88, \eta_p^2 = 0.001$]. Contrast tests revealed that the visual effect is significantly larger when RSD compared to upright ($p = 0.0001, RSD = 29.8^\circ \pm 2.23^\circ, \text{upright} = 27.7^\circ \pm 2.87^\circ$) suggesting a larger reliance on visual information when body and gravity cues are not in alignment (Figure 18).

3.1.4 Hypothesis 2 – tDCS Condition Cybersickness Relative to Sham

The second hypothesis proposed that anodal tDCS during VR would result in lower cybersickness relative to sham and that cathodal tDCS during VR would result in greater cybersickness relative to sham. To examine pre-post changes in sickness, pre-VR FMS scores were compared to post-VR FMS score. The post-VR FMS score could either be the score upon completion of the 20-minute VR session or, in the case that the participant dropped out of the VR session, their score upon stopping the VR session. A Shapiro-Wilk test revealed non-normal distribution of the residuals for pre-VR and post-VR FMS scores therefore a two-way repeated measures ART ANOVA was used to determine the effects of tDCS condition and time on FMS. The factors tDCS condition and time were treated as repeated measures. The ART ANOVA revealed a significant main effect of time [$F_{1,105} = 156.59, p < 0.0001, \eta_p^2 = 0.60$] and tDCS condition [$F_{2,105} = 4.57, p = 0.013, \eta_p^2 = 0.080$]. The interaction between time and tDCS condition was not significant [$F_{2,105} = 1.12, p = 0.33, \eta_p^2 = 0.021$]. The ART contrast tests for time revealed that pre-VR FMS was significantly less than post-VR FMS ($p < 0.0001, \text{pre-VR} = 0.53 \pm 0.12, \text{post-VR} = 5.29 \pm 0.50$). Further, the ART contrast tests for tDCS condition revealed that cathodal FMS was significantly less than sham FMS ($p = 0.0093, \text{cathodal} = 2.45 \pm 0.53, \text{sham} = 3.32 \pm 0.61$). Average pre-VR and post-VR FMS scores are presented in Figure 19.

Table 7. Mean visual effect across body orientations, tDCS conditions and time. SE = standard error.

Body Orientation	tDCS Condition	Time	Mean	SE
Upright	Sham	Pre	23.4°	4.87°
		Post	24.0°	3.79°
Upright	Anodal	Pre	29.8°	8.8°
		Post	31.3°	7.13°
Upright	Cathodal	Pre	30.1°	10.1°
		Post	27.7°	6.04°

RSD	Sham	Pre	27.8°	3.64°
		Post	27.2°	4.22°
RSD	Anodal	Pre	29.4°	5.04°
		Post	30.7°	5.40°
RSD	Cathodal	Pre	33.4°	8.26°
		Post	30.4°	5.60°

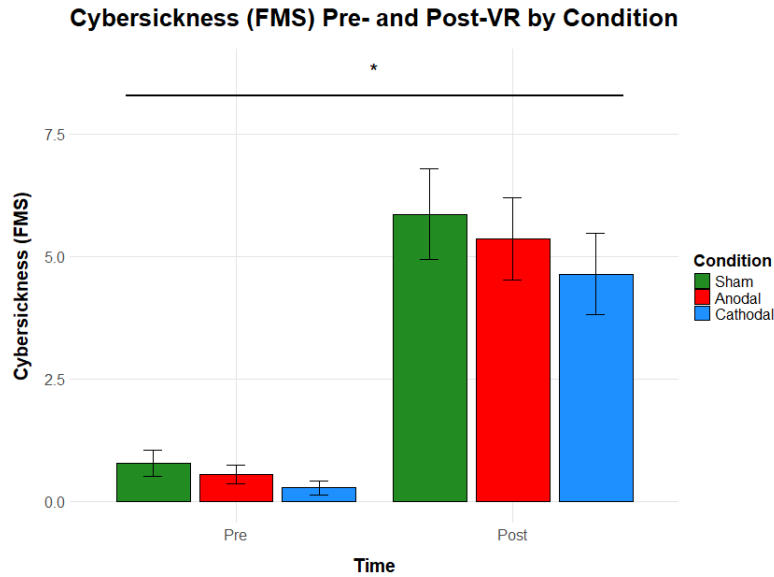


Figure 19. Fast Motion Sickness (FMS) cybersickness comparison of pre-VR to post-VR across tDCS conditions. Error bars represent standard error.

3.1.4.1 Cybersickness Progression Across tDCS Conditions

The four participants who dropped out before the full 20-minute VR exposure in at least one tDCS condition were excluded from the analysis (n=18). Drop out days and conditions are summarized on Table 8 below. The change in FMS (ΔFMS) was calculated by subtracting the participants baseline score (pre-VR) from each subsequent score (Equation 8).

Equation 8. Change in Fast Motion Sickness (ΔFMS_x) scores were calculated by subtracting the pre-VR FMS score (FMS_1) from the FMS score at the time point of interest (FMS_x).

$$\Delta FMS_x = FMS_x - FMS_1$$

Table 8. Number of participants in each condition on each day and number of dropouts in the total sample in the total sample (n=22).

Day	Condition	n	Dropouts
Day 1	Sham	7	3
	Anodal	9	0
	Cathodal	6	1
Day 2	Sham	10	0
	Anodal	7	0
	Cathodal	5	1
Day 3	Sham	5	0
	Anodal	6	0
	Cathodal	11	0

Table 9. Mean Fast Motion Sickness (FMS) and standard error (SE) for each time point averaged across all tDCS conditions.

Time point	Mean	Standard Error
0 minutes	0.54	± 0.13
2 minutes	1.52	± 0.26
4 minutes	2.00	± 0.25
6 minutes	2.52	± 0.28
8 minutes	2.83	± 0.34
10 minutes	3.11	± 0.32
12 minutes	3.52	± 0.37
14 minutes	3.83	± 0.42
16 minutes	3.96	± 0.43
18 minutes	4.04	± 0.40
20 minutes	4.26	± 0.43

Change in Cybersickness (FMS) Across Time by Condition

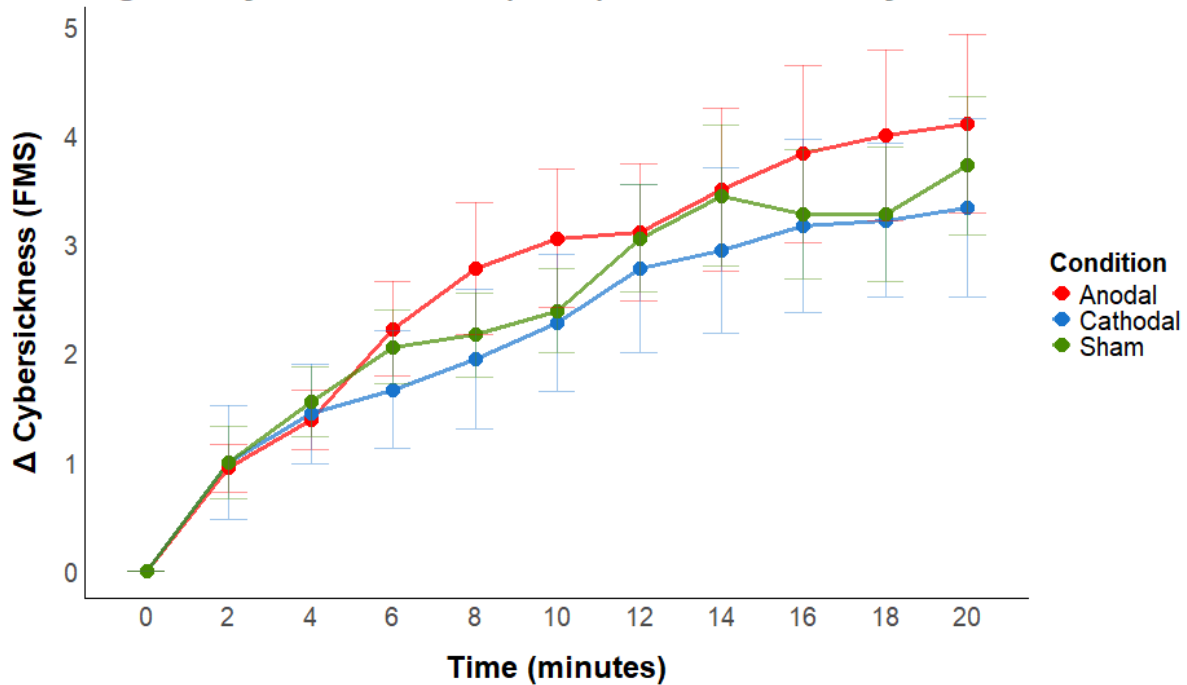


Figure 20. Average change in Fast Motion Sickness (FMS) across 2-minute time points during VR by tDCS condition. Error bars represent standard error.

The average Δ FMS scores across each 2-minute time point in each tDCS condition are represented in Figure 20. A Shapiro-Wilk test confirmed the normality of residuals within Δ FMS. Therefore, a two-way repeated measures ANOVA was used to investigate the effect of tDCS condition and time point on Δ FMS. The factors tDCS condition and time were treated as repeated measures. Mauchly's test for sphericity indicated violations of sphericity for the main effect of time and the interaction between tDCS condition and time; therefore, Greenhouse Geisser corrections were applied to these effects. The two-way repeated measures ANOVA revealed a significant main effect of time point [$F_{10,170} = 21.86$, $\epsilon = 0.17$, $p < 0.001$, $\eta_p^2 = 0.56$] and a non-significant main effect of tDCS condition [$F_{2,34} = 0.65$, $p = 0.53$, $\eta_p^2 = 0.037$]. The interaction between tDCS condition and time point was not significant [$F_{20,340} = 0.75$, $\epsilon = 0.31$, $p = 0.61$, $\eta_p^2 = 0.042$]. Mean and standard error for average Δ FMS at each time are reported in Table 9 and contrast test results for the main effect of time point are summarized in Table 10.

Table 10. Contrast tests for the effect of time point on change in Fast Motion Sickness (Δ FMS).

Comparison	<i>p</i>
0 minutes < 2,4,6,8,10,12,14,16,18,20 minutes	<0.0001
2 minutes < 4 minutes	0.006
2 minutes < 6,8,10,12,14,16,18,20 minutes	<0.0001
4 minutes < 6 minutes	0.02
4 minutes < 8 minutes	0.016
4 minutes < 10 minutes	0.00082
4 minutes < 12,14,16,18,20 minutes	<0.0001
6 minutes < 8 minutes	1.00 (ns)
6 minutes < 10 minutes	0.071 (ns)
6 minutes < 12,14,18,20 minutes	<0.0001
6 minutes < 16 minutes	0.00016
8 minutes < 10 minutes	1.00 (ns)
8 minutes < 12 minutes	0.004
8 minutes < 14 minutes	0.00011
8 minutes < 16 minutes	0.00022
8 minutes < 18 minutes	0.00017
8 minutes < 20 minutes	0.000058
10 minutes < 12 minutes	0.97 (ns)
10 minutes < 14,16,18,20 minutes	0.008
10 minutes < 16 minutes	0.006
10 minutes < 18 minutes	0.002
10 minutes < 20 minutes	0.00086
12 minutes < 8,9,10 minutes	1.00 (ns)
12 minutes < 20 minutes	0.25 (ns)
14 minutes < 16,18,20 minutes	1.00 (ns)
16 minutes < 18,20 minutes	1.00 (ns)
18 minutes < 20 minutes	1.00 (ns)

There was a significant increase in sickness from 0 minutes to 2 minutes, 2 minutes to 4 minutes and 4 minutes to 6 minutes, suggesting the largest progression of sickness took place within the first 6 minutes of the VR exposure.

3.1.4.2 tDCS Condition Cybersickness Order Effects

For all tDCS conditions, FMS was collected every 2 minutes starting before participants entered VR until the end of their 20-minute exposure (11 time points). Four participants dropped out on the first day of their study and only one of the 4 participants had an additional drop-out on the second day of the study. All four participants dropped out on the sham day ($M = 11.6$ minutes, $SD = 3.14$ minutes) and one participant dropped out on the cathodal day at 7 minutes. In the three participants who only dropped out once, their first day was the sham condition. In the participant who dropped out twice, their first day was the cathodal condition and their second day was the sham condition. No participants dropped out on the anodal stimulation days. Further, due to logistical constraints and participant dropouts, there was an unequal number of participants receiving each tDCS condition on each day. Day, tDCS condition assignment and dropout frequency are summarized in Table 8. These results prompted an investigation into how ordering of the days influenced participant cybersickness. Previous research suggests that cybersickness severity decreases with repeated exposure to the same VR content, therefore two additional analyses were conducted to investigate order effects on pre-VR and post-VR sickness across testing days and order effects of cybersickness progression across testing days (Chang et al., 2020).

Order effects of pre-VR and post-VR cybersickness were investigated for all participants ($n=22$). A Shapiro-Wilk test confirmed non-normality of residuals within Δ FMS. Therefore, a two-way repeated measures ART ANOVA was used to investigate the effect of time and day on FMS. The factors day and time were treated as repeated measures. The two-way repeated measures ART ANOVA revealed a significant main effect of time [$F_{1,105} = 193.58, p < 0.001, \eta_p^2 = 0.65$] and day [$F_{2,105} = 4.76, p = 0.01, \eta_p^2 = 0.083$]. The interaction between time and day was also significant [$F_{2,105} = 3.23, p = 0.043, \eta_p^2 = 0.06$]. Contrast tests confirmed no significant differences between pre-VR FMS across any combinations of Day 1 and Day 2 ($p = 1.00$, Day 1 = 0.55 ± 0.21 , Day 2 = 0.68 ± 0.27), Day 1 and Day 3 ($p = 0.9977$, Day 1 = 0.55 ± 0.21 , Day 3 = 0.36 ± 0.14) or Day 2 and Day 3 ($p = 0.9961$, Day 2 = 0.68 ± 0.27 , Day 3 = 0.36 ± 0.14). Contrast tests also confirmed no significant differences between post-VR FMS for Day 1 and Day 2 ($p = 0.3832$, Day 1 = 6.14 ± 0.83 , Day 2 = 4.86 ± 0.96), Day 1 and Day 3 ($p = 0.6958$, Day 1 = $6.14 \pm$

0.83, Day 3 = 4.86 ± 0.79) and Day 2 and Day 3 ($p = 0.9964$, Day 2 = 4.86 ± 0.96 , Day 3 = 4.86 ± 0.79). All contrast test results for the interaction between time and day are summarized in Table 11.

Table 11. Contrast tests for the interaction of time and day on change in Fast Motion Sickness (Δ FMS) in VR.

Comparison	<i>p</i>
Post Day 1 vs Pre Day 1	<0.0001
Post Day 1 vs Pre Day 2	
Post Day 1 vs Pre Day 3	
Post Day 2 vs Pre Day 1	
Post Day 2 vs Pre Day 2	
Post Day 2 vs Pre Day 3	
Post Day 3 vs Pre Day 1	
Post Day 3 vs Pre Day 2	
Post Day 3 vs Pre Day 3	
Post Day 1 vs Post Day 2	0.3832 (ns)
Post Day 1 vs Post Day 3	0.6958 (ns)
Pre Day 2 vs Pre Day 3	0.9961 (ns)
Post Day 2 vs Post Day 3	0.9964 (ns)
Pre Day 1 vs Pre Day 3	0.9977 (ns)
Pre Day 1 vs Pre Day 2	1.00 (ns)

Next order effects of Δ FMS progression were investigated across the testing days for all participants who did not drop out ($n=18$). A Shapiro-Wilk test confirmed the normality of residuals within Δ FMS. Therefore, a two-way repeated measures ANOVA was used to investigate the effect of day and time point on Δ FMS. The factors day and time point were treated as repeated measures. The two-way repeated measures ANOVA revealed a significant main effect of time point [$F_{10,170} = 21.86$, $\epsilon = 0.17$, $p < 0.001$, $\eta_p^2 = 0.56$], a non-significant main effect of day [$F_{2,34} = 1.2$, $p = 0.3$, $\eta_p^2 = 0.066$] and non-significant interaction of time point and day [$F_{20,340} = 1.57$, $p = 0.058$, $\eta_p^2 = 0.084$]. Contrast tests for the significant effect of time point on Δ FMS can be found in Table 10.

3.1.4.3 Time in VR by Day and Condition

Next data from all participants ($n=22$) was used to investigate the effects of day and condition on time spent in VR. A Shapiro-Wilk test confirmed non-normality of residuals within time in VR. Therefore, a two-way repeated measures ART ANOVA was used to investigate the effects of day and condition on time in VR. The factors of day and condition were treated as repeated measures. The two-way repeated measures ART ANOVA revealed a significant main effect of condition [$F_{2,38.14} = 23.78, p < 0.0001, \eta_p^2 = 0.55$] and no significant main effect of day [$F_{2,37.77} = 1.99, p = 0.15, \eta_p^2 = 0.095$]. The interaction between condition and day was also significant [$F_{4,4.88} = 4.87, p = 0.0019, \eta_p^2 = 0.26$]. Contrast tests revealed that participants spent significantly more time in VR if day 1 was the anodal condition than if day 1 was the sham condition ($p = 0.0312$, anodal = 20min \pm 0, $n = 9$, sham = 17.1min \pm 1.4, $n = 7$). Therefore, participants were more likely to stop the VR exposure prematurely if the first day was the sham condition than if it was an anodal condition (Figure 21). Any other significant contrast tests were not of interest as they did not have a shared condition or day. All contrast test results are summarized in Table 12.

Next, we investigated if the difference in time spent in VR in the anodal day 1 and sham day 1 participants extended to differences in ABS Δ Cue Weights on day 1. The Shapiro-Wilk test confirmed the normality of residuals within day 1 ABS Δ Cue Weights. Therefore, a two-way mixed effects ANOVA was used to investigate the effects of tDCS condition and sensory modality on ABS Δ Cue Weights. The factor tDCS condition was treated as a between subjects' factor and the factor sensory modality was treated as a repeated measure.

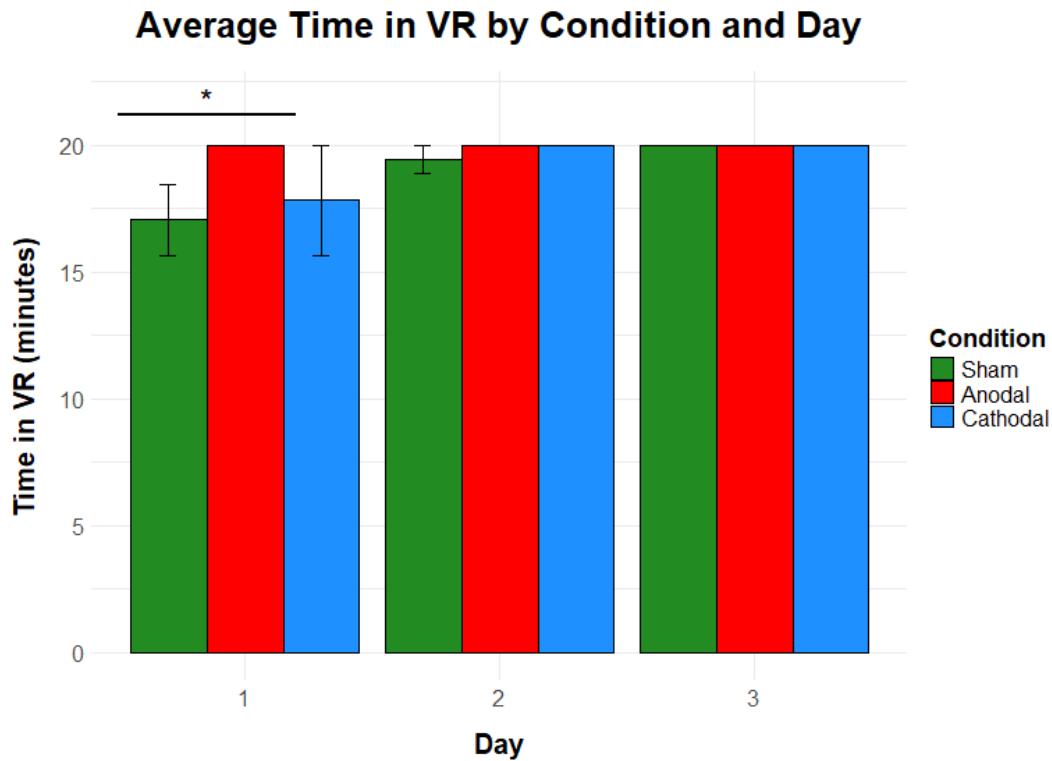


Figure 21. Average time spent in virtual reality (VR) across transcranial direct current stimulation (tDCS) conditions and study days. Participant dropouts only occurred on days 1 and 2 of the study in the sham and cathodal conditions. No participants dropped out in the anodal condition. Error bars represent standard error.

The two-way mixed effects ANOVA revealed a non-significant main effect of sensory modality trending toward significance [$F_{2,22} = 4.26$, $\epsilon = 0.53$, $p = 0.06$, $\eta_p^2 = 0.11$], and a non-significant main effect of tDCS condition [$F_{1,11} = 1.73$, $p = 0.21$, $\eta_p^2 = 0.09$]. The interaction between condition and sensory modality was also non-significant [$F_{2,22} = 1.84$, $\epsilon = 0.53$, $p = 0.20$, $\eta_p^2 = 0.05$]. Therefore, differences in time spent in VR between sham day 1 and anodal day 1 groups were not reflected in the ABS Δ Cue Weights between groups. The trend toward significance for the main effect of sensory modality is unsurprising given earlier analyses which found an increased ABS Δ Cue Weight for gravity and body cues relative to vision cues.

Finally, we investigated if the difference in time spent in VR in the anodal day 1 and sham day 1 participants extended to differences in Δ Cue Weights on day 1. A Shapiro-Wilk test confirmed the non-normality of residuals within Δ Cue Weights. Therefore, a two-way mixed

effects ART ANOVA was used to investigate the effects of condition and sensory modality on Δ Cue Weights. The factor condition was treated as a between subjects' factor and the factor sensory modality was treated as a repeated measure. The two-way mixed effects ART ANOVA revealed a non-significant main effect of condition [$F_{1,11} = 0.01, p = 0.91, \eta_p^2 = 0.001$] and non-significant main effect of sensory modality [$F_{2,22} = 1.74, p = 0.20, \eta_p^2 = 0.14$]. The interaction between condition and sensory modality was also not significant [$F_{2,22} = 0.79, p = 0.47, \eta_p^2 = 0.07$]. Therefore, differences in time spent in VR between the sham day 1 and anodal day 1 groups were not reflected in the Δ Cue Weights between groups.

Table 12. Contrast tests for the interaction of tDCS condition and day on time in VR.

Comparison	<i>p</i>
Cathodal Day 3 > Sham Day 1	0.012
Anodal Day 3 > Sham Day 1	0.0197
Anodal Day 2 > Sham Day 1	0.0283
Anodal Day 1 > Sham Day 1	0.0312
Cathodal Day 2 > Sham Day 1	0.0582 (ns)
Sham Day 3 > Sham Day 1	0.103 (ns)
Sham Day 2 > Sham Day 1	0.117 (ns)
Cathodal Day 1 > Sham Day 1	0.5222 (ns)
Cathodal Day 1 > Anodal Day 3	0.8518 (ns)
Cathodal Day 3 > Cathodal Day 1	0.9657 (ns)
Anodal Day 1 > Cathodal Day 1	0.9712 (ns)
Cathodal Day 2 > Cathodal Day 1	0.9733 (ns)
Anodal Day 2 > Cathodal Day 1	0.9768 (ns)
Anodal Day 3 > Sham Day 2	0.9786 (ns)
Sham Day 3 > Cathodal Day 1	0.9846 (ns)
Cathodal Day 3 > Sham Day 2	0.9983 (ns)
Anodal Day 1 > Sham Day 2	0.9986 (ns)
Cathodal Day 2 > Sham Day 2	0.9988 (ns)
Anodal Day 2 > Sham Day 2	0.9996 (ns)
Sham Day 2 > Cathodal Day 1	0.9996 (ns)
Sham Day 3 > Sham Day 2	0.9998 (ns)

Sham Day 3 > Cathodal Day 3, Anodal Day 3	1.00 (ns)
Anodal Day 1 > Anodal Day 2, Sham Day 3, Cathodal Day 3	
Anodal Day 3 > Sham Day 3, Cathodal Day 2,3, Anodal Day 1,2	
Cathodal Day 2 > Sham Day 3, Cathodal Day 3, Anodal Day 1,2	
Cathodal Day 3 > Anodal Day 2, 3	

3.1.5 Sensory Reweighting and Cybersickness Modelling

3.1.5.1 Linear Mixed Model – Change in PU and Change in FMS

A linear mixed model was used to investigate the association between absolute Δ PU over a grey background in the RSD orientation and Δ FMS. Ideally a comparison between Δ Cue Weight and Δ FMS could also be investigated; however, cue weights were not well estimated by the vector sum model at the individual level. Instead, the absolute Δ PU was used as a measure of sensory reweighting to investigate the association between sensory reweighting and cybersickness.

Homoscedasticity and normality of residuals were confirmed through their respective plots. The results of the linear mixed model are summarized in Table 13. The model intercept indicated that in the sham condition, the average Δ FMS was 5.03 (95% CI [2.93,7.13]) when the absolute Δ PU was 0. The standard deviation for the random intercept (SD = 3.63) suggests moderate variability in Δ FMS in the sham condition. The linear mixed model revealed no meaningful association between absolute Δ PU and Δ FMS in the sham condition ($\beta = -0.009$, 95% CI [-0.124, 0.107]). The interaction in the anodal condition suggests a moderate trend where larger absolute Δ PU was associated with smaller Δ FMS ($\beta = -0.170$, 95% CI [-0.362, 0.022]). For the cathodal condition, the interaction in absolute Δ PU and Δ FMS did not suggest any association ($\beta = 0.003$, CI [-0.164, 0.171]; Figure 22).

Next, 3-parameter Gaussian regression models were used to investigate the relationship between Δ FMS and Δ PU. Only grey background data was used for the Δ PU. The Gaussian regression models were fit to the Δ FMS for each tDCS condition as a function of Δ PU for each body's orientation.

Table 13. Results of a linear mixed model on the association between the absolute change in PU (absolute Δ PU) over a grey background in the right side down (RSD) orientation and change in FMS (Δ FMS). SE = standard error, CI = confidence interval, SD = standard deviation.

	Coefficient (β)	SE	95% CI (lower)	95% CI (upper)	Random effect SD
Sham Intercept	5.03	1.04	2.93	7.13	3.63
Sham Slope	-0.009	0.057	-0.124	0.107	
Anodal vs Sham intercepts	0.80	0.95	-1.13	2.73	
Cathodal vs Sham intercepts	-0.70	0.95	-2.63	1.22	
Δ PU * Anodal Condition	-0.170	0.095	-0.362	0.0218	
Δ PU * Cathodal Condition	0.003	0.083	-0.164	0.171	

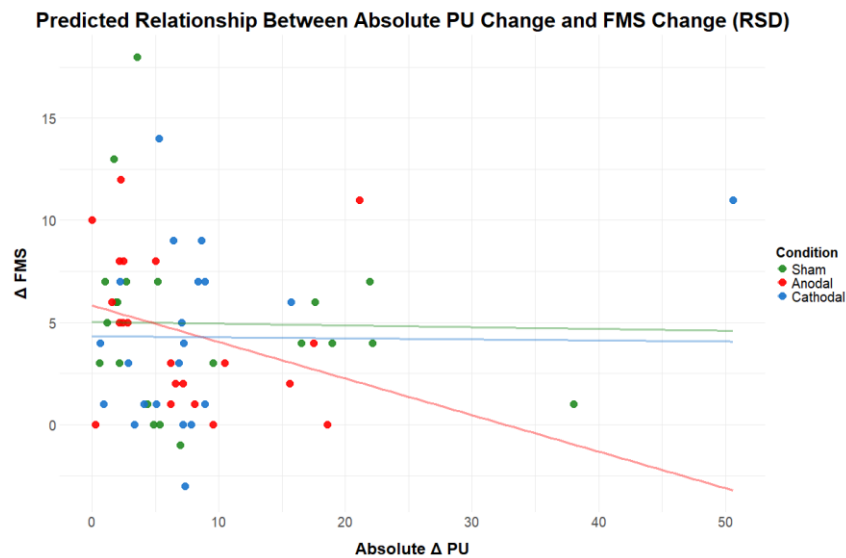


Figure 22. Estimated association between absolute change in perceptual upright (PU) change and Fast Motion Sickness scale (FMS) change for right side down (RSD) grey background data.

The Gaussian regression models revealed that Δ PU in the sham upright [$(R^2 = 0.08)$, $F_{3,18} = 0.78$, $p = 0.47$], sham RSD [$(R^2 = 0.04)$, $F_{3,18} = 0.4$, $p = 0.67$], anodal upright [$(R^2 = 0.01)$, $F_{3,18} = 0.1$, $p = 0.9$] anodal RSD [$(R^2 = 0.06)$, $F_{3,18} = 0.62$, $p = 0.55$] or cathodal upright [$(R^2 = 0.25)$, $F_{3,18} = 3.02$, $p = 0.07$], cathodal RSD [$(R^2 = 0.15)$, $F_{3,18} = 1.6$, $p = 0.23$] tDCS conditions did not have any significant predictive effects on Δ FMS (Figure 23).

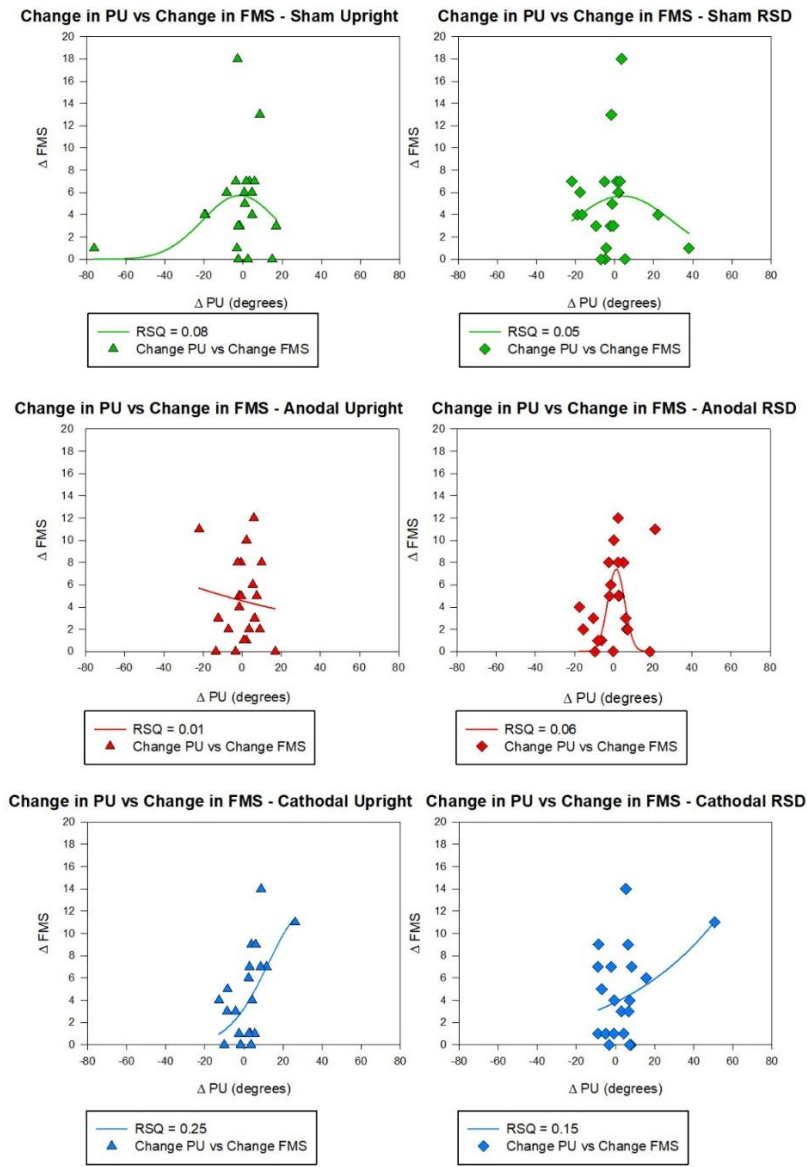


Figure 23. 3-parameter Gaussian regression models of change in FMS (Δ FMS) as a function of change in PU (Δ PU) for right side down (RSD) grey background data across all tDCS conditions.

4.1 Discussion

This study aimed to investigate the effects of the rTPJ on sensory reweighting and cybersickness. Under sensory conflict theory, motion sickness is thought to manifest under conditions where visual, vestibular and proprioceptive cues are in conflict – this theory extends to cybersickness in VR. Through sensory reweighting, our CNS can rely on previous experience and expectations to

reweigh our reliance on certain sensory cues and maintain a veridical perception of the environment. Sensory reweighting is essential for postural control and perception in noisy conditions and inefficient sensory reweighting is associated with postural instability, motion sickness or cybersickness. Previous research has shown that greater changes in the SVV are associated with less susceptibility to cybersickness following a high intensity VR exposure (Chung & Barnett-Cowan, 2023). A separate study found that anodal tDCS to the rTPJ prior to an intense VR exposure reduced disorientation cybersickness symptoms and postural instability relative to a sham condition (Takeuchi et al., 2018). Taken together, these studies point toward sensory reweighting as a cybersickness mitigation strategy, with possible contributions from the rTPJ. The results of the present study are in contrast with previous findings however.

Hypothesis 1 stated that the rTPJ is involved in sensory reweighting and therefore anodal tDCS of the rTPJ would result in more efficient sensory reweighting observed as a greater change in vision (visual), gravity (vestibular) and body (proprioceptive) sensory cues relative to the sham condition. Under this same hypothesis, it was hypothesized that cathodal tDCS of the rTPJ would result in less efficient sensory reweighting observed as a smaller change in vision, gravity, and body sensory cues relative to the sham condition. To test this hypothesis, we examined the effect of tDCS condition and sensory modality on absolute change in cue weight. No significant differences were observed across tDCS conditions when investigating Δ Cue Weight or Δ Cue Weight. This suggests that anodal and cathodal tDCS to the rTPJ during VR did not significantly alter cue weights post-VR within this sample of participants.

The second aim of this study was to investigate the effects of anodal and cathodal tDCS on cybersickness (FMS) outcomes. Informed by previous research by Takeuchi and colleagues (2018), we hypothesized that anodal stimulation would decrease cybersickness FMS relative to sham stimulation. It was also hypothesized that cathodal stimulation would increase cybersickness relative to sham stimulation. When comparing post-VR FMS scores between tDCS conditions, no significant differences between the sham and tDCS conditions were found. Further, no differences in the Δ FMS across tDCS conditions were observed across cybersickness progression. Within our sample, there is limited evidence to suggest that tDCS to the rTPJ during VR alters cybersickness outcomes. Further, our data suggests no association or relationship

between grey RSD Δ PU and Δ FMS across tDCS conditions. Using a similar modelling approach to previous work which did observe a relationship between sensory reweighting on the SVV and cybersickness, similar trends in data distribution were observed within our data set however statistical significance was not reached..

4.1.1 Hypothesis 1 - No Change in Cue Weights across tDCS Conditions

To confirm consistency in baseline cue weights, differences in pre-VR cue weights across tDCS conditions were investigated. It was important to confirm that pre-VR Cue Weights within a sensory modality across tDCS conditions did not differ so that comparisons could be made between pre-VR and post-VR scores across tDCS conditions. No significant differences were found between pre-VR Cue Weights for any of the vision, body or gravity cues across tDCS conditions. This confirms that pre-VR, participant cue weight reliance did not significantly differ between the three testing days.

At the individual level, cue weights for each sensory modality also did not differ pre-VR across the tDCS conditions. This confirms that participants were entering the VR exposures with comparable baseline cue weights across all three days for all three tDCS conditions. Surprisingly, there were no differences in ABS Δ Cue Weight across sensory modalities in the sham condition nor the tDCS conditions. Across all tDCS conditions however, there was a larger change in reliance on body and gravity cues relative to the vision cues. Greater shifts in the body and gravity cue weight reliance suggest that the largest changes in sensory weights post-VR are a trade-off between reliance on body cues and reliance on gravity cues. The non-absolute Δ Cue Weights, however, did not differ across sensory modalities between the three conditions, though visual trends suggest that an increased reliance on gravity cues and a decreased reliance on body cues may occur post-VR.

4.1.1.1 Cue Weight Change Trends for Averaged Data

Participant responses on the OCHART may vary between trials and while this issue is mitigated through repeated trials, the risk cannot be eliminated entirely. When participant responses do not change in a predictable way across visual backgrounds and body orientations, the vector sum model cannot effectively estimate the sensory vectors from the PUs. Therefore, the averaged PU

values across all participants were used to generate one set of sensory vector estimates for the entire sample.

In examining the modelled average PU data, we can observe the weighted vectors contributing to the internal representation of upright orientation. Pre-VR cue weights showed a larger reliance on bodily and gravity cues at baseline in the sham (vision =12%, body = 52%, gravity =36%), anodal (vision =12.9%, body = 50.5% and gravity= 36.6%) and cathodal (vision = 14.4%, body = 49.6% and gravity = 36%) conditions. This reliance on body and gravity cues was preserved post-VR across the sham (vision = 12.2%, body = 50.9%, gravity = 36.9%), anodal (vision = 13.2%, body = 49.3% and gravity = 37.5%), and cathodal (vision = 13.6%, body = 49.7% and gravity = 36.7%) conditions.

Previous research which applied the vector sum model to the averaged PU data also found evidence for a strong reliance on bodily cues for the OCHART. In one group of older adults, perception for the OCHART was similarly dominated by body cues (62%) followed by gravity cues (25%) and finally vision cues (13%; Fraser et al., 2018). By contrast, other studies have found evidence for a larger relative reliance on visual cues (Barnett-Cowan et al., 2013; Dyde et al., 2006). In a study by Barnett-Cowan and colleagues (2013), the vector sum model was fit to pooled PU data across four body postures (30°,45°,60°, and 120°) and found a large contribution of body cues (60%) followed by vision cues (27%) and gravity cues (13%). Similarly, Dyde and colleagues (2006) found a large contribution of body cues (54%) followed by vision (25%) and gravity cues (21%). Notably, the vision cue weights in the present study are smaller than those of previous studies. Further, across all tDCS conditions, there was minimal change observed in the cue weight of vision ($\leq 0.8\%$). This result was surprising as previous research has found evidence for a decrease in reliance on visual cues following VR when measuring postural control (Akizuki et al., 2005; Nishiike et al., 2013; Warchoł et al., 2024). The lack of difference in visual cue weights may point toward a limitation in how visual vectors have been calculated for this study.

The present study uses a modified shortened version of the OCHART to maximize the potential of capturing transient post-VR effects. The OCHART used in this study uses 24 letter probe orientations (rotated at 15° increments), 7 backgrounds (1 grey, 6 visual rotated at

30° increments) and each combination was presented 8 times resulting in total of 1344 trials (24 x 7 x 8). By contrast, previous work by Barnett-Cowan and colleagues (2013) used 24 letter probe orientations (rotated at 15° increments) paired with 19 background options (1 grey, 18 visual rotated at 22.5° increments) with each combination presented 8 times for a total of 3648 (24 x 18 x 8) trials. Work by Dyde and colleagues (2006) used 18 letter probe orientations (15° intervals from 30° to 150° and -30° to -150°) paired with 19 background options (1 grey, 18 visual rotated at 22.5° increments) and each combination was presented 7 times for a total of 2394 (18 x 19 x 7) trials. Our study design included fewer visual backgrounds and therefore less data points per body orientation for the vector sum modelling which may have decreased the accuracy of the visual vector estimate.

The lack of cue weight change post-VR may also point toward a difference in the role of the rTPJ across levels of sensory conflict. In ADR1FT VR, participants have agency and control over the direction and magnitude of motion they experience. By contrast, in a VR roller coaster, participants have no control over the visual motion that is presented. It is possible that the rTPJ is recruited in instances of higher conflict (i.e. roller coaster VR) and therefore stimulation to the rTPJ is more effective under passive motion conditions. Under this same notion, stimulation to the rTPJ may not be effective at facilitating measurable reweighting outcomes following a micro-gravity VR game as the sensory conflict is partially driven by the user and therefore not sufficiently potent for rTPJ intervention.

Further, the older adult study which also found the strongest reliance on body, gravity, then vision cues respectively, used three visual background orientations (Fraser et al., 2018). With less visual backgrounds, the vision vector may be under-represented resulting in a smaller relative contribution of vision compared to other studies. The underrepresentation in visual cue weights poses a limitation in the interpretation of the relative cue weights where visual cues may be contributing more to the PU than estimated by the vector sum model. If vision cue weights are underestimated, this would influence all relative cue weights. While cue weights changes for this study did not reach significance, trends must be interpreted with caution as cue weight estimates for gravity and body may be overestimated relative to vision due to compositional cue interdependence.

Within the average PU data across all tDCS conditions, there was also a small increase in cue weight of gravity ($\leq 0.9\%$). This aligns with previous research which has found that post-VR vestibular cues are upweighted for the SVV (Chung & Barnett-Cowan, 2023), adjusting the VOR and postural control (Di Girolamo et al., 2001; Warchoř et al., 2024). Though small, this trend may indicate a shift in reliance from body to gravity cues post-VR. Following VR, the perceptual bias on the SVV shifted away from the body axis toward alignment with gravity. These shifts were attributed to an increase in vestibular weighting following high intensity VR. In a separate study using the OCHART, astronauts following long-term (~168 days) exposure to microgravity in space shifted their reliance on body cues when making PU judgments (Harris et al., 2017). The present study did not manipulate gravity cues nor did it subject participants in unreliable sensory conditions long-term therefore direct comparisons between their study and our study cannot be made. However, the subtle shift in reliability toward gravity cues observed in the present study and the previous astronaut study align with the Bayesian reweighting model. Under the Bayesian reweighting model, a decrease in reliability of visual and body cues for upright would lead to an increased reliance on vestibular cues and previous experience (prior) when making upright estimations (Clemens et al., 2011; Knill & Pouget, 2004; Křrding & Wolpert, 2004). During the VR exposure, visual cues for orientation in microgravity are unreliable and bodily input may become unreliable due to increased postural sway. In this study, vestibular input and gravity cues are not manipulated and therefore remain reliable despite visual and postural perturbations in VR. However, postural sway and centre of pressure were not measured therefore we cannot say for certain whether the trend suggesting a decrease in body cue weights is attributable to sway.

Contrary to the sham and anodal conditions, cathodal trends in the averaged PU data suggest a small decrease in vision cues (-0.8%). This result may suggest cathodal stimulation to the rTPJ can facilitate a more efficient shift in sensory cue reliance for perception. When exposed to VR, shifting reliance from highly conflicting visual cues on to less conflicting body and gravity cues may be a more efficient strategy for reducing VR discomfort. In VR, depth cues are stimulated artificially and can misrepresent the binocular cues required by the dorsal stream for vision for action. The ventral stream, however, can extract distance cues from monocular

information and therefore is recruited for guiding action in VR (Harris et al., 2019). Evidence for this change in streams was found via fMRI when participants were asked to make spatial judgements on near and far objects in VR. In the real world, objects within arm's length are processed in the dorsal stream while distant objects are processed in the ventral stream. In VR, encoding by ventral and dorsal streams is opposite suggesting different neural mechanisms for visually guided actions in virtual space (Beck et al., 2010; Harris et al., 2019). Disruption to the ventral stream of vision caused by the downstream effects of cathodal rTPJ tDCS may underly the decrease in reliance on visual cues (Cook et al., 2025; Harris et al., 2019; Singh-Curry & Husain, 2009). These trends, however, are extremely small and analysis at the individual level is non-significant, therefore interpretations are limited.

4.1.1.2 PU change

The PU data was examined as an additional measure of sensory reweighting as it can be analyzed independently of the vector sum model. Participant PUs pre-VR and post-VR were compared to determine the reliance on bodily and gravity cues for orientation perception at a certain point in time. First, PUs over the six visual backgrounds were analyzed to determine if there was an effect of tDCS or VR on PU. When comparing pre-VR and post-VR PU data, there were no significant differences in any of the tDCS conditions within the upright or RSD body orientations. The rTPJ, specifically the IPL region, has bidirectional connections with the inferior temporal lobe which supports object recognition and processing in the ventral stream (Conway, 2018; Mars et al., 2012). If the ventral stream is the dominant stream for visual processing in VR, we would anticipate tDCS of the rTPJ to have downstream effects on object recognition via the IPL and for those effects to be reflected in the PU. Further, as stated in the introduction, the rTPJ is involved in the perception of uprightness, making it surprising that OCHART results did not differ from pre-VR to post-VR in the anodal or cathodal conditions (Fiori et al., 2015; Kheradmand et al., 2015). However, the presence of contextual visual cues in the PU judgements may explain why pre-VR and post-VR PU do not differ significantly. In a study which investigated the rTPJ for performance on the rod and frame test, performance on the no-frame-present condition was significantly worse when the rTPJ was inhibited using cTBS compared to a sham condition. When a reference frame was present, accuracy was also impaired following

cTBS to the rTPJ as well as control areas V1- V3. These findings suggest the rTPJ plays a distinct role in the integration of vestibular, proprioceptive and visual cues for verticality judgements in the absence of contextual visual cues (i.e. frames) and that the rTPJ and V1-V3 both contribute to verticality judgements when reference cues are present (Fiori et al., 2015). For the OCHART, the presence of visual cues may provide contextual cues and allow other lower-level areas like V1-V3 to inform verticality judgements when rTPJ function is altered from tDCS.

The effect of visual background and body orientation on PU was also investigated. The PU analysis revealed a strong effect of body orientation on PU. Across all tDCS conditions, both upright and RSD body orientations displayed a slight leftward (counterclockwise) bias of the PU from the body axis. Against a 0° visual background pre-VR, the PU shifted -8.52° away from the upright body orientation and -26.95° from the RSD body orientation. In the RSD condition, there was a larger leftward bias or counterclockwise shift away from the body axis compared to upright. This leftward bias in the RSD condition suggests a larger influence of gravity on the PU when the body axis is not aligned with gravity. These results agree with previous research which has found evidence for the influence of body tilt on upright and verticality perception using the OCHART and the SVV respectively (Aubert, 1861; Barnett- Cowan et al., 2013; De Vrijer et al., 2009; Dyde et al., 2006; H. Jenkin et al., 2007). More specifically, the leftward bias in PU has been found in previous studies which used the OCHART to investigate PU in upright, RSD, and left side down (LSD) body orientations.

Even in LSD body orientations, the leftward bias persists perhaps due to a rightward postural bias or an asymmetric preference in visuospatial attention toward the left visual field (Barnett-Cowan et al., 2013; Mamassian & Goutcher, 2001). Additionally, the PU has been found to shift toward the body axis across various body tilts, providing strong evidence for the influence of body axis in PU (Barnett-Cowan et al., 2013). There was also a small to medium interaction effect between body orientation and visual background. These findings provide further evidence in support of visual cue contributions to upright perception and the combined effect of body orientation and visual background on the PU (Jenkin et al., 2007). In alignment with these findings, previous research using the OCHART supports that manipulating visual cues

during the OCHART can influence task responses. When the OCHART letter probe is superimposed over static or dynamic visual backgrounds which contained orientation cues, there was a large effect of the background orientation on the PU (Jenkin et al., 2011). Further, the dynamic visual scenes had larger visual effects on the PU compared to static visual backgrounds of the same scene suggesting a strong influence of visual motion cues (i.e. depth and laws of physics) on the perception of upright (Jenkin et al., 2011). It is worth noting that larger visual effects do not imply a more accurate perception of upright but rather a larger influence of visual cues on the PU relative to static backgrounds.

4.1.1.3 Grey Background PU

Next, an analysis of PU over the grey background revealed a significant main effect of body orientation where PU was significantly larger when upright than when RSD, confirming an effect of body orientation on PU. There was no significant effect of tDCS condition or time nor significant interactions between any of the factors. A further analysis of the grey background sham PU data confirmed a main effect of body orientation where PU was significantly larger when upright than when RSD. These effects of body emphasize a shift in reliance from body to gravity cues when completing the OCHART in the upright position compared to RSD. This makes sense because body and gravity cues are in alignment when upright but when RSD, gravity cues are more indicative of the gravity-aligned upright and therefore more reliable for informing orientation judgements. Even in the absence of visual orientation cues, differences in pre- and post-VR PU were not observed suggesting there is little effect of rTPJ tDCS or VR on PU.

The absence of change observed in pre- and post-VR PU may also be due to the aspects of vision being evaluated by the OCHART. The OCHART evaluates how changes to the orientation of visual stimuli affects upright perception however the visual changes that occur following a short-term VR exposure are primarily depth and motion-related (Chang et al., 2020). More specifically, changes in VOR, accommodation and vergence have been observed post-VR suggesting that changes in visual processing observed immediately following a short-term VR exposure may not be captured by a static task like the OCHART (Di Girolamo et al., 2001;

Szpak et al., 2020; Warchoł et al., 2024). This may serve as an additional explanation as to why changes in visual cue weights are not observed in the current study.

4.1.1.4 Visual Effect

The visual effect was calculated to investigate how visual background changes altered participant's PU without using the vector sum model. The visual effect analysis found no evidence for a significant interaction between time, tDCS condition and body orientation. However, there was a significantly larger visual effect in the RSD body orientation compared to the upright body orientation. This finding suggests that when RSD, individuals rely more on visual information when making orientation judgements than if they were upright. These findings complement the results of the PU analysis in which participants relied less on body cues and more on gravity cues when RSD. Taken together, these results point toward a reliance on vision and gravity cues for orientation perception when RSD. When RSD, we cannot rely on body cues to inform our orientation judgment as they are no longer aligned with the true gravitational upright. Therefore, in support of the Bayesian model of sensory processing, an adaptive shift to favour gravity and vision cues when in a RSD position occurs.

4.1.2 Hypothesis 2 - No Difference in Change in Cybersickness Between tDCS Conditions

Hypothesis 2 was that activity in the rTPJ contributes to the modulation of cybersickness and therefore anodal tDCS to the rTPJ during VR would decrease cybersickness relative to sham whereas cathodal tDCS to the rTPJ during VR would increase cybersickness relative to sham. Across all tDCS conditions, post-VR cybersickness (FMS) scores were significantly larger than pre-VR scores confirming the sickening effects of ADRIFT as a VR experience. This result is in alignment with sensory conflict theory in that conflicting sensory information from VR causes cybersickness. Further, greater cybersickness was reported in the sham condition compared to the cathodal condition. This difference, however, was not significant at the pre- and post-VR times and therefore the difference may be attributable to pre-existing symptoms at baseline. While symptoms of fatigue, headaches and anxiety were screened for before beginning the experiment, it is possible that tDCS or VR set-up caused anxiety in some participants resulting in higher ratings on the pre-VR FMS.

4.1.3 Cybersickness and Sensory Reweighting

To model the association between Δ PU and Δ FMS, a linear mixed model was run to investigate if absolute Δ PU is predictive of Δ FMS by tDCS condition. The model revealed no significant association between absolute Δ PU and Δ FMS in any of the tDCS conditions. In the anodal condition there was a trend to suggest a greater absolute Δ PU was associated with less Δ FMS. However, the 95% confidence interval includes 0, therefore the effect is uncertain, and we cannot confidently rule out that there was no effect of anodal stimulation. These results provide little evidence to suggest that the absolute Δ PU observed in each tDCS condition is predictive of the Δ FMS outcomes or that the association between absolute Δ PU and Δ FMS differs across tDCS conditions.

Previous research by Chung and Barnett-Cowan (2023) found evidence for a Gaussian relationship between cybersickness as measured by the FMS and change in sensory reweighting as measured by the SVV. In the study by Chung and Barnett-Cowan (2023) the SVV line orientations stimuli were presented over a grey background while the participant was RSD, therefore we chose to use our most analogous OCHART stimuli — letter probes over grey background — to investigate the relationship between Δ PU and Δ FMS. The Δ PU over a grey background for the RSD condition was compared to the Δ FMS for each body orientation in each tDCS condition. The 3-parameter Gaussian regressions found no association of change in PU on change in FMS in any of the tDCS conditions pre-VR or post-VR. Therefore, there is no evidence for a systematic effect between Δ PU and Δ FMS. Despite an increase in cybersickness from pre-VR to post-VR across all tDCS conditions, no change in sensory weights was observed. Why might Δ FMS be related to change in SVV but not Δ PU? The main difference between these tasks is the reliance on different sensory cues. For the SVV, participants are instructed to align a line with gravity and when participants complete the SVV in different body orientations their responses are influenced by the degree of body tilt. However, the SVV estimate remains close to the gravity vector ($\leq 30^\circ$ deviation) even in different body orientations implying a larger effect of gravity on the SVV. By contrast, the OCHART quantifies upright based on the orientation at which a letter probe is most easily recognized (PU). When visual backgrounds are present for the SVV and OCHART, body orientations and visual background orientations have a greater effect

on PU relative to the SVV suggesting a larger effect of body and vision cues over gravity cues on the OCHART (Dyde et al., 2006). Further, the averaged PU cue weight trends observed in this study suggest a shift toward gravity cue reliance and away from bodily cue reliance post-VR – these trends align with those observed by Chung and Barnett-Cowan (2023). As previously established, gravitational effects are larger on the SVV than on the PU therefore the adaptive upweighting of vestibular cues observed following a high intensity VR exposure may be better captured by the SVV which is more sensitive to gravitational effects. Therefore, participants who are resistant to cybersickness may not show large shifts in their PU because changes in gravitational reliance are not strongly reflected in the PU.

Similar tendencies in the data can be noted when comparing the distribution of datapoints on our gaussian regression graphs to those of Chung and Barnett-Cowan (2023). Firstly, most data points along the x-axis are gathered near 0° and are spread between -20° to 20° change. This is evidence that, despite using different tasks to measure sensory reweighting, the degree of change observed post high-intensity VR is similar in magnitude between the SVV and OCHART. The change in the SVV, however, may be more closely linked to Δ FMS because it can better capture the shift in reliance on gravitational cues post-VR. Second, upon examining the gaussian regression curves, many data points fall below the peak of the curve. This indicates that even those that do not get sick or, in the case of this study, those who show little Δ FMS from baseline, do not display changes in their sensory reweighting. This tendency points toward the contributions of other variables in predicting FMS.

While previous research suggests sensory reweighting is an informative variable for cybersickness prediction, there is evidence for other predictive measures as well. For example, participant “presence” or sense of being physically present in a VR experience has been linked to lower sensitivity to sensory conflict and a reduced risk of cybersickness in VR users (Weech et al., 2019). When standing, sway path length duringvection is inversely related to cybersickness and when seated, autonomic measures like changes in gastric electrical activity, blinking and breathing rate have been found to strongly predict post-VR sickness scores (Dennison et al., 2016; Kim et al., 2005; Weech et al., 2018). Combined with autonomic and balance control

measures, sensory reweighting may supplement predictions of cybersickness. However, on its own, sensory reweighting cannot accurately predict cybersickness manifestation with certainty.

4.2 Limitations and Future Directions

4.2.1 PU and OCHART Interpretations

Estimates of participant PU are limited to extrapolations made on the orientations of the letter probe that the participant is presented. More recently, researchers who use the OCHART have employed two Bayesian adaptive staircases to the task to determine the points of maximum ambiguity (Fraser et al., 2018). This approach may be more effective at precisely determining a participant's perceptual upright. A Bayesian staircase approach could reduce instances where OCHART response averages do not fit to a sigmoidal response curve.

Establishing precise points of subjective equality in each participant could also address the limitation in generating cue weights at the individual level. It can be difficult to assess patterns of sensory reweighting in heterogeneous samples or among people who display a lot of uncertainty in responses across all trials. By using an adaptive staircase procedure, the stimuli presented will adapt based on participant responses, ensuring that the point of subjective equality is located precisely rather than estimated based on sigmoidal response curves. An adaptive staircase procedure would also reduce the task completion time and any response errors attributable to fatigue. Future studies using the OCHART should consider employing a Bayesian adaptive staircase to determine PSE and improve precision in PU estimates and optimize vector sum model fit to data.

4.2.2 VR Exposure Limitations

ADR1FT VR was used during the VR exposure as it simulated a microgravity environment and initiated rotation along the roll, yaw and pitch axis. When there is rotation about two or more axes there is a greater chance that participants will experience cybersickness (Chang et al., 2020). In ADR1FT, the presence of unreliable visual cues and dynamic visual stimuli is consistent across exposures however, user experience in ADR1FT may vary across participants based on how the participant engages with the virtual environment. Additionally, experience in

ADR1FT may vary within a participant based on how the participant interacts with the game across the three testing days. The inter and intra-participant variability in VR exposure may limit our interpretations of cybersickness manifestation. Future studies should consider a standardized, non-interactive VR exposure that also simulates frequent rotation along all axes.

4.2.3 Fast Motion Sickness (FMS) Scale vs Simulator Sickness Questionnaire (SSQ)

In the present study cybersickness was measured using the FMS. The FMS was selected because it could be quickly recorded throughout the VR exposure and could be immediately rated following termination of the VR exposure. The Simulator Sickness Questionnaire (SSQ) is a more popular measure of cybersickness and was used by Takeuchi and colleagues (2018) when measuring sickness following a VR rollercoaster experience primed by tDCS to the rTPJ. On the SSQ, participants rank their sickness on a 4-point scale (None, Slight, Moderate or Severe) based on a set of symptoms (e.g. eye strain, nausea, dizziness with eyes open) which correspond with disorientation, nausea and/or oculomotor cybersickness symptom subtypes. The SSQ gives a more specific estimation of an individual's cybersickness at a given time but requires more time to complete than the FMS (Chang et al., 2020). The FMS was used instead of the SSQ post-VR in the interest of time and in hopes of capturing post-VR effects of sensory reweighting through the OCHART. No significant differences in cybersickness across tDCS conditions were observed using the FMS which may suggest that the effects of rTPJ tDCS as observed by Takeuchi and colleagues (2018) are symptom specific.

The FMS is also highly subjective and can even vary within a participant. Among participants who dropped out of the VR portion of the study, one participant dropped out when they reached an FMS of 7 on one testing day (sham) but completed the entire VR exposure on a different testing day despite reporting a peak FMS score of 12 (cathodal). Another participant who dropped out of the VR portion on two separate testing days dropped out at an FMS score of 14 one day (cathodal) but an FMS score of 18 on a different day (sham). Interestingly, on the one day this participant did not drop out of the VR session (anodal) they still reached an FMS score of 14. This suggests that participant ratings of cybersickness and thresholds for unbearable

cybersickness may differ from day to day making FMS a less reliable measurement of cybersickness.

4.2.4 tDCS Limitations

This study design uses tDCS which, as a technique, has its own limitations. Participant anatomy varies and therefore the electrode placement under the 10-20 method and current density may not be optimal for every participant (Chew et al., 2015; Meinzer et al., 2024). Individual variability in white matter, grey matter, cerebrospinal fluid, bone density and hair texture can impact the electric field distribution of tDCS currents and stimulation outcomes (Bikson et al., 2016; Miranda, 2013). The rTPJ is also located at the junction of the temporal and parietal lobes caudal to the sylvian fissure and therefore the surface is dense with cortical folding. Areas with many gyri and sulci are at higher risk of cortical current flow polarity inversions which could result in unpredictable tDCS outcomes (Bikson et al., 2016). Further, a review investigating the polarity effects of tDCS on cognitive and motor domains suggests that cathodal stimulation may be ineffective at disrupting plasticity for associative learning in non-motor regions (Jacobson et al., 2012). The results of the study by Takeuchi and colleagues (2018) agreed with this result and found significant effects of anodal stimulation on cybersickness but not cathodal. Alternatively, research that applied tDCS on the occipital cortex found cathodal stimulation was effective at reducing contrast sensitivity whereas no change was observed following anodal stimulation (Antal et al., 2001). This suggests anodal and cathodal stimulation efficacy may be task or region dependent (Bikson et al., 2016). This study was designed under the assumption that anodal and cathodal tDCS coupled with VR will produce the anticipated enhancements and impairments respectively. However, differences between sham and tDCS conditions were not observed suggesting limited efficacy of tDCS over the rTPJ during VR exposure.

The 1.5mA current delivered through the 35cm² electrodes delivered a maximum current density of 0.04mA/cm². This current density was matched to the current density used by Takeuchi and colleagues (2019). Across other TPJ tDCS studies, the maximum current density is 0.03 – 0.08mA/cm². Therefore, the current density reached in this study is relatively low for stimulation of the TPJ (Donaldson et al., 2015). With a higher current density, the outcomes of

cybersickness may be more pronounced due to greater or more rapid LTP-like effects (Kronberg et al., 2017). However, research using animal models has also suggested that greater current densities could result in plasticity that is no longer input-specific (Jackson et al., 2016; Kronberg et al., 2017). The ratio of reference electrode to stimulating electrode may also be important in focusing tDCS current and improving modulation of cortical excitability. Focality of current can be increased by either decreasing the size of the stimulation electrode or increasing the size of the reference electrode (Nitsche et al., 2007). Future studies should consider a smaller stimulating electrode and a relatively larger reference electrode to improve focality of stimulation currents. The location of the reference electrode (Cz) was also selected as informed by Takeuchi and colleagues' study (2019) and therefore no interference effects were anticipated between stimulation over the rTPJ and area Cz which captures the supplementary motor cortex and sensorimotor cortices. While the possibility of cortical excitability or depression at Cz cannot be ruled out, no significant effects of stimulation were observed in the anodal nor the cathodal conditions.

4.2.5 Online tDCS vs Offline tDCS

The hypotheses and motivation for this study were heavily based on the findings of Takeuchi and colleagues (2018). One key distinction, however, was that participants in the Takeuchi study were stimulated before the VR exposure (offline tDCS) whereas participants of our study were stimulated during the VR exposure (online tDCS). This design decision was made to accommodate the addition of the OCHART in the study design. If offline tDCS was used, the pre-VR OCHART would have to happen either before the offline tDCS, during the offline tDCS or after the offline tDCS. If the OCHART was completed before offline tDCS, changes in sensory processing which may occur as result of offline tDCS would not be captured and therefore comparisons between PU on pre- and post-OCHART would not be representative of the participant's perceptual state upon entering VR. If the OCHART was completed after offline tDCS, there is a risk of the offline tDCS effects wearing off before the participant enters VR therefore limiting our interpretations of the rTPJ's involvement in cybersickness. If the OCHART and offline tDCS were done simultaneously, the 20-minute stimulation period would not span both the upright and RSD OCHARTs. Additionally, some participants may complete

the OCHART faster than others leading to inconsistencies in how soon after stimulation participants enter VR.

In contrast to our study, participants in the Takeuchi study received offline tDCS at rest for 15 minutes before entering VR whereas stimulation for the present study was delivered online throughout the 20 minute VR exposure. . Differences in online and offline stimulation may underly the differences in cybersickness outcomes between Takeuchi and colleagues' (2018) findings and the results of the present study. Previous studies investigating the effect of online vs offline anodal tDCS over the posterior parietal cortex found that offline tDCS improved spatial working memory bilaterally while online tDCS had no such effect. This difference in results was attributed to differences in neuronal activity during active stimulation versus stimulation aftereffects. Online tDCS alters neuron membrane potential and neuronal excitability which changes how input to the area of interest is processed. Alternatively, the aftereffect of offline tDCS is a result of changes in synaptic strength and neurotransmitter activity (Živanović et al., 2021). It is thought that young healthy cortices exercise homeostatic control over inhibitory and excitatory activity and therefore effects of online tDCS may not be observed behaviorally in these populations (Hill et al., 2016; Živanović et al., 2021). The rTPJ shares connections with the posterior parietal cortex and therefore regional stimulation outcomes may be applicable for rTPJ functioning as well. If online tDCS affects rTPJ functions tied to sensory reweighting similarly to how it affects spatial working memory, it would make sense that offline tDCS has no effect but online tDCS does. In this case, the offline tDCS used by Takeuchi and colleagues (2018) would prime participants to enter VR with pre-existing excitation to the rTPJ and facilitate cybersickness mitigation versus online tDCS which would alter input processing but not have any measurable down- stream effects on cybersickness and sensory reweighting. Future studies should use both online and offline stimulation on separate days to compare cybersickness outcomes to determine how timing of rTPJ tDCS influences VR outcomes.

4.2.6 Cybersickness and tDCS Aftereffect Assumptions

A key difference between the present study and the highlighted OCHART studies is the time at which sensory cues are manipulated. In OCHART studies which used microgravity flight and dynamic visual backgrounds, perceptual inputs are actively manipulated as participants complete the OCHART. In this study however, participants complete the OCHART following the termination of the VR exposure and tDCS. This design relies on the assumption that tDCS and VR aftereffects will persist up to 40 minutes following their termination. Previous research investigating cybersickness in an interactive VR environment with highly dynamic motion cues and altered gravity cues (i.e. suspended objects) found participant cybersickness symptoms and accommodation and vergence changes returned to baseline 40 minutes following their exit from VR (Szpak et al., 2020). A separate study found cybersickness symptoms may persist between 10 minutes and 4 hours following VR immersion (Dużmańska et al., 2018). Further, changes in postural control last about 30 minutes and changes in VOR have been observed up to 30 minutes post-VR (Di Girolamo et al., 2001; Warchoń et al., 2024). The VOR and postural control are not assessed in this study, however these short-term changes in ocular mechanisms and sensorimotor interactions following VR suggest lingering effects of VR on perceptual mechanisms. Despite this evidence, we cannot say for certain whether the hypothesized perceptual changes span the entire post-VR OCHART session and whether all participants experience the same duration of aftereffect. The results of this study suggest that any aftereffect in perception following VR with or without tDCS is minimally captured by the OCHART.

By using offline tDCS, the Takeuchi study operates under the assumption that the aftereffect of the tDCS will span the entire duration of the VR rollercoaster (Takeuchi et al., 2018). The aftereffects of tDCS are difficult to quantify but previous research which measured corticospinal activity suggested 13 minutes of tDCS is enough to produce measurable aftereffects for up to 60 minutes (Nitsche & Paulus, 2001; Takeuchi et al., 2018). Further, post-tDCS, cortical activity does not return to baseline immediately. Research has shown that 13 min of stimulation of the motor cortex can have measurable aftereffects of up to 90 min (Nitsche & Paulus, 2001; Thair et al., 2017). This study operates on the same assumption when evaluating sensory weights using the OCHART post-VR however, we cannot say for certain that the

aftereffects of tDCS on the rTPJ are similar to those observed in the motor cortex. Further, we cannot guarantee that the effects of tDCS to the rTPJ are sustained throughout the post-VR OCHARTs or that the transient changes in sensory reweighting post-VR can be captured by the OCHART over approximately 40 minutes. When comparing pre-VR to post-VR sensory cue weights in the sham condition, the results suggest that any effects of VR on sensory reweighting are captured minimally by the OCHART. Though the duration of sensory reweighting following VR is unknown, but the effects of cybersickness may last between 10 minutes and 4 hours suggesting the perceptual changes underlying cybersickness persist in the absence of the sickening VR (Dużmańska et al., 2018). However, considerable individual differences to cybersickness susceptibility and recovery may limit these interpretations of this study. The OCHART task was shortened to increase the chance of capturing effects post-VR. However, the shortened OCHART may reduce the rigor of the task in measuring sensory weights.

4.2.7 Future Measure Suggestions

A measure of postural instability would have contributed to the interpretation of the observed results. Previous research has found that anodal tDCS to the rTPJ improved postural stability in VR and decreased cybersickness (Takeuchi et al., 2018). Anodal tDCS to the rTPJ has also been found to improve postural control with eyes closed on an unstable surface whereas cathodal tDCS to the rTPJ has been found to impair postural stability in the same conditions (Kamada & Takeuchi, 2023). This suggests that under unreliable sensory conditions, the rTPJ contributes to updating the body schema to maintain balance. In the present study, any perturbations to postural control that occurred as result of VR or the different tDCS conditions were not measured, thereby limiting interpretations of tDCS outcomes. As previously established, postural instability is not a requirement for cybersickness manifestation or vice versa therefore we cannot rule out the possibility that postural control was altered by the tDCS despite absence of change in cybersickness. Future studies applying tDCS to the rTPJ for cybersickness mitigation should include a measure of postural stability before, during and after stimulation application. Including a postural stability measure may help determine if the tDCS conditions caused changes in postural sway and if these changes are predictive of cybersickness manifestation.

Participant gaming experience was not collected; however, in a previous VR study, no significant differences were found between gamers (play for >1 hour a week) and non-gamers (play for <1 hour a week) when compared on SVV performance, and FMS scores for high and

low intensity VR exposures (Chung & Barnett-Cowan, 2023). Further, no participants reported prior experience playing ADRIFT, nor did participants report playing ADRIFT between testing sessions. Despite this, we cannot rule out the possible impact of gaming experience as the game was operated on an Xbox controller. A brief explanation on how to navigate the virtual world was given prior to game play. However, those who are familiar with Xbox controllers may become comfortable with the controls faster and therefore be able to navigate the virtual world, adjust their avatars orientation, and interact with objects more easily. Participants with videogame experience may have an advantage over non-gamers when preventing unwanted visual motion in VR, thereby reducing their risk of conflicting sensory cues and cybersickness.

Future studies evaluating sensory reweighting through a psychophysical task should consider using SVV in place of the OCHART. The OCHART was initially selected to measure sensory reweighting as it accounted for changes in reliance on visual, bodily, and gravitational cues. More specifically, the OCHART is especially sensitive to contributions of visual and body cues in participant responses. However, results of this study suggest that the OCHART is not sensitive to the transient changes in vision that occur post-VR in its shortened form. Instead, though not as sensitive to visual changes, the SVV may be better able to quantify the shift in reliance from body to gravity cues post-VR with tDCS to the rTPJ. Previous studies have found significant changes in SVV following non-invasive stimulation to the rTPJ and following high-intensity VR immersion (Chung & Barnett- Cowan, 2023; Kheradmand et al., 2015). Changes in reliance on gravity cues have been most strongly linked to cybersickness outcomes therefore the SVV may be a powerful tool in understanding the relationship between sensory reweighting and cybersickness manifestation under various tDCS conditions. Research interested in evaluating the visual changes that occur following VR should consider testing visual contributions to postural control or the VOR. Previous research suggests that reductions in VOR gain post-VR indicates an increase in vestibular weighting over visual weighting (Di Girolamo et al., 2001; Warchoř et al.,2024). Both the SVV and the VOR can be evaluated quickly post-VR increasing the chance of capturing an effect of VR in those who adapt quickly to environmental changes.

4.2.8 Effect Size and Sample Size Estimation

The main effects we were interested in were the interaction between tDCS condition, sensory modality on absolute Δ Cue Weight where we expected a significant interaction between tDCS condition and sensory modality on cue weights. The other main effect we were interested in was the change in FMS from pre-VR to post-VR across tDCS conditions. Both effects were not significant with a very small effect size suggesting the study was underpowered.

Using the results from the 2 x 2 x 3 x 6 ANOVA investigating the Δ PU across time, body orientation, tDCS condition and visual background, a simulated model estimated a power of 11.5% with 200 participants suggesting that an infeasible sample would need to be collected to find a four-way interaction using this study design. Further, a simulated model investigating the effects of the 2 x 2 ART ANOVA investigating the effects of condition and time on FMS indicated a sample of 200 people would be powered at 48.50%. The outcome of these power analyses suggests that any differences detected with a large sample size may be attributable to chance and not representative of the true population. By contrast, a simulated model of the 3x3 ART ANOVA investigating the ABS Δ Cue Weight across conditions and sensory modalities was powered at 80% with 98 people suggesting a larger effect size that is more easily detected as the sample increase.

4.3 Conclusion

In the current study, tDCS was applied to the rTPJ to investigate the effects of anodal and cathodal stimulation on sensory reweighting and cybersickness outcomes. The results suggest that anodal and cathodal stimulation does not significantly alter sensory reweighting or cybersickness outcomes relative to sham stimulation. Despite this, there are small trends indicating the upweighting of vestibular cues post-VR across all tDCS conditions. Further, no significant differences were observed between the sham and anodal nor the sham and cathodal final cybersickness scores or at any point along the VR exposure. However, across tDCS conditions there was a consistent significant increase in cybersickness up to 6 minutes suggesting early adaptation for cybersickness occurs following at least 6 minutes of VR immersion. Future research should consider using the SVV and assess postural stability before, during, and after VR

immersion to assess changes in sensory reweighting. To quantify cybersickness, future studies should consider using both the SSQ and the FMS to quantify changes in distinct cybersickness symptoms and cybersickness progression, respectively. Additionally, investigating the effect of online and offline rTPJ tDCS within the same VR environment would yield further insights into the role of the rTPJ in cybersickness mitigation, sensory integration and conflict perception.

References

- Akiduki, H., Nishiike, S., Watanabe, H., Matsuoka, K., Kubo, T., & Takeda, N. (2003). Visual- vestibular conflict induced by virtual reality in humans. *Neuroscience Letters*, *340*(3), 197–200. [https://doi.org/10.1016/S0304-3940\(03\)00098-3](https://doi.org/10.1016/S0304-3940(03)00098-3)
- Akizuki, H., Uno, A., Arai, K., Morioka, S., Ohyama, S., Nishiike, S., Tamura, K., & Takeda, N. (2005). Effects of immersion in virtual reality on postural control. *Neuroscience Letters*, *379*(1), 23– 26. <https://doi.org/10.1016/j.neulet.2004.12.041>
- Alais, D., & Burr, D. (2019). Cue Combination Within a Bayesian Framework. In A. K. C. Lee, M. T. Wallace, A. B. Coffin, A. N. Popper, & R. R. Fay (Eds.), *Multisensory Processes* (Vol. 68, pp. 9–31). Springer International Publishing. https://doi.org/10.1007/978-3-030-10461-0_2
- Alais, D., Newell, F., & Mamassian, P. (2010). *Multisensory Processing in Review: From Physiology to Behaviour*. <https://doi.org/10.1163/187847510X488603>
- Allison, R. S., Harris, L. R., Jenkin, M., Jasiobedzka, U., & Zacher, J. E. (2001). Tolerance of temporal delay in virtual environments. *Proceedings IEEE Virtual Reality 2001*, 247–254. <https://doi.org/10.1109/VR.2001.913793>
- American Psychological Association. (2018, April 19). *APA Dictionary of Psychology*. APA Dictionary of Psychology. <https://dictionary.apa.org/>
- Amso, D., & Scerif, G. (2015). The attentive brain: Insights from developmental cognitive neuroscience. *Nature Reviews Neuroscience*, *16*(10), 606–619. <https://doi.org/10.1038/nrn4025>
- Antal, A., Nitsche, M. A., & Paulus, W. (2001). External modulation of visual perception in humans. *Neuroreport*, *12*(16), 3553–3555. <https://doi.org/10.1097/00001756-200111160-00036>
- Arcioni, B., Palmisano, S., Apthorp, D., & Kim, J. (2019). Postural stability predicts the likelihood of cybersickness in active HMD-based virtual reality. *Displays*, *58*, 3–11. <https://doi.org/10.1016/j.displa.2018.07.001>
- Assländer, L., & Peterka, R. J. (2014). Sensory reweighting dynamics in human postural control. *Journal of Neurophysiology*, *111*(9), 1852–1864. <https://doi.org/10.1152/jn.00669.2013>

- Aubert, H. (1861). Eine scheinbare bedeutende Drehung von Objecten bei Neigung des Kopfes nach rechts oder links. *Archiv für Pathologische Anatomie und Physiologie und für Klinische Medicin*, 20(3–4), 381–393. <https://doi.org/10.1007/BF02355256>
- Balslev, D., Nielsen, F. Å., Paulson, O. B., & Law, I. (2005). Right temporoparietal cortex activation during visuo-proprioceptive conflict. *Cerebral Cortex*, 15(2), 166–169. <https://academic.oup.com/cercor/article-abstract/15/2/166/343556>
- Barnett-Cowan, M., Jenkin, H., Dyde, R., Jenkin, M., & Harris, L. (2013). Asymmetrical representation of body orientation. *Journal of Vision*, 13. <https://doi.org/10.1167/13.2.3>
- Beck, L., Wolter, M., Mungard, N. F., Vohn, R., Staedtgen, M., Kuhlen, T., & Sturm, W. (2010). Evaluation of Spatial Processing in Virtual Reality Using Functional Magnetic Resonance Imaging (fMRI). *Cyberpsychology, Behavior and Social Networking*, 13(2), 211–215. <https://doi.org/10.1089/cyber.2008.0343>
- Bikson, M., Grossman, P., Thomas, C., Zannou, A. L., Jiang, J., Adnan, T., Mourdoukoutas, A. P., Kronberg, G., Truong, D., Boggio, P., Brunoni, A. R., Charvet, L., Fregni, F., Fritsch, B., Gillick, B., Hamilton, R. H., Hampstead, B. M., Jankord, R., Kirton, A., ... Woods, A. J. (2016). Safety of Transcranial Direct Current Stimulation: Evidence Based Update 2016. *Brain Stimulation*, 9(5), 641– 661. <https://doi.org/10.1016/j.brs.2016.06.004>
- Blanke, O., & Arzy, S. (2005). The out-of-body experience: Disturbed self-processing at the temporo- parietal junction. *The Neuroscientist: A Review Journal Bringing Neurobiology, Neurology and Psychiatry*, 11(1), 16–24. <https://doi.org/10.1177/1073858404270885>
- Blanke, O., Mohr, C., Michel, C. M., Pascual-Leone, A., Brugger, P., Seeck, M., Landis, T., & Thut, G. (2005). Linking Out-of-Body Experience and Self Processing to Mental Own-Body Imagery at the Temporoparietal Junction. *Journal of Neuroscience*, 25(3), 550–557. <https://doi.org/10.1523/JNEUROSCI.2612-04.2005>
- Bos, J. E., de Vries, S. C., van Emmerik, M. L., & Groen, E. L. (2010). The effect of internal and external fields of view on visually induced motion sickness. *Applied Ergonomics*, 41(4), 516–521. <https://doi.org/10.1016/j.apergo.2009.11.007>

- Brown, L. L., Schneider, J. S., & Lidsky, T. I. (1997). Sensory and cognitive functions of the basal ganglia. *Current Opinion in Neurobiology*, 7(2), 157–163. [https://doi.org/10.1016/S0959-4388\(97\)80003-7](https://doi.org/10.1016/S0959-4388(97)80003-7)
- Caramenti, M., Lafortuna, C. L., Mugellini, E., Khaled, O. A., Bresciani, J.-P., & Dubois, A. (2018). Matching optical flow to motor speed in virtual reality while running on a treadmill. *PLOS ONE*, 13(4), e0195781. <https://doi.org/10.1371/journal.pone.0195781>
- Chang, E., Kim, Hyun Taek, & Yoo, B. (2020). Virtual Reality Sickness: A Review of Causes and Measurements. *International Journal of Human–Computer Interaction*, 36(17), 1658–1682. <https://doi.org/10.1080/10447318.2020.1778351>
- Chew, T., Ho, K.-A., & Loo, C. K. (2015). Inter- and Intra-individual Variability in Response to Transcranial Direct Current Stimulation (tDCS) at Varying Current Intensities. *Brain Stimulation*, 8(6), 1130–1137. <https://doi.org/10.1016/j.brs.2015.07.031>
- Chung, W., & Barnett-Cowan, M. (2023). Sensory reweighting: A common mechanism for subjective visual vertical and cybersickness susceptibility. *Virtual Reality*, 27(3), 2029–2041. <https://doi.org/10.1007/s10055-023-00786-z>
- Ciechanski, P., Carlson, H. L., Yu, S. S., & Kirton, A. (2018). Modeling Transcranial Direct-Current Stimulation-Induced Electric Fields in Children and Adults. *Frontiers in Human Neuroscience*, 12. <https://doi.org/10.3389/fnhum.2018.00268>
- Clemens, I. A. H., Vrijer, M. D., Selen, L. P. J., Gisbergen, J. A. M. V., & Medendorp, W. P. (2011). Multisensory Processing in Spatial Orientation: An Inverse Probabilistic Approach. *Journal of Neuroscience*, 31(14), 5365–5377. <https://doi.org/10.1523/JNEUROSCI.6472-10.2011>
- Clower, D. M., West, R. A., Lynch, J. C., & Strick, P. L. (2001). The Inferior Parietal Lobule Is the Target of Output from the Superior Colliculus, Hippocampus, and Cerebellum. *The Journal of Neuroscience*, 21(16), 6283–6291. <https://doi.org/10.1523/JNEUROSCI.21-16-06283.2001>
- Cohen, B., Dai, M., Yakushin, S. B., & Cho, C. (2019). The neural basis of motion sickness. *Journal of Neurophysiology*, 121(3), 973–982. <https://doi.org/10.1152/jn.00674.2018>
- Collard, M. (1994). [The vestibular system: From structure to function]. *La Revue Du Praticien*, 44(3), 295–298.

- Conway, B. R. (2018). The Organization and Operation of Inferior Temporal Cortex. *Annual Review of Vision Science*, 4, 381–402. <https://doi.org/10.1146/annurev-vision-091517-034202>
- Cook, A. J., Im, H. Y., & Giaschi, D. E. (2025). Large-scale functional networks underlying visual attention. *Neuroscience & Biobehavioral Reviews*, 173, 106165. <https://doi.org/10.1016/j.neubiorev.2025.106165>
- Corbetta, M., & Shulman, G. L. (2002). Control of goal-directed and stimulus-driven attention in the brain. *Nature Reviews Neuroscience*, 3(3), 201–215. <https://doi.org/10.1038/nrn755>
- Costello, P. J. (1997). *Health and Safety Issues associated with Virtual Reality—A Review of Current Literature*.
- Curry, C. (2019). *Simulator Sickness Questionnaire*. University of Minnesota Twin Cities.
- Davis, S., Nesbitt, K., & Nalivaiko, E. (2015). *Comparing the onset of cybersickness using the Oculus Rift and two virtual roller coasters*. 167.
- De Vrijer, M., Medendorp, W. P., & Van Gisbergen, J. a. M. (2009). Accuracy-precision trade-off in visual orientation constancy. *Journal of Vision*, 9(2), 9.1-15. <https://doi.org/10.1167/9.2.9>
- Decety, J., & Lamm, C. (2007). The Role of the Right Temporoparietal Junction in Social Interaction: How Low-Level Computational Processes Contribute to Meta-Cognition. *The Neuroscientist*, 13(6), 580–593. <https://doi.org/10.1177/1073858407304654>
- Denise, P., & Darlot, C. (1993). The cerebellum as a predictor of neural messages—II. Role in motor control and motion sickness. *Neuroscience*, 56(3), 647–655. [https://doi.org/10.1016/0306-4522\(93\)90362-J](https://doi.org/10.1016/0306-4522(93)90362-J)
- Dennison, M. S., Wisti, A. Z., & D’Zmura, M. (2016). Use of physiological signals to predict cybersickness. *Displays*, 44, 42–52. <https://doi.org/10.1016/j.displa.2016.07.002>
- Di Girolamo, S., Picciotti, P., Sergi, B., Di Nardo, W., Paludetti, G., & Ottaviani, F. (2001). Vestibulo-ocular reflex modification after virtual environment exposure. *Acta Oto-Laryngologica*, 121(2), 211–215. <https://doi.org/10.1080/000164801300043541>
- Donaldson, P. H., Rinehart, N. J., & Enticott, P. G. (2015). Noninvasive stimulation of the temporoparietal junction: A systematic review. *Neuroscience and Biobehavioral Reviews*, 55,

547–572. <https://doi.org/10.1016/j.neubiorev.2015.05.017>

Dużmańska, N., Strojny, P., & Strojny, A. (2018). Can Simulator Sickness Be Avoided? A Review on Temporal Aspects of Simulator Sickness. *Frontiers in Psychology, 9*, 2132.

<https://doi.org/10.3389/fpsyg.2018.02132>

Dyde, R. T., Jenkin, M. R., & Harris, L. R. (2006). The subjective visual vertical and the perceptual upright. *Experimental Brain Research, 173*(4), 612–622.

<https://doi.org/10.1007/s00221-006-0405-y>

Dyde, R. T., Jenkin, M. R., Jenkin, H. L., Zacher, J. E., & Harris, L. R. (2009). The effect of altered gravity states on the perception of orientation. *Experimental Brain Research, 194*(4), 647–660. <https://doi.org/10.1007/s00221-009-1741-5>

Eddy, C. M. (2016). The junction between self and other? Temporoparietal dysfunction in neuropsychiatry. *Neuropsychologia, 89*, 465–477.

<https://doi.org/10.1016/j.neuropsychologia.2016.07.030>

Eördegh, G., Tót, K., Kiss, Á., Kéri, S., Braunitzer, G., & Nagy, A. (2022). Multisensory stimuli enhance the effectiveness of equivalence learning in healthy children and adolescents. *PLoS ONE, 17*(7), e0271513. <https://doi.org/10.1371/journal.pone.0271513>

Fiori, F., Candidi, M., Acciarino, A., David, N., & Aglioti, S. M. (2015). The right temporoparietal junction plays a causal role in maintaining the internal representation of verticality. *Journal of Neurophysiology, 114*(5), 2983–2990. <https://doi.org/10.1152/jn.00289.2015>

Fogassi, L., & Luppino, G. (2005). Motor functions of the parietal lobe. *Current Opinion in Neurobiology, 15*(6), 626–631. <https://doi.org/10.1016/j.conb.2005.10.015>

Frank, S. M., & Greenlee, M. W. (2018). The parieto-insular vestibular cortex in humans: More than a single area? *Journal of Neurophysiology, 120*(3), 1438–1450.

<https://doi.org/10.1152/jn.00907.2017>

Fraser, L. E., Mansfield, A., Harris, L. R., Merino, D. M., Knorr, S., & Campos, J. L. (2018). The Weighting of Cues to Upright Following Stroke With and Without a History of Pushing. *Canadian Journal of Neurological Sciences, 45*(4), 405–414. <https://doi.org/10.1017/cjn.2017.297>

Friedrich, F. J., Egly, R., Rafal, R. D., & Beck, D. (1998). *Spatial Attention Deficits in Humans: A Comparison of Superior Parietal and Temporal-Parietal Junction Lesions.*

- Fulvio, J. M., Ji, M., & Rokers, B. (2021). Variations in visual sensitivity predict motion sickness in virtual reality. *Entertainment Computing*, 38.
- Gallagher, M., & Ferrè, E. R. (2018). Cybersickness: A Multisensory Integration Perspective. *Multisensory Research*, 31(7), 645–674. <https://doi.org/10.1163/22134808-20181293>
- Giordano, J., Bikson, M., Kappenman, E. S., Clark, V. P., Coslett, H. B., Hamblin, M. R., Hamilton, R., Jankord, R., Kozumbo, W. J., McKinley, R. A., Nitsche, M. A., Reilly, J. P., Richardson, J., Wurzman, R., & Calabrese, E. (2017). Mechanisms and Effects of Transcranial Direct Current Stimulation. *Dose-Response*, 15(1), 1559325816685467. <https://doi.org/10.1177/1559325816685467>
- Godefroy, O. (2013). *The Behavioral and Cognitive Neurology of Stroke*. Cambridge University Press.
- Gonzalez-Franco, M., Abtahi, P., & Steed, A. (2019). Individual Differences in Embodied Distance Estimation in Virtual Reality. *2019 IEEE Conference on Virtual Reality and 3D User Interfaces (VR)*, 941–943. <https://doi.org/10.1109/VR.2019.8798348>
- Halligan, P. W., Fink, G. R., Marshall, J. C., & Vallar, G. (2003). Spatial cognition: Evidence from visual neglect. *Trends in Cognitive Sciences*, 7(3), 125–133. [https://doi.org/10.1016/S1364-6613\(03\)00032-9](https://doi.org/10.1016/S1364-6613(03)00032-9)
- Harris, D. J., Buckingham, G., Wilson, M. R., & Vine, S. J. (2019). Virtually the same? How impaired sensory information in virtual reality may disrupt vision for action. *Experimental Brain Research*, 237(11), 2761–2766. <https://doi.org/10.1007/s00221-019-05642-8>
- Harris, Jenkin, M., Jenkin, H., Zacher, J. E., & Dyde, R. T. (2017). The effect of long-term exposure to microgravity on the perception of upright. *NPJ Microgravity*, 3, 3. <https://doi.org/10.1038/s41526-016-0005-5>
- Henley, C. (2021). *Planning of Movement*. <https://openbooks.lib.msu.edu/neuroscience/chapter/planning-of-movement/>
- Hill, A. T., Fitzgerald, P. B., & Hoy, K. E. (2016). Effects of Anodal Transcranial Direct Current Stimulation on Working Memory: A Systematic Review and Meta-Analysis of Findings From Healthy and Neuropsychiatric Populations. *Brain Stimulation*, 9(2), 197–208.

<https://doi.org/10.1016/j.brs.2015.10.006>

Holmes, N. P., & Spence, C. (2005). Multisensory Integration: Space, Time and Superadditivity. *Current Biology*, *15*(18), R762–R764. <https://doi.org/10.1016/j.cub.2005.08.058>

Huff, T., Mahabadi, N., & Tadi, P. (2025). Neuroanatomy, Visual Cortex. In *StatPearls*. StatPearls Publishing. <http://www.ncbi.nlm.nih.gov/books/NBK482504/>

Hughes, B. P., Naeem, H. N., & Davidenko, N. (2024). Factors affecting vection and motion sickness in a passive virtual reality driving simulation. *Scientific Reports*, *14*(1), 30214. <https://doi.org/10.1038/s41598-024-80778-4>

Jackson, M. P., Rahman, A., Lafon, B., Kronberg, G., Ling, D., Parra, L. C., & Bikson, M. (2016). Animal models of transcranial direct current stimulation: Methods and mechanisms. *Clinical Neurophysiology: Official Journal of the International Federation of Clinical Neurophysiology*, *127*(11), 3425–3454. <https://doi.org/10.1016/j.clinph.2016.08.016>

Jacobson, L., Koslowsky, M., & Lavidor, M. (2012). tDCS polarity effects in motor and cognitive domains: A meta-analytical review. *Experimental Brain Research*, *216*(1), 1–10. <https://doi.org/10.1007/s00221-011-2891-9>

Javed, K., Reddy, V., & M Das, J. (2023). Neuroanatomy, Posterior Cerebral Arteries. In *StatPearls*. StatPearls Publishing. <http://www.ncbi.nlm.nih.gov/books/NBK538474/>

Jenkin, H., Barnett-Cowan, M., Islam, A., Mazour, E., Dyde, R., Sanderson, J., Jenkin, M., & Harris, L. (2007). The Effect of Tilt on the Perceptual Upright. In *Perception* (Vol. 36).

Jenkin, M., Zacher, J., Dyde, R., Harris, L., & Jenkin, H. (2011). Perceptual Upright: The Relative Effectiveness of Dynamic and Static Images Under Different Gravity States. *Seeing and Perceiving*, *24*(1), 53–64. <https://doi.org/10.1163/187847511X555292>

Kamada, H., & Takeuchi, N. (2023). Transcranial Direct Current Stimulation over the Temporoparietal Junction Modulates Posture Control in Unfamiliar Environments. *Brain Sciences*, *13*(11), 1514. <https://doi.org/10.3390/brainsci13111514>

Kaski, D., Quadir, S., Nigmatullina, Y., Malhotra, P. A., Bronstein, A. M., & Seemungal, B. M. (2016). Temporoparietal encoding of space and time during vestibular-guided orientation. *Brain*, *139*(2), 392–403. <https://doi.org/10.1093/brain/awv370>

- Keshavarz, B., & Hecht, H. (2011). Validating an efficient method to quantify motion sickness. *Human Factors*, 53(4), 415–426. <https://doi.org/10.1177/0018720811403736>
- Kheradmand, A., Lasker, A., & Zee, D. S. (2015). Transcranial Magnetic Stimulation (TMS) of the Supramarginal Gyrus: A Window to Perception of Upright. *Cerebral Cortex*, 25(3), 765–771. <https://doi.org/10.1093/cercor/bht267>
- Kheradmand, A., & Winnick, A. (2017). Perception of Upright: Multisensory Convergence and the Role of Temporo-Parietal Cortex. *Frontiers in Neurology*, 8, 552. <https://doi.org/10.3389/fneur.2017.00552>
- Kim, Y. Y., Kim, H. J., Kim, E. N., Ko, H. D., & Kim, H. T. (2005). Characteristic changes in the physiological components of cybersickness. *Psychophysiology*, 42(5), 616–625. <https://doi.org/10.1111/j.1469-8986.2005.00349>
- Knierim, J. (2020, October 20). *Motor Cortex (Section 3, Chapter 3)*—The University of Texas Medical School at Houston. Neuroscience Online. <https://nba.uth.tmc.edu/neuroscience/m/s3/chapter03.html>
- Knill, D. C., & Pouget, A. (2004). The Bayesian brain: The role of uncertainty in neural coding and computation. *Trends in Neurosciences*, 27(12), 712–719. <https://doi.org/10.1016/j.tins.2004.10.007>
- Körding, K. P., & Wolpert, D. M. (2004). Bayesian integration in sensorimotor learning. *Nature*, 427(6971), 244–247. <https://doi.org/10.1038/nature02169>
- Krol, L. (2020). *EEG 10-10 system with additional information*. Wikimedia Commons. https://commons.wikimedia.org/wiki/File:EEG_10-10_system_with_additional_information.svg
- Kronberg, G., Bridi, M., Abel, T., Bikson, M., & Parra, L. C. (2017). Direct Current Stimulation Modulates LTP and LTD: Activity Dependence and Dendritic Effects. *Brain Stimulation*, 10(1), 51–58. <https://doi.org/10.1016/j.brs.2016.10.001>
- Kronberg, G., Rahman, A., Sharma, M., Bikson, M., & Parra, L. C. (2020). Direct current stimulation boosts hebbian plasticity in vitro. *Brain Stimulation*, 13(2), 287–301. <https://doi.org/10.1016/j.brs.2019.10.014>

- Kropf, E., Syan, S. K., Minuzzi, L., & Frey, B. N. (2018). From anatomy to function: The role of the somatosensory cortex in emotional regulation. *Revista Brasileira de Psiquiatria*, *41*(3), 261–269. <https://doi.org/10.1590/1516-4446-2018-0183>
- Kucyi, A., Hodaie, M., & Davis, K. D. (2012). Lateralization in intrinsic functional connectivity of the temporoparietal junction with salience- and attention-related brain networks. *Journal of Neurophysiology*, *108*(12), 3382–3392. <https://doi.org/10.1152/jn.00674.201>
- LaViola, J. J. (2000). A discussion of cybersickness in virtual environments. *ACM SIGCHI Bulletin*, *32*(1), 47–56. <https://doi.org/10.1145/333329.333344>
- Lefaucheur, J.-P., & Wendling, F. (2019). Mechanisms of action of tDCS: A brief and practical overview. *Neurophysiologie Clinique*, *49*(4), 269–275. <https://doi.org/10.1016/j.neucli.2019.07.013>
- León-Domínguez, U., Vela-Bueno, A., Froufé-Torres, M., & León-Carrión, J. (2013). A chronometric functional sub-network in the thalamo-cortical system regulates the flow of neural information necessary for conscious cognitive processes. *Neuropsychologia*, *51*(7), 1336–1349. <https://doi.org/10.1016/j.neuropsychologia.2013.03.012>
- Litleskare, S. (2021). The relationship between postural stability and cybersickness: It's complicated – An experimental trial assessing practical implications of cybersickness etiology. *Physiology & Behavior*, *236*, 113422. <https://doi.org/10.1016/j.physbeh.2021.113422>
- Mamassian, P., & Goutcher, R. (2001). Prior knowledge on the illumination position. *Cognition*, *81*(1), B1–B9. [https://doi.org/10.1016/S0010-0277\(01\)00116-0](https://doi.org/10.1016/S0010-0277(01)00116-0)
- Mars, R. B., Jbabdi, S., Sallet, J., O'Reilly, J. X., Crosson, P. L., Olivier, E., Noonan, M. P., Bergmann, C., Mitchell, A. S., Baxter, M. G., Behrens, T. E. J., Johansen-Berg, H., Tomassini, V., Miller, K. L., & Rushworth, M. F. S. (2011). Diffusion-Weighted Imaging Tractography-Based Parcellation of the Human Parietal Cortex and Comparison with Human and Macaque Resting-State Functional Connectivity. *The Journal of Neuroscience*, *31*(11), 4087–4100. <https://doi.org/10.1523/JNEUROSCI.5102-10.2011>
- Mars, R. B., Sallet, J., Schuffelgen, U., Jbabdi, S., Toni, I., & Rushworth, M. F. S. (2012). Connectivity-Based Subdivisions of the Human Right 'Temporoparietal Junction Area': Evidence

for Different Areas Participating in Different Cortical Networks. *Cerebral Cortex*, 22(8), 1894–1903. <https://doi.org/10.1093/cercor/bhr268>

Martin, J. H. (2012). 12. The Vestibular System and Eye Movements. In *Neuroanatomy Text and Atlas* (4th ed.). McGraw-Hill.

Masina, F., Pezzetta, R., Lago, S., Mantini, D., Scarpazza, C., & Arcara, G. (2022). Disconnection from prediction: A systematic review on the role of right temporoparietal junction in aberrant predictive processing. *Neuroscience & Biobehavioral Reviews*, 138, 104713. <https://doi.org/10.1016/j.neubiorev.2022.104713>

Masseti, T., Crocetta, T. B., Silva, T. D. da, Trevizan, I. L., Arab, C., Caromano, F. A., & Monteiro, C. B. de M. (2017). Application and outcomes of therapy combining transcranial direct current stimulation and virtual reality: A systematic review. *Disability and Rehabilitation: Assistive Technology*, 12(6), 551–559. <https://doi.org/10.1080/17483107.2016.1230152>

Matsushashi, M., Ikeda, A., Ohara, S., Matsumoto, R., Yamamoto, J., Takayama, M., Satow, T., Begum, T., Usui, K., Nagamine, T., Mikuni, N., Takahashi, J., Miyamoto, S., Fukuyama, H., & Shibasaki, H. (2004). Multisensory convergence at human temporo-parietal junction – epicortical recording of evoked responses. *Clinical Neurophysiology*, 115(5), 1145–1160. <https://doi.org/10.1016/j.clinph.2003.12.009>

McManus, M., & Harris, L. R. (2023). Enhancement of visual cues to self-motion during a visual/vestibular conflict. *PLOS ONE*, 18(3), e0282975. <https://doi.org/10.1371/journal.pone.0282975>

Meinzer, M., Shahbabaie, A., Antonenko, D., Blankenburg, F., Fischer, R., Hartwigsen, G., Nitsche, M. A., Li, S.-C., Thielscher, A., Timmann, D., Waltemath, D., Abdelmotaleb, M., Kocataş, H., Caisachana Guevara, L. M., Batsikadze, G., Grundei, M., Cunha, T., Hayek, D., Turker, S., ... Flöel, A. (2024). Investigating the neural mechanisms of transcranial direct current stimulation effects on human cognition: Current issues and potential solutions. *Frontiers in Neuroscience*, 18. <https://doi.org/10.3389/fnins.2024.1389651>

Merchant, W., & Kirolos, R. (2022). An Overview of Cybersickness Self-Report Measures for use in Defence Research and Development Canada Experiments. *Defence Research and Development Canada*.

Miranda, P. C. (2013). IS 1. The electric field in the brain during tDCS. *Clinical Neurophysiology*, 124(10), e39. <https://doi.org/10.1016/j.clinph.2013.04.020>

Mittelstaedt, H. (1983). A new solution to the problem of the subjective vertical. *Naturwissenschaften*, 70(6), 272–281. <https://doi.org/10.1007/BF00404833>

Moraes, D., & Gustavo, C. (2013). Anatomy of the Visual Pathways. *Journal of Glaucoma*, 22, S2. <https://doi.org/10.1097/IJG.0b013e3182934978>

Morley, A., & Hill, L. (2016). *10-20 system EEG Placement*.

Murray, M. M., Lewkowicz, D. J., Amedi, A., & Wallace, M. T. (2016). Multisensory Processes: A Balancing Act across the Lifespan. *Trends in Neurosciences*, 39(8), 567–579. <https://doi.org/10.1016/j.tins.2016.05.003>

Nagy, A., Eördegh, G., Paróczy, Z., Márkus, Z., & Benedek, G. (2006). Multisensory integration in the basal ganglia. *European Journal of Neuroscience*, 24(3), 917–924. <https://doi.org/10.1111/j.1460-9568.2006.04942.x>

Nesbitt, K., Davis, S., Blackmore, K., & Nalivaiko, E. (2017). Correlating reaction time and nausea measures with traditional measures of cybersickness. *Displays*, 48, 1–8. <https://doi.org/10.1016/j.displa.2017.01.002>

neuroConn Programmable Direct Current Stimulator DC-STIMULATOR User manual. (2024, October 14). neuroConn.

Ng, A. K. T., Chan, L. K. Y., & Lau, H. Y. K. (2018). A Study of Cybersickness and Sensory Conflict Theory Using a Motion-Coupled Virtual Reality System. *2018 IEEE Conference on Virtual Reality and 3D User Interfaces (VR)*, 643–644. <https://doi.org/10.1109/VR.2018.8446269>

Nishiike, S., Okazaki, S., Watanabe, H., Akizuki, H., Imai, T., Uno, A., Kitahara, T., Horii, A., Takeda, N., & Inohara, H. (2013). The effect of visual-vestibulosomatosensory conflict induced by virtual reality on postural stability in humans. *The Journal of Medical Investigation: JMI*, 60(3–4), 236–239. <https://doi.org/10.2152/jmi.60.236>

Nitsche, M. A., Doemkes, S., Karaköse, T., Antal, A., Liebetanz, D., Lang, N., Tergau, F., & Paulus, W. (2007). Shaping the effects of transcranial direct current stimulation of the human motor cortex. *Journal of Neurophysiology*, 97(4), 3109–3117. <https://doi.org/10.1152/jn.01312.2006>

- Nitsche, M. A., & Paulus, W. (2001). Sustained excitability elevations induced by transcranial DC motor cortex stimulation in humans. *Neurology*, *57*(10), 1899–1901.
<https://doi.org/10.1212/wnl.57.10.1899>
- Olman, E. by D. C. (2022). *Motion Processing: MT and MST*.
<https://pressbooks.umn.edu/sensationandperception/chapter/motion-processing-mt-and-mst/>
- Oman, C. M. (1982). *A Heuristic Mathematical Model for the Dynamics of Sensory Conflict*. *Acta Oto-laryngologica*.
- Palmisano, S., Allison, R. S., Teixeira, J., & Kim, J. (2023). Differences in virtual and physical head orientation predict sickness during active head-mounted display-based virtual reality. *Virtual Reality*, *27*(2), 1293–1313. <https://doi.org/10.1007/s10055-022-00732-5>
- Papeo, L., Longo, M. R., Feurra, M., & Haggard, P. (2010). The role of the right temporoparietal junction in intersensory conflict: Detection or resolution? *Experimental Brain Research*, *206*(2), 129–139. <https://doi.org/10.1007/s00221-010-2198-2>
- Pearson, K. (2000). Motor Systems. *Current Opinion in Neurobiology*. [https://doi.org/10.1016/S0959-4388\(00\)00130-6](https://doi.org/10.1016/S0959-4388(00)00130-6)
- Pelletier, S. J., & Cicchetti, F. (2015). Cellular and Molecular Mechanisms of Action of Transcranial Direct Current Stimulation: Evidence from In Vitro and In Vivo Models. *International Journal of Neuropsychopharmacology*, *18*(2), pyu047.
<https://doi.org/10.1093/ijnp/pyu047>
- Peterka, R. J. (2018). Sensory integration for human balance control. *Handbook of Clinical Neurology*, *159*, 27–42. <https://doi.org/10.1016/B978-0-444-63916-5.00002-1>
- Polanía, R., Nitsche, M. A., & Ruff, C. C. (2018). Studying and modifying brain function with non-invasive brain stimulation. *Nature Neuroscience*, *21*(2), 174–187.
<https://doi.org/10.1038/s41593-017-0054-4>
- Popa, L. S., & Ebner, T. J. (2019). Cerebellum, Predictions and Errors. *Frontiers in Cellular Neuroscience*, *12*. <https://doi.org/10.3389/fncel.2018.00524>

- Purves, D., Augustine, G. J., Fitzpatrick, D., Katz, L. C., LaMantia, A.-S., McNamara, J. O., & Williams, S. M. (2001a). Anatomical Distribution of Rods and Cones. In *Neuroscience. 2nd edition*. Sinauer Associates. <https://www.ncbi.nlm.nih.gov/books/NBK10848/>
- Purves, D., Augustine, G. J., Fitzpatrick, D., Katz, L. C., LaMantia, A.-S., McNamara, J. O., & Williams, S. M. (2001b). The Association Cortices. In *Neuroscience. 2nd edition*. Sinauer Associates. <https://www.ncbi.nlm.nih.gov/books/NBK11109/>
- Raju, H., & Tadi, P. (2022). Neuroanatomy, Somatosensory Cortex. In *StatPearls*. StatPearls Publishing. <http://www.ncbi.nlm.nih.gov/books/NBK555915/>
- Ramnani, N. (2012). Frontal Lobe and Posterior Parietal Contributions to the Cortico-cerebellar System. *The Cerebellum*, *11*(2), 366–383. <https://doi.org/10.1007/s12311-011-0272-3>
- Reason, J. T. (1978). Motion Sickness Adaptation: A Neural Mismatch Model. *Journal of the Royal Society of Medicine*, *71*(11), 819–829. <https://doi.org/10.1177/014107687807101109>
- Reason, J. T., & Brand, J. (1975). *Motion Sickness*. Academic Press.
- Riccio, G. E., & Stoffregen, T. A. (1991). An ecological Theory of Motion Sickness and Postural Instability. *Ecological Psychology*, *3*(3), 195–240. https://doi.org/10.1207/s15326969eco0303_2
- Saredakis, D., Szpak, A., Birkhead, B., Keage, H. A. D., Rizzo, A., & Loetscher, T. (2020). Factors Associated With Virtual Reality Sickness in Head-Mounted Displays: A Systematic Review and Meta-Analysis. *Frontiers in Human Neuroscience*, *14*, 96. <https://doi.org/10.3389/fnhum.2020.00096>
- Singh-Curry, V., & Husain, M. (2009). The functional role of the inferior parietal lobe in the dorsal and ventral stream dichotomy. *Neuropsychologia*, *47*(6), 1434–1448. <https://doi.org/10.1016/j.neuropsychologia.2008.11.033>
- Souvestre, P. A., Landrock, C. K., & Blaber, A. P. (2008). Reducing Incapacitating Symptoms during Space Flight: Is Postural Deficiency Syndrome an Applicable Model? *Hippokratia*, *12*(Suppl 1), 41–48. <https://www.ncbi.nlm.nih.gov/pmc/articles/PMC2577399/>

Spence, C. (2012). Multisensory Perception, Cognition and Behaviour: Evaluating the Factors Modulating Multisensory Integration. In *The New Handbook of Multisensory Processing*. Massachusetts Institute of Technology.

Stanney, K., Lawson, B. D., Rokers, B., Dennison, M., Fidopiastis, C., Stoffregen, T., Weech, S., & Fulvio, J. M. (2020). Identifying Causes of and Solutions for Cybersickness in Immersive Technology: Reformulation of a Research and Development Agenda. *International Journal of Human-Computer Interaction*, 36(19), 1783–1803.

<https://doi.org/10.1080/10447318.2020.1828535>

Stein, B. E., & Stanford, T. R. (2008). Multisensory integration: Current issues from the perspective of the single neuron. *Nature Reviews Neuroscience*, 9(4), 255–266.

<https://doi.org/10.1038/nrn2331>

Swenson, R. S. (2017). Chapter 8—The Vestibular System. In P. M. Conn (Ed.), *Conn's Translational Neuroscience* (pp. 167–183). Academic Press. <https://doi.org/10.1016/B978-0-12-802381-5.00014-2>

Szpak, A., Michalski, S. C., & Loetscher, T. (2020). Exergaming With Beat Saber: An Investigation of Virtual Reality Aftereffects. *Journal of Medical Internet Research*, 22(10), e19840. <https://doi.org/10.2196/19840>

Takeda, N., Morita, M., Horii, A., Nishiike, S., Kitahara, T., & Uno, A. (2001). Neural mechanisms of motion sickness. *The Journal of Medical Investigation: JMI*, 48(1–2), 44–59.

Takeuchi, N., Mori, T., Suzukamo, Y., & Izumi, S.-I. (2018). Modulation of Excitability in the Temporoparietal Junction Relieves Virtual Reality Sickness. *Cyberpsychology, Behavior, and Social Networking*, 21(6), 381–387. <https://doi.org/10.1089/cyber.2017.0499>

Taylor, J. L. (2009). Proprioception. In L. R. Squire (Ed.), *Encyclopedia of Neuroscience* (pp. 1143–1149). Academic Press. <https://doi.org/10.1016/B978-008045046-9.01907-0>

Thair, H., Holloway, A. L., Newport, R., & Smith, A. D. (2017). Transcranial Direct Current Stimulation (tDCS): A Beginner's Guide for Design and Implementation. *Frontiers in Neuroscience*, 11, 641. <https://doi.org/10.3389/fnins.2017.00641>

- Treisman, A. M., & Gelade, G. (1980). A feature-integration theory of attention. *Cognitive Psychology*, *12*(1), 97–136. [https://doi.org/10.1016/0010-0285\(80\)90005-5](https://doi.org/10.1016/0010-0285(80)90005-5)
- Treisman, M. (1977). Motion Sickness: An Evolutionary Hypothesis. *Science*, *197*(4302), 493–495. <https://doi.org/10.1126/science.301659>
- Tuthill, J. C., & Azim, E. (2018). Proprioception. *Current Biology*, *28*(5), R194–R203. <https://doi.org/10.1016/j.cub.2018.01.064>
- Uno, A., Takeda, N., & Tadas. (2000). Effects of Vestibular Cerebellum Lesion on Motion Sickness in Rats. *Acta Oto-Laryngologica*, *120*(3), 386–389. <https://doi.org/10.1080/000164800750000612>
- Ventre, J., & Faugier-Grimaud, S. (1988). Projections of the temporo-parietal cortex on vestibular complex in the macaque monkey (*Macaca fascicularis*). *Experimental Brain Research*, *72*(3), 653–658. <https://doi.org/10.1007/BF00250611>
- Ventre-Dominey, J. (2014). Vestibular function in the temporal and parietal cortex: Distinct velocity and inertial processing pathways. *Frontiers in Integrative Neuroscience*, *8*, 53. <https://doi.org/10.3389/fnint.2014.00053>
- Ventre-Dominey, J., Nighoghossian, N., & Denise, P. (2003). Evidence for interacting cortical control of vestibular function and spatial representation in man. *Neuropsychologia*, *41*(14), 1884–1898. [https://doi.org/10.1016/S0028-3932\(03\)00126-X](https://doi.org/10.1016/S0028-3932(03)00126-X)
- Vossel, S., Geng, J. J., & Fink, G. R. (2014). Dorsal and Ventral Attention Systems. *The Neuroscientist*, *20*(2), 150–159. <https://doi.org/10.1177/1073858413494269>
- Warburton, M., Mon-Williams, M., Mushtaq, F., & Morehead, J. R. (2023). Measuring motion-to-photon latency for sensorimotor experiments with virtual reality systems. *Behavior Research Methods*, *55*(7), 3658–3678. <https://doi.org/10.3758/s13428-022-01983-5>
- Warchoń, J., Tetych, A., Tomaszewski, R., Kowalczyk, B., & Olchowik, G. (2024). Virtual Reality- Induced Modification of Vestibulo–Ocular Reflex Gain in Posturography Tests. *Journal of Clinical Medicine*, *13*(10), 2742. <https://doi.org/10.3390/jcm13102742>

- Warwick-Evans, L. A., Symons, N., Fitch, T., & Burrows, L. (1998). Evaluating sensory conflict and postural instability. Theories of motion sickness. *Brain Research Bulletin*, *47*(5), 465–469. [https://doi.org/10.1016/S0361-9230\(98\)00090-2](https://doi.org/10.1016/S0361-9230(98)00090-2)
- Weech, S., Kenny, S., & Barnett-Cowan, M. (2019). Presence and Cybersickness in Virtual Reality Are Negatively Related: A Review. *Frontiers in Psychology*, *10*. <https://www.frontiersin.org/articles/10.3389/fpsyg.2019.00158>
- Weech, S., Varghese, J. P., & Barnett-Cowan, M. (2018). Estimating the sensorimotor components of cybersickness. *Journal of Neurophysiology*, *120*(5), 2201–2217. <https://doi.org/10.1152/jn.00477.2018>
- Weech, S., Wall, T., & Barnett-Cowan, M. (2020). Reduction of cybersickness during and immediately following noisy galvanic vestibular stimulation. *Experimental Brain Research*, *238*(2), 427–437. <https://doi.org/10.1007/s00221-019-05718-5>
- Winnick, A. A., Wang, C.-H., Ko, Y.-H., & Chang, T.-P. (2022). Subjective visual vertical imprecision during lateral head tilt in patients with chronic dizziness. *Experimental Brain Research*, *240*(1), 199–206. <https://doi.org/10.1007/s00221-021-06247-w>
- Woo, Y. S., Jang, K.-M., Nam, S. G., Kwon, M., & Lim, H. K. (2023). Recovery time from VR sickness due to susceptibility: Objective and quantitative evaluation using electroencephalography. *Heliyon*, *9*(4), e14792. <https://doi.org/10.1016/j.heliyon.2023.e14792>
- Wurtz, R., & Kandel, E. (2021). Central Visual Pathways. In *Principles of Neural Science* (6th ed.). McGraw-Hill. https://www.weizmann.ac.il/brain-sciences/labs/ulanovsky/sites/neurobiology.labs.ulanovsky/files/uploads/kandel_ch27_ch28_visioncentralmotiondepthform.pdf
- Yamada, Y., & Sumiyoshi, T. (2021). Neurobiological Mechanisms of Transcranial Direct Current Stimulation for Psychiatric Disorders; Neurophysiological, Chemical, and Anatomical Considerations. *Frontiers in Human Neuroscience*, *15*, 631838. <https://doi.org/10.3389/fnhum.2021.631838>
- Yin, K., He, Z., Xiong, J., Zou, J., Li, K., & Wu, S.-T. (2021). Virtual reality and augmented reality displays: Advances and future perspectives. *Journal of Physics: Photonics*, *3*(2), 022010. <https://doi.org/10.1088/2515-7647/abf02e>

Yip, D. W., Awosika, A. O., & Lui, F. (2025). Physiology, Motor Cortical. In *StatPearls*. StatPearls Publishing. <http://www.ncbi.nlm.nih.gov/books/NBK542188/>

Zhan, T., Yin, K., Xiong, J., He, Z., & Wu, S.-T. (2020). Augmented Reality and Virtual Reality Displays: Perspectives and Challenges. *iScience*, 23(8). <https://doi.org/10.1016/j.isci.2020.101397>

Živanović, M., Paunović, D., Konstantinović, U., Vulić, K., Bjekić, J., & Filipović, S. R. (2021). The effects of offline and online prefrontal vs parietal transcranial direct current stimulation (tDCS) on verbal and spatial working memory. *Neurobiology of Learning and Memory*, 179, 107398. <https://doi.org/10.1016/j.nlm.2021.1073>